CORRELATIVE SPECT IMAGING OF NEURAL STEM/PROGENITOR CELL TRANSPLANTS IN A RAT MODEL OF PARKINSON'S DISEASE

By

JACQUELINE A GLEAVE, BSc

A Thesis

Submitted to the School of Graduate Studies

in Partial Fulfillment of the Requirements

for the Degree

Doctor of Philosophy

McMaster University

DOCTOR OF PHILSOPHY (2009) McMaster University

(Medical Sciences) Hamilton, ON

TITLE: Correlative SPECT imaging of neural stem/progenitor cell transplants in a rat model of Parkinson's disease

AUTHOR: Jacqueline A Gleave, BSc (Simon Fraser University)

SUPERVISOR: Dr. L.C. Doering

NUMBER OF PAGES: xv, 184

Abstract

Cell therapy for Parkinson's disease will greatly benefit from progress in methods aimed at visualizing the dopamine system and cell replacement techniques. Currently, cell therapy has been met with varied success, in part due to differences in cell sources, transplantation procedures, and our lack of understanding of cell fate post-transplantation. The standardization of transplantation procedures will enhance our ability to draw comparisons between studies and improve cell therapy outcomes. We developed a method to label neural stem/progenitor cells (NSPCs) with technetium-99m and then visualize the cells with single photon emission computed tomography (SPECT) subsequent to grafting in the brain. This labeling method permitted a high uptake of the tracer into the cells without causing damage to the DNA or altering cell viability. The labeling caused a significant decrease (75%) in the proliferative capacity of the NSPCs and caused a trend towards an increase in neuronal differentiation. Using this technique paves the way to standardize the location of the transplant and quantify the number transplanted cells while increasing the production of neurons.

Experiments were performed to visualize the dopamine system with [^{123}I]altropane at pre- and post-transplant time points in the 6-OHDA rat model of Parkinson's disease. [^{123}I]altropane binding correlated with the content of dopamine in the striatum. However, [^{123}I]altropane binding was not correlated with dopamine content in the substantia nigra and did not show a correlation with the amphetamine rotations. However, there was a significant correlation with the cylinder test and the postural

instability test. When the data was assessed using linear regression, the r^2 value of the linear relationship was low indicating that [^{123}I]altropane SPECT is not a good predictor of behavioural outcome due to a weak linear relationship. Our data indicates that [^{123}I]altropane predicts the integrity of the striatal dopamine nerve terminals, but does not predict the integrity of the nigrostriatal system. The results are discussed in relation to the use of [^{123}I]altropane in comparison to other dopamine SPECT and PET agents.

Acknowledgements

I would like to thank my family who has continually supported me and encouraged me in pursuing my educational goals. My husband, Dennis, has been supportive, encouraging, and wonderfully patient - I could not have done this without him. My supervisor, Dr. Doering, has given me guidance while allowing me to work independently and has been great to work with over the years. My committee members, Dr. Farncombe, Dr. Mishra, and Dr. Vallaint have been supportive in this project and I owe them many thanks. This has truly been a team effort and I thank all of my colleagues and friends who helped me by showing me new techniques or helping me relax. Final thanks to God the Father from whom all blessings flow.

Table of Contents

List of Figures and Tables

Chapter 2 – Literature Review

Chapter 3 – Materials and Methods

Chapter 4 – In vitro labeling of neural stem/progenitor cells with $[^{99m}Tc(CO)_3SAACQHIVTat_{48-57}]^+$

Chapter 5 – Imaging neural stem/progenitor cells labeled with $[^{99m}Tc(CO)_3SAACQHIVTat_{48-57}]^+$ in rodents

Abbreviations

[^{123}I]altropane	[^{123}I]-2β-carbomethoxy-3β-(4-fluorophenyl)-*N*-(3-iodo-*E*-allyl)nortropane
[^{99m}Tc]TRODAT	[2-[[2-[[[3-(4-chlorophenyl)-8-methyl-8-azabicyclo[3,2,1]oct-2-yl]methyl](2-mercaptoethyl)amino]ethyl]amino]ethanethiolato-(3-)-N2,N2',Se,Se']oxo-[1R-(exo-exo)]-[99mTc]technetium
^{99m}Tc-SAACQ	$[^{99m}Tc(CO)_3SAACQHIVTat_{48-57}]^+$
Re-SAACQ	$[Re(CO)_3SAACQHIVTat_{48-57}]^+$
6-OHDA	6-hydroxydopamine
AAAD	Aromatic amino acid decarboxylase
AP	Anterio-posterion
BrdU	Bromodeoxyuridine
CAT	Catalase
COMT	Catechol *O*-methyltransferase
CNS	Central nervous system
CT	Computed tomograpy
DA	Dopamine
DAPI	4',6-diamidino-2-phenylindole
DAergic	Dopaminergic
DAT	Dopamine transporter

DV	Dorsal ventral
ESCs	Embryonic stem cells
EGF	Epidermal growth factor
FDOPA	6-[^{18}F]Fluoro-L-dopa
FGF-2	Basic fibroblast growth factor
FITC	Fluorescein isothiocyanate
FMT	6-[^{18}F]fluoro-L-*m*-tyrosine
FOV	Field of view
GABA	Gamma aminobutyric acid
GDNF	Glial cell line derived neurotrophic factor
GFAP	Glial fibrillary acidic protein
GSH	Glutathione
GSH-Px	Glutathione peroxidase
HIV-1	Human immunodeficiency virus 1
HPLC	High performance liquid chromatography
LB	Lewy bodies
L-DOPA	Levodopa
MAO	Monoamine oxidase
MFB	Median forebrain bundle
ML	Medial-lateral
MPTP	1-methyl-4-phenyl-1,2,3,6-tetrahydropyridine
MRI	Magnetic resonance imaging

NAT	Noradrenaline transporter
NPCs	Neural progenitor cells
NSCs	Neural stem cells
NSPCs	Neural stem/progenitor cells
OB	Olfactory bulb
PBS	Phosphate buffered saline
PD	Parkinson's disease
PIT	Postural instability test
PMT	Photomultiplier tube
PET	Positron emission tomography
RCF	Relative centrifugal force
RMS	Rostral migratory stream
ROI	Region of interest
ROS	Reactive oxygen species
SAAC	Single amino acid chelate
SAACQ	Single amino acid chelate bisquinoline
SAACQ	[SAACQHIVTat$_{48-57}$]
SNpc	Substantia nigra pars compacta
SOD	Superoxide dismutase
SPECT	Single photon emission computed tomography
SVZ	Subventricular zone
TBS	Tris buffered saline

TBST	Tris buffered saline with Tween 20
TFA	Trifluoroacetic acid
TH	Tyrosine hydroxylase
THir	Tyrosine hydroxylase immunoreactivity
UPDRS	Unified Parkinson's Disease Rating Scale
VM	Ventral mesencephalon

Chapter 1: Introduction and Objectives

Parkinson's disease (PD) is the second most common neurodegenerative disorder following Alzheimer's disease. PD is characterized by the loss of dopamine (DA) neurons that project from the substantia nigra pars compacta (SNpc) to the striatum and by the formation of protein occlusions called Lewy bodies (LB). There is currently no cure for PD and treatment focuses on alleviating the motor symptoms associated with this disease through the oral administration of DA antagonists or more invasively by surgical procedures.

Neural stem cells (NSCs) are undifferentiated cells that persist into adulthood. They have the ability to self-renew and differentiate into the main cell types in the central nervous system (CNS): astrocytes, oligodendrocytes, and neurons. They can be expanded *in vitro* as neurospheres, which are free-floating, heterogeneous aggregates of cells. Expansion of the neurospheres is required to generate large numbers of neural stem/progenitor cells (NSPCs) for transplantation purposes. These cells can be altered *in vitro* to express and release growth factors, directed to a dopaminergic (DAergic) lineage, or they can be used in an unmanipulated state. NSPCs have been transplanted into the intact and lesioned animal brain. Once transplanted, these cells have been shown to differentiate into neurons and glia.

Although NSPC transplants are promising for neurological therapy, there are limitations to this form of treatment. Currently, the fate of the cells is difficult to predict after transplantation and the optimal transplantation conditions, such as cell number, location, and age of the host, are not well defined for effective results. Differences between cell types, donor source, and the *in vitro* culture conditions make comparisons between studies difficult. Non-invasive imaging of the cell transplant and the DA nigrostriatal system would help to address some of these issues and imaging will offer certain information that other standard techniques cannot provide. In addition, non-invasive imaging is suited to quantitative, longitudinal studies, which decreases the subject-to-subject variability and the costs associated with pre-clinical studies.

To this end, we demonstrated the ability to label cells *in vitro* for non-invasive *in vivo* imaging with single photon emission computed tomography (SPECT). Using a novel probe based on the permeation peptide HIVTat$_{48-57}$, the single amino acid chelate quinoline (SAACQ) was incorporated into the peptide as a natural amino acid and either Re or ^{99m}Tc was coordinated into the peptide. The labeled cells could be visualized by fluorescence microscopy or with SPECT when they were labeled with [Re(CO)$_3$SAACQHIVTat$_{48-57}$][Br] (Re-SAACQ) or [^{99m}Tc(CO)$_3$SAACQHIVTat$_{48-57}$]$^+$ (^{99m}Tc-SAACQ) respectively.

The first objective of this study was to label NSPCs with Re-SAACQ or with ^{99m}Tc-SAACQ and determine the amount of activity that could be taken up into the

cells. In order for the labeling system to be a viable option, the biological integrity of the cells must be unaffected. We examined cell viability, DNA damage, and the proliferation and differentiation characteristics of the cells. There was no significant change in the viability of the cells or in the amount of DNA damage of the labeled NSPCs when compared to controls. The proliferation of the cells was significantly decreased when the cells were labeled with ^{99m}Tc-SAACQ and there was a trend towards an increase in neuronal differentiation.

The second objective of this study was to use SPECT to visualize the cell transplants *in vivo*. Initial studies were completed in mice and planar, dynamic, and parallel hole and pinhole SPECT/CT was performed. We found that there was no significant loss of the ^{99m}Tc from the cells and we established methods to quantify the number of transplanted cells. We also demonstrated the specificity of the SPECT image by correlating it with phosphorimaging and histology.

In addition to imaging the cell transplants, we assessed the DA system using [2-[[2-[[[3-(4-chlorophenyl)-8-methyl-8-azabicyclo[3,2,1]oct-2-yl]methyl](2-mercaptoethyl)amino]ethyl]amino]ethanethiolato-(3-)-N2,N2',Se,Se']oxo-[1R-(exo-exo)]-[99mTc]technetium ([^{99m}Tc]TRODAT), 6-[^{18}F]fluoro-L-*m*-tyrosine ([^{18}F]FMT), and [^{123}I]-2β-carbomethoxy-3β-(4-fluorophenyl)-*N*-(3-iodo-*E*-allyl)nortropane ([^{123}I]altropane). We were unable to obtain consistent images with [^{99m}Tc]TRODAT or [^{18}F]FMT. Using [^{123}I]altropane we could consistently visualize the DA system pre- and

post-lesion and pre- and post-transplantion with SPECT. **The third objective was to correlate the [^{123}I]altropane SPECT images with the histology, neurochemistry, and/or behavioural tests in the animals.** To our knowledge, this is the first time [^{123}I]altropane has been used to visualize the DA system in small animals. The SPECT images showed a strong correlation with the DA content in the striatum, but not with the substantia nigra. In addition, [^{123}I]altropane images were unable to predict functional recovery assessed by behavioural testing indicating that SPECT images should not be used to predict behavioural outcomes.

Chapter 2: Literature Review

2.1 Parkinson's disease

Parkinson's disease (PD) is the most common neurodegenerative movement disorder (Dawson and Dawson, 2003). It is a progressive disease characterized by the loss of DAergic neurons that project from the SNpc to the striatum and by the formation of LB. A loss of 50-70% of the DA neurons is necessary before obvious symptoms of the disease appear. Common symptoms include resting tremor, rigidity, bradykinesia and akinesia. The mean onset age for PD is 60 years with a mean duration of 13 years (Hughes *et al.*, 1993). Apart from the nigrostriatal lesions, there are non-nigral lesions that lead to cognitive and psychological impairments (Aarsland *et al.*, 1996).

2.1.1 Etiology of Parkinson's disease

PD is thought to operate through common molecular pathways. One hypothesized mechanism suggests that the misfolding and aggregation of proteins in the DAergic neurons of the SNpc leads to cell death while another proposes that mitochondrial dysfunction and resulting oxidative stress leads to toxicity of the DAergic neurons. Previous work indicates that oxidative stress to α-synuclein, a protein linked to inherited PD, resulted in an increase in misfolding and aggregation (Giasson *et al.*, 2000). It is possible that a combination of both mechanisms leads to the pathogenesis of PD.

2.1.2 Protein misfolding

Abnormal protein folding and aggregation have been linked to age-related neurodegenerative diseases such as Alzheimer's disease and PD. It is thought that protein aggregation caused by misfolded proteins may directly lead to neuronal death by interfering with intracellular trafficking or sequestering proteins required for cell survival (Bussell, Jr. and Eliezer, 2001). Alternatively, it may indirectly cause cell death through the process which the cell uses to sequester soluble misfolded proteins (Dauer and Przedborski, 2003). As the cell ages, its ability to handle misfolded proteins appears to decline (Sherman and Goldberg, 2001). Proteins may become damaged and misfolded due to insult caused by reactive oxygen species (ROS). The cell's ability to recruit chaperones, used for protein refolding, or proteasomes, used to degrade misfolded proteins, decreases with age (Dauer and Przedborski, 2003). Neurons may be more susceptible to these changes because they are post-mitotic. The increase in protein aggregation is characterized by the presence of LB in PD. Therefore, the combination of cell aging and oxidative stress resulting in the formation of ROS may result in an increase in protein aggregation leading to DAergic neuronal death.

2.1.3 Mitochondrial dysfunction

Since the discovery that 1-methyl-4-phenyl-1,2,3,6-tetrahydropyridine (MPTP) caused DAergic neurodegeneration through the inhibition complex I of the electron transport chain, mitochondrial dysfunction and resulting oxidative stress have been investigated in the pathogenesis of PD. Abnormalities in complex I activity in PD have

been identified and inhibition of complex I may subject the cells to oxidative stress and energy failure (Greenamyre *et al.*, 2001). In the SNpc of PD brains there are elevated levels of biological markers of oxidative damage (Parker, Jr. *et al.*, 1989). DA neurons may be more susceptible because the metabolism of DA produces hydrogen peroxide and superoxide radicals (Graham *et al.*, 1978). Mitochondrial-related energy failure may disrupt the vesicular DA storage releasing DA into the cytosol of the cell, which in turn increase the presence of ROS (Dauer and Przedborski, 2003). An increase in ROS in the cytosol may result in an increase in protein aggregation and demand on the molecular mechanisms used by the cell to handle the increase in protein misfolding. Despite compelling evidence towards the involvement of DA metabolism in DAergic cell death, there is an inability to confirm this as the primary cause of death due to the absence of DA neurons in post-mortem studies. It is possible that the increase in ROS production is a nonspecific future that occurs in dying cells (Dauer and Przedborski, 2003).

2.1.4 Oxidative stress

Oxidative stress is thought to be a prominent part of the etiology of PD. Oxygen radical species can be produced by both endogenous and exogenous sources. Endogenously, the auto-oxidation of catecholamines and their breakdown via monoamine oxidase (MAO) causes the formation of O_2^- and H_2O_2 repectively. Although H_2O_2 is not a ROS because it does not contain a free electron, it produces hydroxyl radicals through its reaction with iron (the Fenton reaction[1]).

[1] $H_2O_2 + Fe^{2+} \rightarrow OH^- + OH\cdot + Fe^{3+}$

DA itself can cause free radical production. In addition to the MAO breakdown of DA, the auto-oxidation of chatecholamines (6-hydroxydopamine (6-OHDA) and DA) forms quinones that are damaging to the cells. The anti-oxidant defense system is comprised of superoxide dimutase (SOD), glutathione peroxidase (GSH-Px), catalase (CAT), and glutathione (GSH). The ROS produced by DA causes cellular damage because of its action on phospholipids, proteins, and nucleic acids. The attack on the cell membrane leads to lipid peroxidation and ROS can cause damage to the DNA nucleosides and the phosphodiester backbone. Because differentiated neurons do not go through the full cell cycle, oxidative stress can lead to the accumulation of DNA damage over time, which may play a key role in the aging process. In conclusion, DA toxicity from its own oxidation can lead to the production of radicals, toxic quinonic compounds and melanin (Offen *et al.*, 1996).

In post-mortem studies in PD patients, there is an increase in lipid peroxidation products and abnormal iron metabolism in the basal ganglia (Gerlach *et al.*, 1994). The iron levels are specifically increased in the SNpc, which is involved in the nigrostriatal pathway (Gerlach *et al.*, 1994). In addition, the levels of free radical scavengers are abnormal in PD patients. There is a decrease in GSH-Px in the lateral ventral portion of the SNpc, which is the area most susceptible to DA cell death in PD (Damier *et al.*, 1993). This would lead to a defect in the basal detoxification capabilities of this area of the brain which decreases its ability to deal with ROS.

2.1.5 Therapeutic options

Current therapies for PD focus around controlling the symptoms associated with this disease. These include pharmacological interventions (levodopa (L-DOPA) and MAO inhibitors) and surgical options (deep brain stimulation and pallidotomy). The most effective drug used clinically is L-DOPA, a DA precursor. Oral administration of L-DOPA replaces striatal DA and relieves many of the symptoms of PD (Dauer and Przedborski, 2003). However, prolonged use of L-DOPA leads to side effects such as dyskinesias, influencing the patients' quality of life (Chapuis *et al.*, 2005). In addition, therapies available do not halt disease progression; therefore, there is a need for future therapeutic strategies to focus on relieving symptoms and protecting or rescuing degenerating neurons in order to slow or halt disease progression.

2.2 The 6-hydroxydopamine Model

In order to study the effectiveness of potential therapies, animal models of PD have been developed. These include toxin-based models, such as 6-OHDA, paraquat, rotenone, and MPTP models (Dauer and Przedborski, 2003). The 6-OHDA rat model of PD is a widely implemented model due to its characterized behavioural phenotypes. 6-OHDA is a neurotoxin that is structurally analogous to the catecholamines DA and noradrenaline. It is taken up by the DA transporter (DAT) and the noradrenergic transporter (NAT) (Luthman *et al.*, 1989) resulting in the death of these neuronal types. The initial model was a bilateral model developed by Ungerstedt (Ungerstedt, 1968).

This model was later modified to the currently implemented unilateral model (Ungerstedt and Arbuthnott, 1970).

2.2.1 Mechanism of Neurotoxicity

6-OHDA is unable to cross the blood brain barrier and therefore must be injected directly into the brain parenchyma of rats using stereotaxic surgery. The toxic effects of 6-OHDA occurs in 2 steps: 1) accumulation in the neuron, 2) changes in cell homeostasis and resultant neuronal damage (Simola *et al.*, 2007). The intracellular storage of 6-OHDA is mediated by DAT and NAT. The changes in cell homeostasis and the resultant neuronal damage are thought to be largely caused by oxidative stress (Figure 2.1) (Cadet and Brannock, 1998; Blum *et al.*, 2001). The production of cytotoxic species occurs by both enzymatic and non-enzymatic mechanisms, which are amplified by the trace elements manganese and iron (Cadet and Brannock, 1998; Choi *et al.*, 1999).

Enzymatically, 6-OHDA is broken down by MAO generating H_2O_2 that triggers the production of oxygen radicals (Cohen, 1984). The auto-oxidation of 6-OHDA produces H_2O_2, ROS, and chatecolamine quinones that attack the endocellular nucleophilic groups (Palumbo *et al.*, 1999). The increase in ROS decreases the endocellular antioxidants amplifying the neurotoxic effects of 6-OHDA causing abnormalities in the cell structure and metabolism which eventually leads to neuronal death (Blum *et al.*, 2001). This mechanism was determined because infusion of free radical scavengers into the rat brain caused attenuation of 6-OHDA neurotoxicity (Cadet

Figure 2.1. The proposed mechanism of 6-OHDA neurotoxicity. 6-OHDA is taken up by the DAT and can induce cell toxicity by three main mechanisms: 1) reactive oxygen species 2) inhibition of complex 1 of the mitochondrial electron transport chain 3) hydrogen peroxide formation. One or a combination of these events leads to oxidative stress amplified by cytoplasmic free calcium and a decrease in the cellular production of ATP ultimately resulting in cell death. (Figure from Blum 2001).

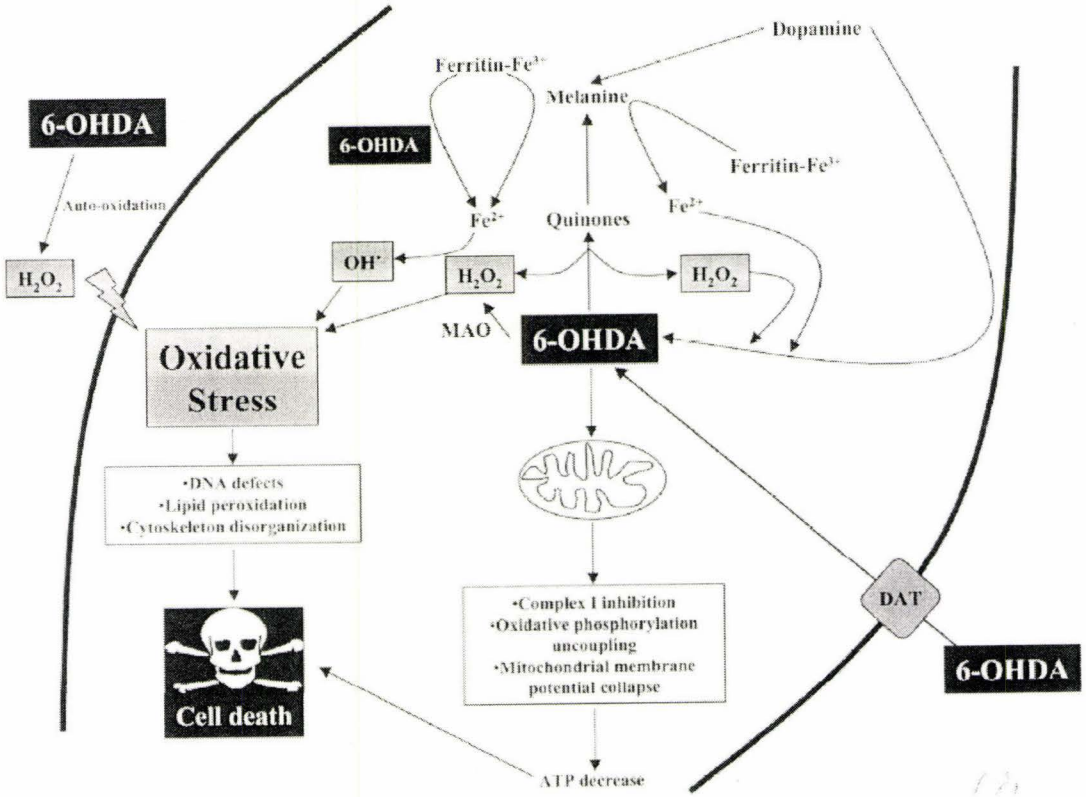
6-OHDA
Auto-oxidation
H_2O_2
Oxidative Stress
•DNA defects
•Lipid peroxidation
•Cytoskeleton disorganization
Cell death
6-OHDA
Ferritin-Fe^{3+}
Fe^{2+}
$OH^{\cdot}$
H_2O_2
MAO
Dopamine
Melanine
Ferritin-Fe^{3+}
Fe^{2+}
Quinones
H_2O_2
6-OHDA
•Complex I inhibition
•Oxidative phosphorylation uncoupling
•Mitochondrial membrane potential collapse
ATP decrease
DAT
6-OHDA

and Brannock, 1998; Perumal *et al.*, 1989; Soto-Otero *et al.*, 2000; Zbarsky *et al.*, 2005). There are also lines of evidence for the involvement of mitochondrial complex I (Glinka and Youdim, 1995), however, this result is controversial (Hirsch *et al.*, 2003). It is apparent that oxidative stress plays a major role in 6-OHDA neurotoxicity.

2.2.2 Motor Deficits

Motor deficits are prevalent in the 6-OHDA rat model with the most widely used experimental paradigm being rotational behaviour (Ungerstedt and Arbuthnott, 1970). Motor deficits are tested after infusion of the toxin into the median forebrain bundle (MFB) that connects the SNpc and the striatum. Less common is the infusion of the neurotoxin into the SNpc because it also results in denervation of the substantia nigra reticulate and the ventral tegmental area.

Rotational behaviour can be used to screen new experimental compounds that affect the DA system (Figure 2.2). Rotational behaviour can be caused by drugs that directly stimulate the DA receptor such as apomorphine or L-DOPA. This causes the rats to rotate contralaterally due to denervation supersensitivity. Ipsilateral rotations are caused by drugs, such as amphetamine, that act directly on the DA terminals causing DA to be released.

Rotational behaviour can parallel the side effects of the drugs used to treat PD. After chronic administration of L-DOPA, contralateral rotations are reduced over time

Figure 2.2. Rotational behaviour can be induced by challenge with amphetamine or apomorphine after injection of the neurotoxin 6-OHDA into the MFB. Amphetamine causes DA release and apomorphine directly stimulates the DA receptors. Because of receptor supersensitivity, there is greater stimulation of DA receptors on the lesioned side with apomorphine challenge. With amphetamine administration, there is greater DA release and resultant signaling on the intact side. The rats will rotate away from the greatest DA stimulation; therefore, apomorphine challenge causes contralateral rotations whereas amphetamine challenge causes ipsilateral rotations.

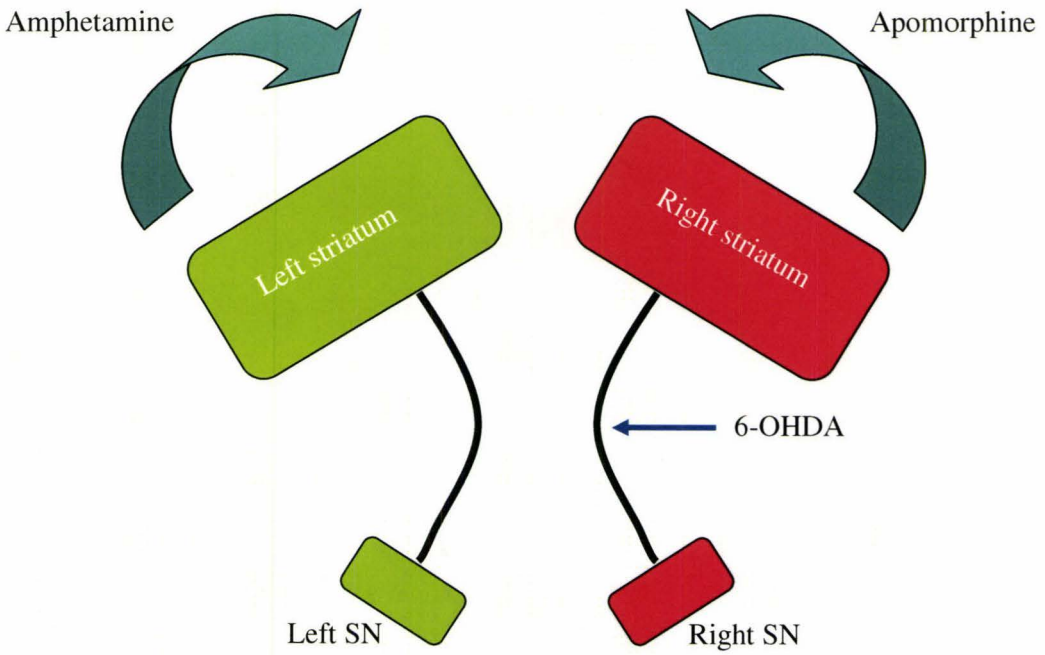
Amphetamine
Apomorphine
Left striatum
Right striatum
6-OHDA
Left SN
Right SN

which is thought to parallel the "wearing off" period seen after prolonged treatment in PD patients (Marin *et al.*, 2005). Despite the reduction in the duration intensity of the contralateral rotations, there is turning sensitization during chronic administration of L-DOPA which is thought to reflect the dyskinesia, a common side effect with chronic L-DOPA treatment (Henry *et al.*, 1998). Chronic treatment also results in abnormal involuntary movements in rats which are also thought to be indicative of dyskinetic movements (Lundblad *et al.*, 2002).

A drawback of using contralateral rotations as a behavioural indicator is the need for a near complete lesion in order to see a behavioural effect (> 90%) (Deumens *et al.*, 2002). The forepaw adjusting step test is also used to test for motor deficits. This test is a more direct measurement of the underlying motor deficits because it does not use a drug challenge to see the motor deficit, which is analogous to the limb akinesia seen in PD (Olsson *et al.*, 1995). This test requires an 80% striatal DA loss in order to see a deficit (Chang *et al.*, 1999). The forepaw use asymmetry test (cylinder test) also directly measures motor deficits that parallel limb akinesia in PD patients (Schallert and Woodlee, 2005). This test is sensitive and only requires a 50% loss of striatal DA neurons (Schallert and Woodlee, 2005). The postural instability test (PIT) mimics the postural instability that is characteristic of patients with PD (Woodlee *et al.*, 2008). Sensory-motor deficits can also be tested in the 6-OHDA rat model of PD. MFB lesions prevent the ability of vibrissae touching to induce forepaw placement on the side ipsilateral to the lesion (Schallert *et al.*, 2000; Woodlee *et al.*, 2005).

2.2.3 Relevance of the 6-OHDA model

This model of PD has the advantage of mimicking many of the key features of the disease, namely the loss of nigrostriatal DA neurons. Cellular studies have demonstrated the development of neuroplasticity in the basal ganglia mimicking the neuroplastic changes that occur in the basal ganglia of PD patients (Simola *et al.*, 2007). This model can be used to investigate the cellular mechanisms underlying the motor deficits and drug induced motor complications by applying the model to molecular, morphological, and electrophysiological studies (Simola *et al.*, 2007). Although this model has many benefits, it cannot replicate many of the neuropathological features of human PD and therefore cannot be used to study the molecular mechanisms of DA degeneration. Despite this, there is an overlap between 6-OHDA-induced DAergic cell death and the DAergic cell death that develops in PD. In the 6-OHDA model there is a preferential sensitivity to the SNpc, the most affected area in PD and this effect is influenced by iron (Youdim and Riederer, 2004), which is reflected in the role that iron is thought to play in PD (Kienzl *et al.*, 1999). There is a key role of oxidative stress in the 6-OHDA damage to DA neurons, and although it remains to be confirmed, it is postulated that oxidative stress plays a role in idiopathic PD as well. However the formation of LB, a hallmark feature of PD, is not present in 6-OHDA lesioned animals (Dauer and Przedborski, 2003). However, for investigating cell replacement therapies and neuroprotective strategies, this model allows the examination of motor deficits and DA cell loss.

2.3 Cell Replacement Therapy for Parkinson's Disease

Cell replacement therapy has gained a great amount of interest over the past decade. The purpose of cell replacement therapy is to alleviate the symptoms and restore neuronal circuitry and function by protecting the remaining neurons or replacing lost neurons. PD symptoms are not evident until there is at least a 50% reduction of the DAergic innervation in the striatum. Therefore, theoretically, there is only a need to restore 50% of the nigrostriatal system in order for a therapy to be effective. The potential sources for cells and tissues are discussed below.

2.3.1 Autografted Tissue

2.3.1.1 Carotid Body

The carotid body is a chemosensory organ found at the bifurcation of the carotid artery. It releases DA in response to hypoxia and these cells divide in a hypoxic environment, which may promote good graft survival after transplantation (McGregor *et al.*, 1984; Espejo *et al.*, 1998). When tested in animal models of PD, the carotid body contributed to partial functional recovery (Espejo *et al.*, 1998; Toledo-Aral *et al.*, 2003; Luquin *et al.*, 1999). However, when used in a clinical trial, concern was raised in regards to the potential to exacerbate the non-motor, autonomic features of PD (Arjona *et al.*, 2003).

2.3.1.2 Adrenal Medulla

The use of the adrenal medulla as a source of DAergic neurons has been explored in clinical trials. Results from trials indicated minimal clinical improvement with poor survival of the graft and a high risk of morbidity and mortality (Ahlskog *et al.*, 1990; Goetz *et al.*, 1991). Co-grafting with a peripheral nerve segment demonstrated improved graft survival and a better functional outcome in animal models (Date *et al.*, 1994; Howel *et al.*, 2000). However, in a clinical setting there was reduced efficacy over time (Date *et al.*, 1995; Date *et al.*, 1996; Lopez-Lozano *et al.*, 1996; Watts *et al.*, 1997; Lopez-Lozano *et al.*, 1999).

2.3.2 Primary Allografted Tissue

The use of primary neural tissue from the fetal ventral mesencephalon (VM) presented itself as a promising source of DA neurons for cell therapy in PD. Initial studies were undertaken in 1979 by Perlow and Bjorklund when they grafted fetal tissue from the VM into the 6-OHDA rat model (Bjorklund and Stenevi, 1979; Perlow *et al.*, 1979). Subsequent studies showed a reduction in motor asymmetries, but no improvement in contralateral sensory neglect (Bjorklund *et al.*, 1980; Dunnett *et al.*, 1981). It was hypothesized that the density of the tissue prevented full recovery, so DA-rich cell suspensions were used (Bjorklund *et al.*, 1980). In this study there was survival and functional recovery post-transplantation in the 6-OHDA rat model. Placing the DA-rich cell suspensions in different areas of the forebrain demonstrated recovery of most motor asymmetries (Dunnett *et al.*, 1983).

Following these experiments, the use of human fetal tissue for cell replacement in PD was investigated. Cell suspensions from human fetal tissue transplanted into immunosuppressed rats lead to the alleviation of motor asymmetries (Wictorin *et al.*, 1992). This study showed graft survival and a DAergic phenotype by tyrosine hydroxylase (TH) positive staining. These promising results led to numerous clinical trials (Lindvall *et al.*, 1990; Lindvall *et al.*, 1994; Freed *et al.*, 2001). The transplants showed long-term survival in the human brain and the formation of functional synaptic connections; however, there was variable efficacy and some patients showed graft-induced dyskinesias.

The heterogeneity of these clinical results may result from the heterogeneity of the cells transplanted into the patients. Although there were DA neurons transplanted into the patients, they were accompanied by a large number of cells lacking a DAergic phenotype. There is also the possibility of a non-uniform distribution of the transplanted cells within the striatum and the lack of proper afferent control due to the ectopic placement of the cells (Goldman, 2005; Ma *et al.*, 2002). A factor hindering the use of primary allografted tissue is the large number of fetuses required per patient and the ethical considerations surrounding this tissue source.

2.3.3 Stem Cells

NPCs can be obtained from both embryonic and adult tissue. In contrast to true stem cells, NPCs have a more restricted potential; however, they maintain the ability to

differentiate into the astrocytes, neurons, and oligodendrocytes. This gives NPCs the potential to be a relatively uniform starting population of cells and an accessible source of neurons following differentiation.

2.3.3.1 Fetal Neural Progenitor Cells

Fetal NPCs have been isolated from many species including human, non-human primates, porcine, and rodents. They can be cultured *in vitro* using mitogens such as basic fibroblast growth factor (FGF-2). These cells can then be influenced in culture to differentiate into TH positive neurons. NPCs have the potential to alleviate the motor deficits seen in PD. It was demonstrated that transplantation of fetal rat NPCs offset the motor asymmetries in the 6-OHDA rat model (Studer *et al.*, 1998). Findings from this study were confirmed by Sawamoto, who demonstrated that fetal mouse NPCs have the ability to reduce symptoms after transplantation into a rodent model of PD (Sawamoto *et al.*, 2001). Human mesencephalic precursors have also been shown to reduce the motor asymmetries in the 6-OHDA rat model (Sanchez-Pernaute *et al.*, 2001). These grafts consisted of TH positive cells indicating that some of the transplanted cells adopted a DAergic phenotype.

This source of the tissue for transplantation offers some benefit because it provides a more uniform source of cells. Using *in vitro* expansion, it is possible to enrich the number of DAergic cells, which would decrease the amount of fetal tissue required for transplantation. However, because this method still requires fetal tissue, it is still

faced by the same ethical dilemmas as primary allografted tissue. There is also a reluctance of primary NPCs to adopt a DAergic phenotype (Armstrong *et al.*, 2003).

2.3.3.2 Embryonic Stem Cells

Embryonic stem cells (ESCs) are unrestricted cells obtained from the blastocyst. These cells can be expanded *in vitro* and differentiated into NPCs (Conti *et al.*, 2005). They can also be differentiated into DAergic neurons by a variety of growth and transcription factors including FGF-8, sonic hedgehog, ascorbic acid, and stable Nurr1 expressing ESC lines (Lee *et al.*, 2000; Kim *et al.*, 2002). ESCs have demonstrated functional benefits without teratoma formation when transplanted into a rodent model (Kim *et al.*, 2002). However, other studies have shown that there is a need to differentiate these cells before they are transplanted as naïve cells caused teratoma formation in almost half of the transplanted animals (Bjorklund *et al.*, 2002).

2.4 Neural Stem Cells

It had been long thought that neurogenesis did not exist in the adult mammalian nervous system until the discovery of a population of cells that continue neurogenesis throughout adult life (Reynolds and Weiss, 1992). These cells were classified as NSCs and they have the ability to self-renew and differentiate into the three main cell types of the CNS: astrocytes, neurons, and oligodendrocytes (Lois and Alvarez-Buylla, 1993; Reynolds and Weiss, 1992). These cells were discovered in the embryonic remnant of the germinal zone (Weiss *et al.*, 1996). NSCs in this area produce cells that migrate

down the rostral migratory stream (RMS) to the olfactory bulb (OB) where they replace dead/dying granular neurons (Lois and Alvarez-Buylla, 1994).

2.4.1 Neural stem cells *in vitro*: the neurosphere assay

Once isolated from the adult brain, NSCs can be cultured as heterogeneous cell aggregates called neurospheres. The first neurosphere assay was developed by Reynolds and Weiss in 1992. These cells are cultured in media containing B27, putrescine, progesterone, heparin, insulin, and the mitogens epidermal growth factor (EGF) and/or FGF-2 (Tropepe *et al.*, 1999). Initial use of this assay grew cells in EGF (Reynolds and Weiss, 1992) with subsequent studies using FGF-2 (Gritti *et al.*, 1999; Tropepe *et al.*, 1999). The addition of EGF and FGF-2 is not required for the survival of the cells, but it is important as studies have shown that withdrawal of these mitogens restricts cell fate to a glial lineage (Erickson *et al.*, 2008).

This assay is useful for examining the self-renewal and multipotency of NSCs (Figure 2.3). However, the neurosphere assay is highly variable with slight changes in cell density having the ability to alter the microenvironment and change the proliferative capacity (Tropepe *et al.*, 1999) as well as causing changes in positional cues (Hack *et al.*, 2004). The heterogeneity of the composition of the neurosphere is proposed to be due to the number of passages the cells undergo, the methodology of performing the cell passages, and the concentration of the media factors (Jensen and Parmar, 2006). Another study indicated that the heterogeneity of the sphere is reflective of the differences in the

Figure 2.3. Schematic of the neurosphere assay. Neurospheres are heterogenous clusters of cells containing true NSCs, NPCs, and cells undergoing early differentiation. NSCs and NPCs are able to self-renew and differentiate into astrocytes, oligodendrocytes, and neurons.

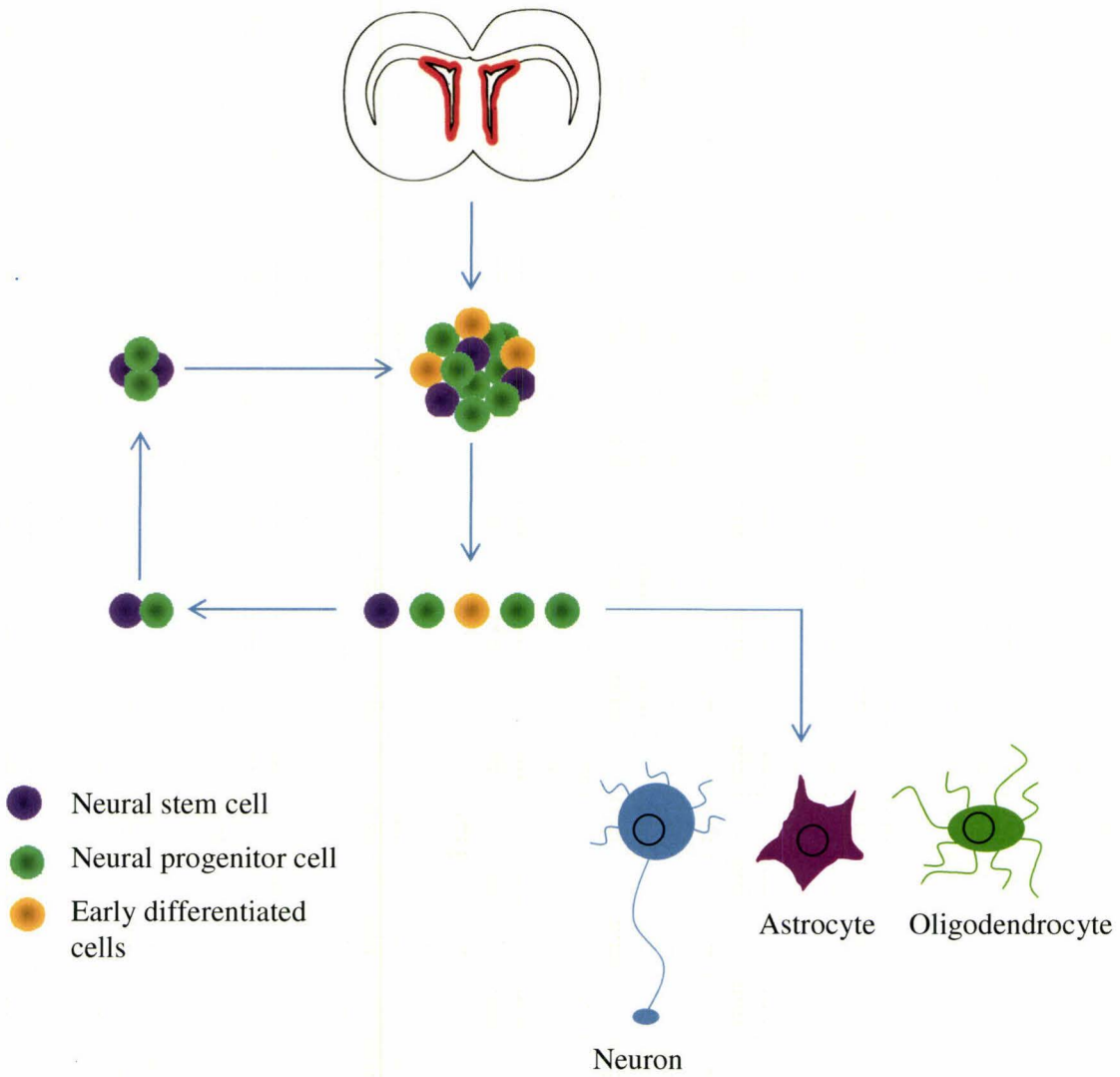
Neural stem cell
Neural progenitor cell
Early differentiated cells
Neuron
Astrocyte
Oligodendrocyte

developmental potential of the parent clone-forming cells. The isolated population of cells is heterogeneous and includes cells with distinct molecular phenotypes; therefore, there may be variable developmental commitment in the parent clone (Suslov *et al.*, 2002). The neurogeneic capacity of the cells within the neurosphere decreases with increasing time *in vitro* (Fricker *et al.*, 1999).

Despite the drawbacks of the neurosphere assay, it has many positive attributes. This culture system allows the cells to maintain their ability to differentiate into a neuronal subtype characteristic of their region of origin; therefore, they reflect the normal cell fate of the progenitors from their region in situ (Hitoshi *et al.*, 2002; Ostenfeld *et al.*, 2002; Klein *et al.*, 2005). Consequently, cells isolated from the VM produce a greater number of DA neurons compared to cells isolated from other parts of the CNS (Ostenfeld *et al.*, 2002; Schwarz *et al.*, 2006).

2.4.1 Neural stem cell niche

There has been debate over the precise location of the NSC niche. Niches are primarily found in the germinal zone of the developing brain that is adjacent to what eventually develops into the cells lining the ventricles (Morshead and van der Kooy, 2001). There are two layers that surround the lateral ventricles in the adult: the ependymal layer and the subependymal layer. Conflicting evidence was published on which layer NSCs are restricted too. One group found the ependymal layer to be the location of the NSC niche (Johansson *et al.*, 1999). Using lipophilic dyes to mark the

ependymal layer, microdissection of the layer was done. Cells marked with the lipophilic dye formed spheres and differentiated into multiple lineages (Johansson *et al.*, 1999). Conflicting results were published stating that NSCs reside in the subependymal layer of the mature germinal zone (Chiasson *et al.*, 1999). It is possible that that the DiI used in the Johansson study marked the subependymal layer cells as well as cells from the ependymal layer. Upon repetition of experiments done by Johansson *et al.* (1999), they reported that the ependymal cells were unable to self-renew indicating that it was likely that there was contamination of the subependymal cells in the ependymal cell population used in the study (Morshead and van der Kooy, 2001). It has also been demonstrated that NSCs may reside outside of this niche as they have been shown to be present in the optic nerve (Palmer *et al.*, 1999), the spinal cord (Weiss *et al.*, 1996), and in other brain regions (Palmer *et al.*, 1995). One of these brain regions is the dentate gyrus of the hippocampus (Cameron *et al.*, 1993). The cells from this region can be supported *in vitro* using the growth factor FGF-2 (Palmer *et al.*, 1995). However, the ability for self-renewal of these cells has been brought into question and some studies have indicated that these cells may be multipotent progenitor cells and not true stem cells (Seaberg and van der Kooy, 2002; Bull and Bartlett, 2005).

2.4.2 Astrocytes as NSCs

The subventricular zone (SVZ) that surrounds the lateral ventricles develops into the subependymal layer. It has been proposed that the NSCs found in the subependymal layer may be a type of astrocyte as cells with the characteristics of NSCs were positively

stained for the glial fibrillary astrocytic protein (GFAP) (Doetsch *et al.*, 1999a). The SVZ has a population of relatively quiescent NSCs (type B cells) that give rise to a population of actively proliferating cells that function as intermediate progenitor cells (type C cells) (Doetsch *et al.*, 1999b). Type C cells then give rise to immature neuroblasts (type A cells) that migrate down the RMS to the OB (Lois and Alvarez-Buylla, 1994). Type B cells have the same properties as NSC; if the type C cells in the SVZ are selectively killed, they are replenished from the type B cells and these cells eventually differentiate into neurons (Doetsch *et al.*, 1999b). Type B cells also have the ultrastructural characteristics and markers of astroglial cells (Kriegstein and Alvarez-Buylla, 2009), express GFAP, the astrocyte-specific glutamate-aspartate transporter (Doetsch *et al.*, 1997), and they are frequently called SVZ astroctyes (Kriegstein and Alvarez-Buylla 2009). Selectively ablating GFAP-positive cells prior to culturing prevents the formation of neurospheres further supporting the idea of NSCs being a subpopulation of cells with astrocyte feature (Morshead *et al.*, 2003).

Although there have been questions raised about the presence of true NSCs in the dentate gyrus of the hippocampus, the cells present in this area also show properties of astrocytes. The radial astrocytes in the subgranular zone function as primary precursors for new neurons in the dentate gyrus of the hippocampus (Seri *et al.*, 2001; Morshead *et al.*, 2003; Garcia *et al.*, 2004). In other parts of the brain, GFAP positive cells give rise to proliferative neural precursors (Ganat *et al.*, 2006). Taken together, numerous reports

support the idea that adult NSCs form a population of GFAP-expressing cells that are indicative of an astrocyte.

2.4.4 Transplantation

NSCs have the ability to self-renew, are multipotent, and are found in the adult CNS. When these cells are expanded *in vitro* and characterized, they represent excellent candidates for therapeutic purposes. Initial transplantation studies directed towards PD treatment used human fetal ventral mesencephalic tissues as a donor source, but carried ethical and logisitical problems. In addition, the survival of the fetal tissue in the brain is low (Hagell *et al.*, 1999). The use of NSPCs is a practical and effective alternative to fetal tissue for transplantation purposes. A number of different studies have utilized xenograft or allograft NSPC transplants in different animal models of neurological disease. Functional improvement has been shown in PD (Kim *et al.*, 2002; Redmond, Jr. *et al.*, 2007), Huntington's disease (McBride *et al.*, 2004), amyotrophic lateral sclerosis (Thonhoff *et al.*, 2009), multiple sclerosis (Copray *et al.*, 2006), stroke (Takagi *et al.*, 2005), and Alzheimer's disease (Wu *et al.*, 2008).

NSPCs can be isolated from multiple areas in the adult brain, be expanded *in vitro* to produce large numbers of cells for transplantation, and have the differentiation potential to replace lost cells in the CNS. *In vitro*, NSPCs have been shown to produce functional neurons capable of forming synaptic connections, releasing neurotransmitters in response to synaptic stimuli, and generating an action potential (Song *et al.*, 2002).

Neurons differentiated from NSPCs *in vitro* have similar electrophysiological properties to neurons *in vivo* (Westerlund *et al.*, 2003). When transplanted into healthy animals and animals disease models, NSPCs have been shown to produce astrocytes, oligodendrocytes, and neurons (Yang *et al.*, 2002; Fricker *et al.*, 1999; Lepore *et al.*, 2006; Shihabuddin *et al.*, 2000; Tabar *et al.*, 2005). Transplanted cells have been shown to migrate towards the site of injury (Lepore *et al.*, 2006; Fricker *et al.*, 1999), integrate into the host tissue (Lepore *et al.*, 2006; Eriksson *et al.*, 2003), and form functional synapses (Benninger *et al.*, 2003). Lepore *et al.* (2006) demonstrated long-term survival of transplanted cells up to 15 months. Taken together, these cells are an attractive option for cell therapy in CNS disease.

NSPC therapy has been used for cell replacement strategies in conjunction with gene therapy and delivery procedures. Transfecting cells with glial derived neurotrophic factor (GDNF) enhance cell survival and increases neuronal differentiation and integration into the host tissue (Yasuhara *et al.*, 2006; Muraoka *et al.*, 2008). In addition, NPCs can be genetically engineered to express genes to correct genetic neurological disorders (Lacorazza *et al.*, 1996; Flax *et al.*, 1998). In these studies, cells were engineered to express the α-subunit of the β-hexosaminidase gene (the gene defect in Tay-Sachs disease) and both studies found that cells could produce and secrete the appropriate transcript and protein (Flax *et al.*, 1998; Lacorazza *et al.*, 1996).

2.4.5 Regulation after transplantation

2.4.5.1 NSCs characteristics may reflect tissue of origin

The characteristics of the NSPCs influence their fate *in vivo* after transplantation. It has been suggested that cells isolated from different areas of the CNS produce cell types from their region of origin (Suslov *et al.*, 2002). *In vitro*, sphere forming cells have been isolated from the striatum (Reynolds and Weiss, 1992), the spinal cord (Weiss *et al.*, 1996), the cerebellum (Klein *et al.*, 2005), and the SVZ (Morshead and van der Kooy, 2001). Although cells isolated from these sites have the ability to form neurospheres in culture, this does not imply they are true stem cells (Chojnacki and Weiss, 2008). It has been demonstrated that cells isolated from the SVZ maintain properties of the SVZ; when transplanted they had the ability to migrate to the OB and differentiate into neurons (Herrera *et al.*, 1999). However, cells transplanted outside of the OB did not produce neurons and differentiated into astrocytes. Likewise, Klein *et al.* (2005) showed that cerebellar derived cells transplanted into the same region failed to produce neurons and only differentiated into glia. This is indicative of cells' inherent genetic programming to produce a certain cell type regardless of the environmental cues.

In addition to the tissue the origin of cells, the "stemness" of the cells can affect the differentiation after transplantation. Uncommitted cells tended to differentiate into glia, whereas cells that were further restricted had a greater neuronal potential *in vivo* (Lepore *et al.*, 2006). Neuronal and glial restricted progenitors, had better viability and migrated extensively in comparison to less differentiated cells (Lepore *et al.*, 2004). This

suggests that the migratory capacity of cells is influenced by the stage of cell differentiation (Lepore *et al.*, 2004). Glial restricted progenitors migrate long distances in comparison to neuronal restricted progenitors which stay close to the graft site (Lepore *et al.*, 2004; Svendsen *et al.*, 1997; Fricker *et al.*, 1999). The age of the animal used for the dissection of NPCs affects the differentiation potential and graft survival *in vivo* (Hahn *et al.*, 2009). In addition, the age of the animal from which the NPCs are isolated also influences the graft volume and graft-derived TH-positive fiber reinnervation (Hahn *et al.*, 2009). Similar results were reported in another study, although the ideal age for the isolation of the cells was different (Sinclair *et al.*, 1999). It has also been shown that adult SVZ NSPCs from aged mice (22-26 months) show reduced expression of genes for NSPC markers and important developmentally regulated transcription factors (Ahlenius *et al.*, 2009); however it has been shown that adult NPCs have the same differentiation and therapeutic potential as embryonic NPCs (Muraoka *et al.*, 2008).

2.4.5.2 Environmental effect on transplanted cells

Although cells may contain intrinsic cues responsible for the selection of a specific cell fate, interaction with the host can also influence the transplanted cells. In particular, the age of the host can influence the outcome of the transplant. Human NPCs from the VM showed tyrosine hydroxylase immunoreactivity (THir) and functional benefits when transplanted into 8 week old rats (Hovakimyan *et al.*, 2008); however, when the same cells were transplanted into juvenile rats, THir was present but there was no resultant functional benefit (Hovakimyan *et al.*, 2008). This may be due to differences

in the host environment, specifically the release of trophic factors from host glial cells (Hovakimyan *et al.*, 2008).

The location of the transplanted cells also greatly influences the survival, migration, integration, and differentiation of the cells. Intrastriatal grafts showed greater and more extensive behavioural recovery compared with grafts in the nucleus accumbens (Falkenstein *et al.*, 2009). Intrastriatal grafts had the ability to alleviate more complex motor behaviours, whereas grafts placed in the nucleus accumbens alleviated the rotational asymmetry, but did not affect the complex motor deficits (Falkenstein *et al.*, 2009). Lateral ganglion eminence progenitor cells transplanted into the striatum, hippocampus, cortex, and olfactory bulb showed a difference in their differentiation capacity (Eriksson *et al.*, 2003). When transplanted into the striatum and hippocampus the transplanted cells underwent gliogenesis in contrast to the cortex and the OB where neuronal differentiation occurred (Eriksson *et al.*, 2003). This study also demonstrated differences in the survival of the grafted cells. There was greater survival in the striatum in comparison to the cortex and the hippocampus.

Transplanted cells have been shown to acquire a cell fate according to the surrounding tissue. Fricker *et al.* (1999) demonstrated that transplanted human NPCs responded to *in vivo* cues in both neurogenic and non-neurogenic regions. Cells that were grafted into the RMS expressed markers of DAergic and GABAergic cells that are normally present in this region (Fricker *et al.*, 1999). Similarly, cells grafted into the

dentate gyrus migrated along endogenous pathways and expressed markers of granule cells (Fricker *et al.*, 1999). This is in contrast to other studies showing that NSPCs maintain properties of their tissue of origin (Suslov *et al.*, 2002). This discrepancy has been suggested to be due to differences in the culture conditions that may influence how the cells respond *in vivo* (Fricker *et al.*, 1999).

2.4.5.3 Effect of a lesion on cell transplants

It has been proposed that injury to the brain can induce proliferation of endogenous NSCs and initiate molecular cues for transplanted NSPCs. NSPCs migrated towards the area of the injury in models of hemorrhage and ischemia (Takagi *et al.*, 2005). In models of multiple sclerosis, NSPCs migrated towards the de-myelinated areas (Yandava *et al.*, 1999) and in models of PD, these cells have been shown to migrate towards the lesioned striatum and/or substantia nigra (Bjugstad *et al.*, 2008). *In vitro* work has demonstrated an increase in THir in cells exposed to media from the VM or the striatum (Anwar *et al.*, 2008). This study showed that the damaged striatum caused TH-induction when compared to the healthy striatum (Anwar *et al.*, 2008). The ability of the lesioned striatum to cause TH-induction of transplanted cells has also been demonstrated *in vivo* (Bjorklund *et al.*, 2002; Yang *et al.*, 2002). Cell survival is also enhanced in the lesioned striatum in comparison to the intact striatum (Nikkhah *et al.*, 2009). Taken together, these results demonstrate that there are cellular and molecular cues present in damaged areas of the brain that promote migration, cell survival, and differentiation.

The damaged brain has been shown to affect endogenous NSCs. In models of ischemia, reports showed increased proliferation of the NPCs residing in the anterior horn of the lateral ventricles and suggested an enhanced neurogenic response to cerebral ischemia (Tonchev *et al.*, 2005). In a model of PD there was increased proliferation in response to lesioning the striatum with 6-OHDA (Aponso *et al.*, 2008). In this study it was found that a large number of the newborn cells in the striatum expressed the astrocytic marker GFAP and did not express neuronal markers indicating that the majority of new cells become glial cells (Aponso *et al.*, 2008). The authors did not see doublecortin immunoreactivity (a marker for cell migration) of the cells indicating that there was a lack of progenitor cell migration from the SVZ to the damaged striatum and that the new cells originate in the striatum. The new cells did not undergo neurogenesis which may be due to the lack of stimulatory cues and the restrictive environment of the lesioned striatum (Aponso *et al.*, 2008).

2.4.5.4 Effect of cell number on the transplant

The characteristics of the initial transplant may affect cell survival and therefore the therapeutic potential. Studies have shown that the number of grafted cells is important because it affects the functional benefit of the transplants, cell survival, and the ability of the cells to adopt a DAergic phenotype. By varying the number of transplanted cells from 25,000 to 200,000 cells it was shown that animals receiving a greater number of cells had significant improvements in their functional recovery in comparison to animals receiving a smaller graft (Terpstra *et al.*, 2007). In addition, larger grafts

contained more THir neurons and had enhanced survival rate of the transplanted cells (Terpstra *et al.*, 2007). This was supported by a recent study demonstrating a decrease in graft volume, cell survival, and THir in transplants when injecting a low number of cells (Nikkhah *et al.*, 2009). Larger graft volumes may stimulate the release of trophic factors and establish a better cell-cell environment to increase survival and the ability to adopt a DAergic cell fate.

2.4.6 NSPCs transplants in PD

In summary, transplants of NSPCs into different CNS disease models have been reported over the past few decades. Once transplanted, these cells are able to differentiate and survive in multiple brain regions (Gage *et al.*, 1995; Suhonen *et al.*, 1996). In rodent models of PD, NSPCs have been shown to improve motor function, which is proposed to be due to potential protective effects in addition to DA neuron replacement (Yang *et al.*, 2002; Wei *et al.*, 2007). NSPCs have been induced to produce DA neurons *in vitro* prior to transplantation and have been shown to alleviate motor deficits in rodent models of PD (O'Keeffe *et al.*, 2008).

2.5 Molecular Imaging

Molecular imaging can be broadly defined as investigating cellular and molecular events involved in normal and pathological conditions by non-invasive techniques *in vivo*. Current techniques include magnetic resonance imaging (MRI), SPECT, and positron emission tomography (PET), ultrasound, and optical imaging. The sensitivity of

PET and SPECT are both several orders of magnitude higher than MRI with the sensitivity of PET typically being higher than that of SPECT (Meikle et.al., 2005). PET and SPECT rely on radioactive decay in order to obtain an image within an animal. PET and SPECT generate tomographic images where a virtual slice of the animal is obtained to generate quantitative or semiquantitative data. Tomographic images are also capable of displaying internal anatomical structures and functional information.

2.5.1 Single photon emission computed tomography

SPECT imaging uses single photon gamma-emitting isotopes which produce an image as a result of the isotope's decay. Gamma cameras rotate around the subject gathering planar images at different angles, which are then used to reconstruct a three-dimensional image (Peremans *et al.*, 2005). The gamma camera detects gamma rays by the interaction of the photon released with NaI crystals within the camera (Peremans *et al.*, 2005). The interaction produces a scintillation, or light flash, which is detected by photomultiplier tubes (PMT). The location of the scintillation can be computed from the response in each PMT to each scintillation event (Peremans *et al.*, 2005). Because there is only one photon emitted from the nucleus of the decaying tracer, there is a need to pre-define the direction of the photon to follow the distribution and concentration of the tracer. The direction of flight of the photon is determined by geometric collimation, which restricts the gamma ray to a pre-defined direction (Massoud and Gambhir, 2003).

A parallel-hole lead collimator consists of lead with multiple elongated holes that allow photons traveling parallel to the holes to interact with the NaI crystals (Peremans *et al.*, 2005). With parallel-hole collimation, a spatial resolution of 2-3 mm can be obtained. To increase spatial resolution pinhole SPECT was designed, which can achieve a resolution of 1 mm. Pinhole collimators deliver high spatial resolution by magnifying the image of the object projected onto the NaI crystals, which is ideal for small animal imaging (Meikle *et al.*, 2005). Because the image is magnified using pinhole SPECT, the image changes with distance; therefore, a somewhat distorted image can be obtained because the distance of the source planes vary in a three dimensional object (Peremans *et al.*, 2005). Distortion can also occur from changes in the center of rotation due to the rotation of the heavy pinhole collimators (Peremans *et al.* 2005). This can be compensated for by performing a center of rotation correction to account for the displacement of the midplane of the pinhole collimator or by rotating the subject instead of the collimators.

2.5.2 Positron emission tomography

PET imaging uses radioisotopes that emit positrons as they decay, which annihilate a nearby electron. The annihilation results in the formation of two gamma rays which are emitted simulatenously in opposite directions with equal energy. Similar to SPECT, the detectors emit a pulse of light after interaction with a gamma ray. The signal is amplified by a PMT in response to each scintillation event. A coincidence, or

simultaneous detection, of the gamma rays from the detectors allows the determination of a line of response and the location of the origin of the signal (Turkington, 2001).

2.5.3 Imaging the dopamine system with SPECT and PET

Both PET and SPECT allow for the evaluation of biological processes in a non-invasive manner. Using this technology, quantitative, longitudinal studies can be completed in a single animal. Therefore, this technology has the potential to increase the accuracy of the study and decrease the cost and time associated with laboratory animal work.

Over the last decade, CNS molecular probes for PET and SPECT imaging have been developed for diagnostic purposes. In particular, those used to assess presynaptic DA integrity are 6-[^{18}F]Fluoro-L-dopa ([^{18}F]DOPA), [^{18}F]FMT for PET imaging and [^{123}I]altropane, and [^{99m}Tc]TRODAT for SPECT imaging (Figure 2.4).

2.5.3.1 Imaging the dopamine system with PET

2.5.3.1.1 [^{18}F]DOPA

[^{18}F]DOPA has long been used as the gold standard for imaging the DA system. [^{18}F]DOPA mimics many of the characteristics of L-DOPA and it is metabolized in a similar way resulting in the formation of metabolites by aromatic amino acid decarboxylase (AAAD) and catechol *O*-methyltransferase (COMT) which are neutral and can cross the blood brain barrier (Doudet *et al.*, 1999). This leads to complications in

Figure 2.4. DAT ligands mark the pre-synapse of DA neurons. Because of this, they have the potential to show the integrity of the DA system. Examples of SPECT DAT ligands are shown.

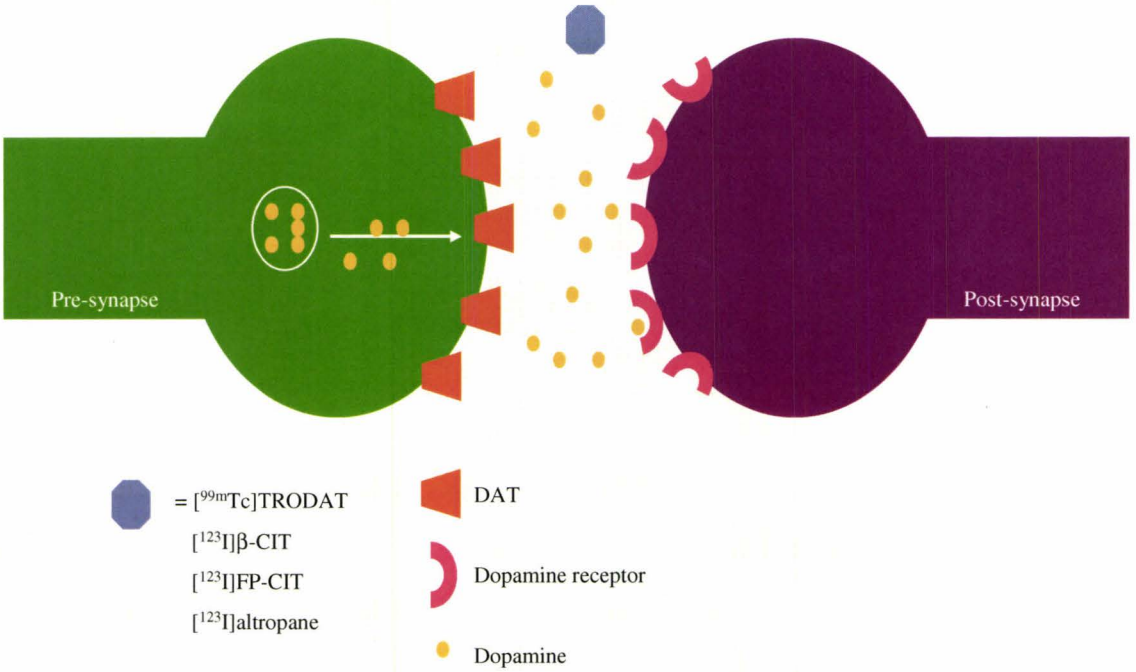
Pre-synapse
Post-synapse
= [99mTc]TRODAT
[123I]β-CIT
[123I]FP-CIT
[123I]altropane
DAT
Dopamine receptor
Dopamine

data interpretation despite the use of AAAD and COMT inhibitors.

2.5.3.1.2 [^{18}F]FMT

[^{18}F]FMT has also been used to evaluate presynaptic DA integrity (DeJesus *et al.*, 1997; Honer *et al.*, 2006). [^{18}F]FMT, like [^{18}F]DOPA, is a substrate for AAAD, but not for COMT (Doudet *et al.*, 1999). The main metabolite of [^{18}F]FMT, 6-fluoro-hydroxyphenylacetic acid, is polar and therefore does not cross the blood brain barrier. It is slowly cleared essentially "trapping" ^{18}F radioactivity in the striatum (DeJesus *et al.*, 1997). This gives a simpler metabolic profile, better counting statistics, and a lower nonspecific background (Doudet *et al.*, 1999). Using carbidopa, an AAAD inhibitor, the metabolism of [^{18}F]FMT is reduced resulting in an increased signal-to-noise ratio between the striatum and cerebellum (Barrio *et al.*, 1996). [^{18}F]FMT has been used to image the normal and diseased striatum in humans (Nahmias *et al.*, 1995) and in MPTP treated primates (Jordan *et al.*, 1997).

2.5.3.2 Imaging the dopamine system with SPECT

SPECT imaging is more cost effective and widely available than PET imaging; therefore, there has been an effort to develop DA imaging agents for SPECT. These imaging agents target the DAT to image the integrity of presynaptic DA. The DAT is embedded in the pre-synaptic compartment and consistently corresponds to the presence of DA neurons (Huang *et al.*, 2003). Imaging of the DAT may reflect the severity of

striatal DA loss in PD. This has been shown where the DAT imaging was correlated with behavioural analysis and ex vivo histology in rodent models of PD (Tatsch, 2001; Andringa *et al.*, 2005). Two DAT imaging compounds for SPECT are [^{99m}Tc]TRODAT and [^{123}I]altropane.

2.5.3.2.1 [^{99m}Tc]TRODAT

[^{99m}Tc]TRODAT is a desirable imaging agent because of the incorporation of ^{99m}Tc. ^{99m}Tc is widely available, has a convenient 6 hour physical half life, is cost effective, and has a greater photon flux per unit dose of radiation when applied to a patient in comparison with other radionuclides (Kung *et al.*, 1997). The biodistribution of [^{99m}Tc]TRODAT has been studied in rats (Kung *et al.*, 1997; Hwang *et al.*, 2002) and imaging in mice has been preformed (Acton *et al.*, 2002). TRODAT is available in a kit formulation allowing for ease of labeling with ^{99m}Tc. This is advantageous and makes [^{99m}Tc]TRODAT an ideal option for imaging the DA system in small animals.

2.5.3.2.2 [^{123}I]altropane

[^{123}I]altropane is a DAT binding imaging agent that was developed for imaging the pre-synapse of DA neurons (Elmaleh *et al.*, 1996). [^{123}I]altropane gives good striatum-to-cerebellum, striatum-to-cortex, and striatum-to-thalamus binding ratios (10.8, 7.2, and 8.3 respectively) (Elmaleh *et al.*, 1996). In addition to having good signal-to-background ratios, it is highly selective for the DAT in comparison to the 5-HT transporter (Fischman *et al.*, 1997). This imaging agent has been used for diagnosing PD

(Fernandez *et al.*, 2001) and attention deficit hyperactivity disorder (Spencer *et al.*, 2007). [^{123}I]altropane binds with high affinity to the DAT and allows for visualization of the DA system (Hettiarachchi *et al.*, 2001). [^{123}I]altropane has been used to image the striatum of nonhuman primates (Madras *et al.*, 1998c; Madras *et al.*, 1998b), healthy volunteers, and patients with PD (Madras *et al.*, 1998a; Fischman *et al.*, 1998). [^{123}I]altropane may provide useful information for the evaluation of certain therapies in small animal models of PD.

Chapter 3: Materials and Methods

3.1 Maintenance of animal colonies

All animal experiments were carried out in accordance with the guidelines specified by the Canadian Council on Animal Care and were approved by the Animal Research Ethics Board of McMaster University.

3.2 HPLC

Analytical HPLC for DA detection was performed using a Varian Pro Star model 330 PDA detector, a model 230 solvent delivery system, a Pursuit C18 5μm 2.4mm metaguard column (Varian) a C18 Varian column (4.6 mm x 250 mm), and a Carroll Ramsey Associater model 105S pindiode radiometric detector with a Star 800 module interface analog to digital convertor using Star chromatography workstation software v.6.41. The mobile phase consisted of Solvent A = H_2O containing 20 mM Triethylamine (adjusted to pH 3 with TFA) and Solvent B = acetonitrile containing 20 mM Triethylamine (pH 3). The elution protocol consisted of a gradient running from 90% solution A and 10 % solution B to 10% solution A and 90% solution B over 20 minutes. The flow rate was 1.0 mL min^{-1}, and all runs were monitored at λ=254 nm.

Semipreparative HPLC was performed using a Varian Pro Star model 330 PDA detector, a model 230 solvent delivery system, and a C-18 3μm Luna sermipreparitive column (Phenomenex; 150 x 10 mm) and a Carroll Ramsey Associater model 105S pindiode radiometric detector with Star 800 module interface analog to a digitized

convertor using Star chromatography workstation software v.6.41. The solvents used were: Solvent A = H_2O containing 0.05% TFA and Solvent B = acetonitrile containing 0.05% TFA. These solvents were run using the elution gradient described above. The flow rate was 4.0 ml min^{-1} and runs were monitored at λ=254 nm.

3.3 Solid-phase peptide synthesis

Solid-phase peptide synthesis was carried out as previously described (Schaffer *et al.*, 2008). Briefly, peptides were prepared following conventional Fmoc automated peptide synthesis protocols using 1-H-Benzotriazolium,1-[bis(dimethylamino)methylene]-hexafluorophosphate(1-),3-oxide as a coupling agent and a glycine-loaded WANG resin as the support. The peptides were isolated using a standard cleavage cocktail and were purified by semipreparative HPLC. The peptide was lyophilized yielding NAcGRKKRRQRRR(SAACQ)G (SAACQ) and $[NAcGRKKRRQRRR(Re(CO)_3\text{-}SAACQ)G]^+$ (Re-SAACQ).

3.4 Preparation of $[^{99m}Tc(CO)_3(OH_2)_3]^+$

A 20 ml Biotage microwave vial containing $K_2[BH_3{\cdot}CO_2]$ (8.5 mg, 6.3×10^{-5} mol), $Na_2B_4O_7{\cdot}10H_2O$ (2.9 mg, 7.6×10^{-6} mol), Na/K-tartrate (15.0 mg, 5.3×10^{-5} mol) and Na_2CO_3 (4.0 mg, 3.8×10^{-5} mol) was sealed with a rubber septum and flushed with $N_{2(g)}$ for 10 min. ^{99m}Tc-generator eluate (100-130 mCi) in 5.0 ml 0.9% saline was added using a syringe and the solution was microwaved (Biotage) at 130°C for 3 min. After

cooling, the pH of the solution was adjusted to approximately 7 by the addition of 1M HCl.

3.5 Peptide labeling with ^{99m}Tc.

4.0 mg (2.1×10^{-6} mol) of AcGRKKRRQRRR(SAACQ)G (SAACQHIVTat$_{48-57}$) in 100 µl of distilled deionized water was added to the $[^{99m}Tc(CO)_3(OH_2)_3]^+$ solution using a syringe. The reaction was microwaved (Biotage) at 120°C for 5 min. The solvent was removed using a V10 (Biotage) and crude product was redissolved in 0.5 ml of distilled H_2O using the V10 (Biotage). The crude reaction was purified using semipreparative HPLC (see above). Radiochemical purity was determined using analytical γ-HPLC (see above). The radiochemical purity was greater than 98% (Figure 3.1).

3.6 Preparation of neurospheres

Neurospheres were prepared as previously described (Schaffer *et al.*, 2008). Briefly, neural stem/progenitor cells were harvested from one to three day old B6.129.FMR1/FvBn mouse pups. They were cultured as neurospheres and used for subsequent experiments between the first and fifth passage.

3.7 Labeling of dissociated neurospheres with $[^{99m}Tc(CO)_3$SAACQHIVTat$_{48-57}]^+$

Neurospheres were transferred from the 24-well plate to a 15 ml Falcon tube and centrifuged at 180 rcf for 5 min. The resulting pellet was incubated with 2 ml of TrypLE

Figure 3.1. (A) UV trace of the Re-SAACQ peptide and (B) the corresponding γ-trace of the ^{99m}Tc-SAACQ peptide after purification.

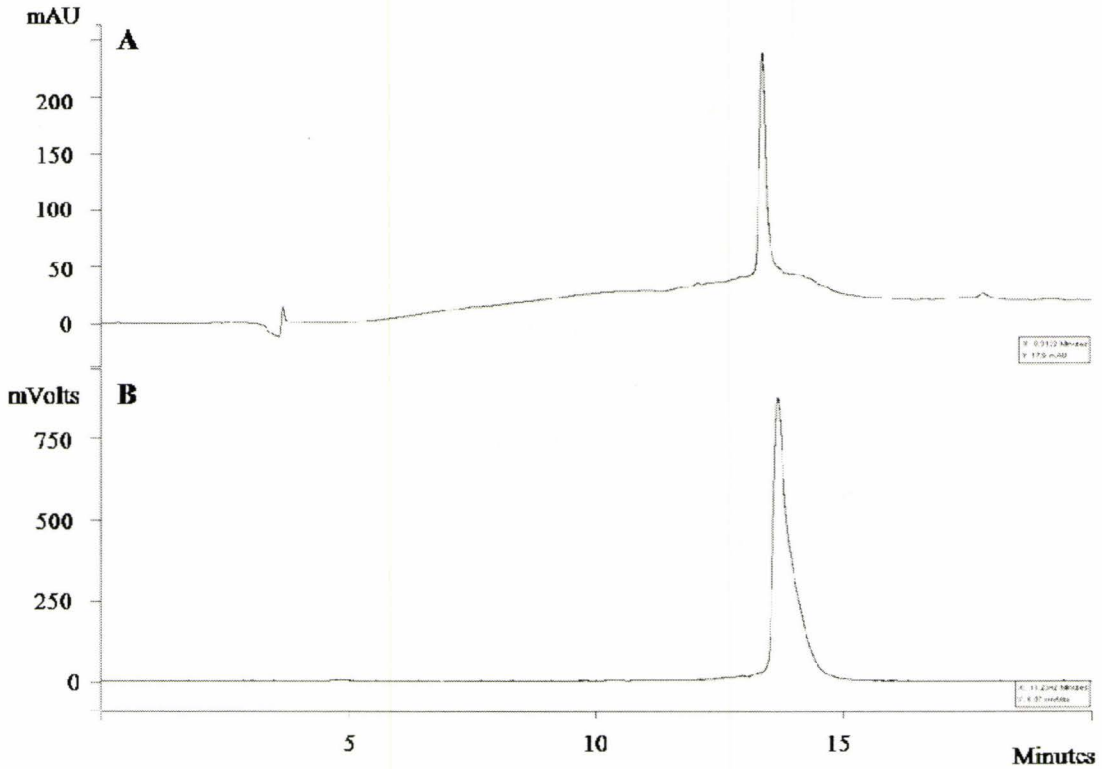
mAU
A
200
150
100
50
0
mVolts
B
750
500
250
0
5
10
15
Minutes

Express (Invitrogen) for 30 min at 37°C in a water bath. The mixture was centrifuged at 180 rcf for 5 min and the pellet was resuspended in 250 µl of serum free media. The pellet was titurated with a fire-polished, small-borehole pipette. The cell counts were determined using trypan blue exclusion dye. Cells were plated in 100 x 20 mm tissue culture dishes at a concentration of 10,000 cells/ml. The cells were incubated with 0.006 MBq/cell of ^{99m}Tc-SAACQ in 0.01 M phosphate buffered saline (PBS) at 37°C for 20 min in a 95% O_2, 5% CO_2 incubator. Initially, various amounts of ^{99m}Tc-SAACQ were incubated with the NSPCs for various amounts of time. We did not find an increase in uptake after 20 minutes. We chose 0.006 MBq/cell with the intent of minimizing the risk of radiolytic damage while maximizing the uptake of activity into the cells. The labeled cells were transferred to siliconized glass capped centrifuge tubes and centrifuged at 180 rcf for 10 min. The supernatant was removed and the cells resuspended in 2 ml of serum free media. The cells were then centrifuged at 180 rcf for 10 min. The supernatant was removed and the cells finally resuspended in the appropriate amount of media or 0.9% sterile saline for the subsequent experiments. Labeling efficiency was determined using a dose calibrator that had been calibrated using a NIST traceable standard over a range of activities. Control cells were prepared in an identical manner. For some experiments a portion of the labeled cells was co-incubated with cell tracker orange (Molecular Probes) in order to label the cells for identification by fluorescence microscopy.

3.8 Washout studies

Efflux of the tracer from cells was determined at 30, 50, 70, and 100 minutes post-labeling in serum free media at room temperature. At the given time points the cells were centrifuged at 180 rcf for 10 minutes. The amount of activity in the media and the amount of activity in the cell pellet was determined. The activity in the cell pellet was decay-corrected and expressed as a percentage of the initial cell uptake activity.

3.9 Viability of labeled neural stem/progenitor cells

Cells were labeled with ^{99m}Tc-SAACQ as described above. Control cells were labeled with an equal volume of 0.01 M PBS. Cells were prepared for labeling with the rhenium version of the peptide, Re-SAACQ or the unlabeled peptide SAACQHIVTat$_{48-57}$ (SAACQ) in an identical manner to the preparation of ^{99m}Tc-SAACQ-labeled cells. The cells were labeled with the same amount (27.3 pmol) of either Re-SAACQ or SAACQ and control cells for these groups were incubated with an identical volume of 0.01M PBS. Viability was determined using trypan blue at 2 and 24 hours after labeling using 20 000 cells.

3.10 Single cell gel electrophoresis assay

A modified literature protocol was used to perform the Comet assay as previously described (Schaffer *et al.*, 2008). Briefly, the cell culture was diluted 1:1 with 1% low-melting point agarose. 120 µL of the suspension was cast into a two well chamber attached to GelBond film. The gels were incubated in a lysis buffer and then in a DNA

unwinding buffer. Electrophoresis of the gels was performed and they were subsequently dehydrated and air dried. The gels were stained by SYBR Gold nucleic acid stain and examined by fluorescence microscopy. Cells were classified as normal, damaged, or apoptotic based on the fragmentation pattern of the DNA observed in the comet tail. 20 000 cells were used for this assay.

3.11 Proliferation of labeled neural stem/progenitor cells

100 000 cells were labeled with ^{99m}Tc-SAACQ as described above. Control cells were labeled with an equal volume of 0.01 M PBS. Cells were labeled with Re-SAACQ or SAACQ as described above. Proliferation was monitored using a BrdU Cell Proliferation Assay (Chemicon International) according to the manufacturer's instructions. Briefly, cells were incubated for 24 hours with a BrdU reagent and BrdU incorporation was detected using an ELISA.

3.12 Differentiation of labeled neural stem/progenitor cells

100 000 cells were labeled with SAACQ, Re-SAACQ or ^{99m}Tc-SAACQ as described above. After labeling with the above probes, the cells were plated onto coverslips coated with poly-L-lysine (Sigma) and laminin (Invitrogen) in a 1:1 ratio of serum-free media to serum-free media without EGF, FGF-2, and heparin containing 1% fetal bovine serum (Biowest). The cells were differentiated for 10 days at 37°C in 95% O_2, 5% CO_2.

3.13 Immunocytochemistry and histology

The media from the differentiated cells was removed and the cells were washed in 0.01 M PBS. The cells were fixed for 10 min at -20°C with ice cold acetone and then washed three times for 5 minutes with 0.01 M PBS. The cells were treated with the following primary antibodies at 4°C overnight: monoclonal anti-βIII-tubulin (Promega; 1:1000) and polyclonal anti-cow GFAP (DAKO; 1:100). Following the primary incubation, the cells were washed three times for 5 minutes with 0.01 M PBS and then incubated with the following secondary antibodies for 3 hours at room temperature: goat anti-rabbit FITC (Cedarline; 1:100) and goat anti-mouse AlexaFluor 594 (Invitrogen; 1:1500). The cells were finally washed three times for 5 minutes with 0.01 M PBS and then for 5 minutes with dH_2O. Coverslips were removed, allowed to air dry, and then mounted using Vectashield with DAPI (Vector Laboratories Inc.).

Cryosections of the rat brains were washed three times for 5 minutes with 1XTris buffered saline (TBS) pH 7.4. The sections were incubated with 0.8% sodium borohydride (Sigma) for 10 minutes at room temperature and then washed once for 5 minutes with 0.01 M PBS. Sections were incubated in 0.01 M sodium citrate buffer (pH 6) for 30 minutes at 90°C and then cooled to room temperature. Sections were washed three times for 5 minutes in 1XTBS pH 7.4 and then incubated for one hour in 20% normal goat serum or normal donkey serum in 1XTBST pH 7.4. Sections were incubated in the following primary antibodies overnight at 4°C: monoclonal anti-tyrosine hydroxylase (Calbiochem; 1:500) or chicken anti-MAP2 (Neuromics; 1:1500) with 5%

normal goat serum or normal donkey serum. Sections were washed three times for 5 minutes with 1XTBST pH 7.4 before incubation for one hour with the following secondary antibodies made in 5% normal goat serum or normal donkey serum: goat anti-mouse FITC (Cedarline; 1:200) or donkey anti-chicken AlexaFluor 594 (Invitrogen; 1:1500). Sections were finally treated three times for 5 minutes with 1XTBST pH 7.4 and then once for 5 minutes with dH_2O and air dried. Sections were mounted with Vectashield with DAPI (Vector Laboratories Inc.).

3.14 6-OHDA lesions

Two-month old Spraque Dawley rats (approximately 250g) were anesthetized by the gaseous anesthetic Isoflurane (2.5-3.0%). Temgesic™ in sterile saline was injected subcutaneously as an analgesic. 30 minutes prior to lesioning, rats were given desipramine (15mg/kg i.p.). Rats were placed in a Kopf stereotaxic apparatus in preparation for surgery. A second analgesic, xylocaine, was applied topically on the surface of the scalp prior to the incision. The brain was infused with 6-OHDA (8µg in 4µL in 0.1% ascorbic acid) at a rate of 1µL/min in the right MFB (AP, ML, DV; 2µL at -4.4, -1.2, -7.8 nose-bar –2.5; 3µL -4.0, -1.0, -8.0 nose-bar +3.5 from Bregma and the dura) using a 10-µL Hamilton syringe. The syringe was left in place for 10 minutes and then slowly removed. Doses of 6-OHDA were calculated as a weight of the base.

3.15 Neural stem/progenitor cell transplants

3 weeks after the 6-OHDA lesion, the rats were randomly placed into a control (n=10) or transplant (n=17) group. NSPCs were labeled as previously described. After the final wash the labeled NSPCs were re-suspended in 2mL of serum free media. Washout of the tracer from the cells was performed for 30 minutes at room temperature. The cells were then centrifuged at 180 rcf and the media was removed. The labeled cells were re-suspended in 8μL of 0.9% saline and a dose calibrator was used to determine the activity.

Briefly, an incision was made along the top of the skull and the overlying muscle was scraped away from the skull surface. At the coordinates given below (from Bregma and the dura) a Dremal drill was used to make a small hole through the skull. The cells were transplanted using a 10-μL Hamilton syringe lowered into the right striatum of 6-OHDA lesioned rats (AP, ML, DV; 3 μL –1.0, -3.0, -4.0 nose-bar 0). The syringe was left in place for 10 minutes and then slowly removed. The incision was closed with 4-0 silk sutures and the rat was allowed to recover from the anesthetic.

3.16 Immunosuppression

Rats were immunosuppressed using cyclosporin A (Sigma or Alexis Biochemicals) to minimize immune rejection of the transplant. 10 mg/kg in 0.9% saline was administered subcutaneously everyday starting one day prior to transplantation for the duration of the experiment.

3.17 SPECT imaging of cell transplants

The rats were anesthetized using isoflurane (2.5-3.0%). SPECT images were acquired using a Gamma Medica-Ideas X-SPECT system (Northridge, California, US) and a high resolution parallel-hole collimator followed by a CT. The dual head SPECT/CT system has a SPECT FOV of 10 cm x 10 cm with a spatial resolution of 2-3 mm. The gamma cameras were fitted with low energy high resolution parallel-hole collimators. One rotation was acquired over 64 projections at 100 seconds/projection. Mice were imaged using the same system as described above with the gamma cameras fitted with low energy high resolution pinhole collimators. With the pinhole collimators the system has as SPECT FOV of 4.1 cm x 4.1 cm with a spatial resolution of 1 mm.

SPECT images were reconstructed using OSEM iterative reconstruction with detector response compensation. A total of two iterations with eight subsets were used and reconstructed images were filtered with a 3D Gaussian filter with FWHM of 2 mm. Analysis was done by drawing a 3D region of interest (ROI) around the cell transplant using Amide Medical Image Data Examiner 0.9.1 or Amira. The mean counts/acquisition time were obtained and compared to a calibration curve.

The CT component of the X-SPECT system, which has a flat panel detector FOV of 10 cm x 10 cm, was used for anatomical co-registration. CT information was acquired using 75-kVp X-rays, and a tube current of 265 μA with a spot size of 50 μm. 512 projections were acquired over 360° and reconstructed with a modified FeldKamp cone-

beam reconstruction (Cobra-Exxim version 6.0). The resulting image had a matrix of 512 x 512 x 512 and a reconstructed voxel size of 155μm.

3.18 Phosphorimaging on dissected rat brains

Immediately after imaging, the rat was sacrificed and the brain removed. The brain was flash-frozen in liquid N_2 and 20 micron sections were cut in the cryostat. The sections were exposed to phosphorimaging film for 15 minutes and developed using a Storm 840 Phosphor Imager and ImageQuant TL (GE Healthcare).

3.19 Imaging of the dopamine system with [^{123}I]altropane

An average of 33.9 MBq of [^{123}I]altropane (Alceres Pharmaceuticals Inc.) was injected intravenously via the tail vein in anesthetized rats (isoflurane 2.5-3.0 %). All images were acquired using a Gamma Medica-Ideas X-SPECT. The gamma cameras were fitted with low energy high resolution parallel-hole collimators. Dynamic SPECT imaging was started immediately after injection of the [^{123}I]altropane. Dynamic images were taken over 8 rotations, 64 projections per rotation with 2 seconds per projection. A high resolution CT was acquired immediately following the SPECT for anatomical co-registration as described above. Image reconstruction was carried out using the same algorithm as described above. A summed image was obtained by adding all dynamic projections and reconstructed using the same method.

Imaging analysis was done over the course of 12 weeks. A timeline for the SPECT imaging, behavioural testing, 6-OHDA lesions, and transplants is shown in Figure 3.2).

3.20 Analyzing [^{123}I]altropane SPECT images

Analysis of the images was performed by two methods: Logan analysis with reference regions and using a simple ratio of the mean counts from the left striatum to the right striatum using Amide Medical Image Data Examiner 0.9.1. For the latter, 2D regions of interest on transaxial slices through the striatum were obtained. Within each region, the most intense 25% of the counts were obtained for the right and left striatum. The cerebellum was used as a background tissue. The counts from the background tissue were subtracted from the striatal counts on the left and right side. The ratio of the background corrected right side to left side counts was calculated and used as the "altropane ratio". This was done on the summed image. Logan analysis relies on a reference region devoid of signal to act as an input function and is described in Appendix 1. This method of analysis did not give binding ratios reflective of the image and was not used for the study.

3.21 Neurochemistry

The striatum and substantia nigra were isolated from the rat brains and stored frozen at -80°C. Samples were thawed, weighed, and homogenized in 1.5 mls (striatum) or 700 µls (substantia nigra) of 0.12 M perchloric acid and 9 pM dihydroxybenzylamine

Figure 3.2. Timeline for 6-OHDA lesions, NSPC transplants, [^{123}I]altropane SPECT imaging and behvaioural testing. All three behavioural tests were run at each of the time points given.

3 weeks	**Animals handled daily until the testing starts**
7 weeks	**Pre-lesion behavioural test and [^{123}I]altropane SPECT**
8 weeks	**6-OHDA lesion**
10 weeks	**Post-lesion behavioural test [^{123}I]altropane SPECT**
11 weeks	**Transplant**
12 weeks	**1 week behavioural test [^{123}I]altropane SPECT**
13 weeks	**2 week behavioural test [^{123}I]altropane SPECT**
14 weeks	**3 week behavioural test [^{123}I]altropane SPECT**
15 weeks	**4 week behavioural test [^{123}I]altropane SPECT**
17 weeks	**6 week behavioural test [^{123}I]altropane SPECT**
18 weeks	**7 week behavioural test [^{123}I]altropane SPECT**
19 weeks	**8 week behavioural test [^{123}I]altropane SPECT**
19 weeks	**Animals sacrificed for histology**

(DHBA) used as an internal standard. Homogenates were centrifuged at 10,800 rpm for 5 min and the supernatants were removed and filtered through a 22 μm centrifugal filter (Millipore). The filtered supernatant (10 μls) was injected into an ESA Coulochem II high performance liquid chromatography system with electrochemical detection to determine the dopamine content in the samples. Samples were run through a Zorbax reverse phase C18 column (4.6 mm x 15 cm) and the analytes were quantified with a graphite coulometric detector cell with a positive potential of 300 mV. Mobile phase consisted of 10% MeOH, 0.09 M sodium acetate, 130 μM ethylenediamine tetraacetic acid (EDTA), 0.035 M citric acid and 460 μM sodium heptane sulfonate with the pH adjusted to 4.25. The flow rate was set to 1.0 ml/min.

3.22 Behavioural Testing

3.22.1 Postural Instability Test

Rats were held almost vertically in a wheelbarrow-like position with one forelimb held off the ground against the torso. The free forelimb was placed on a small piece of emery board alongside a ruler. The position of the nose on the ruler was noted. The animal was moved forward over the planted forelimb until making a "catch-up" step (Figure 3.3). The new nose position was noted and the difference between the two positions indicated the displacement of the body needed to trigger a "catch-up" step in the unrestrained forelimb. Three trials were performed for each forelimb on a given day of testing and the average of the three trials was used.

Figure 3.3. (A) The starting and ending positions are shown for the contralateral limb. (B) The starting and ending positions are shown for the ipsilateral limb.

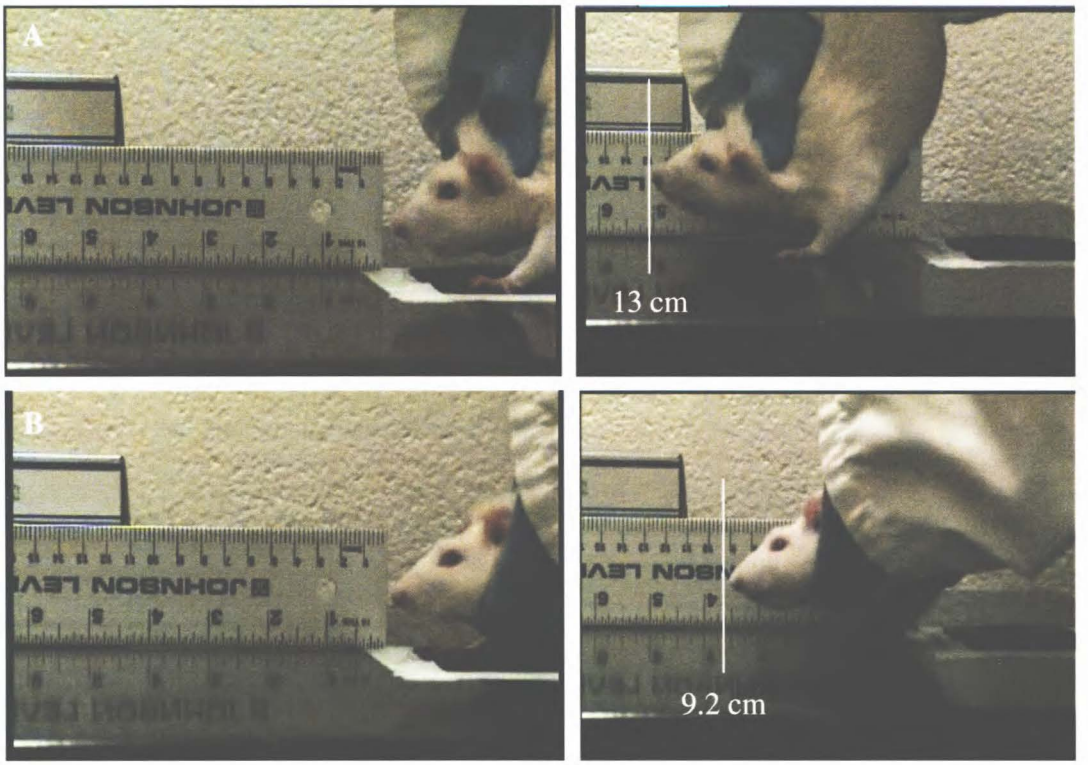
A
13 cm
B
9.2 cm

3.22.2 Cylinder Test

The rats were placed in a clear, plexiglass cylinder (diameter = 20.3 cm, height = 30.5 cm or diameter = 29.2 cm, height = 29.2 cm) on a clear, plexiglass platform over a mirror angled at 45°. Rats in the cylinder engage in exploratory behaviour and rear up on their hindlimbs placing their forepaws on the wall of the cylinder. The forepaw used to contact the wall of the cylinder is recorded along with any lateral movements of the rat along the cylinder. When both forepaws contact the wall of the cylinder it is recorded as "both". The asymmetry score is calculated by adding the number of ipsilateral observations plus ½ of "both" divided by the total number of observations multiplied by 100. The rats were tested for 10-minute intervals with several minutes between tests on each day of testing until 20 observations were made.

3.22.3 Rotational Behaviour

Rats received an injection of d-amphetamine sulfate salt (5mg/kg i.p.) and placed into a rotometer and videotaped for 90 minutes post injection. The number of ipsilateral and contralateral rotations performed by the rat was determined over the 90 minute period.

3.23 Statistical analysis

Data is presented as the mean ± SEM. Statistical analysis was performed using a one-way ANOVA, two-way ANOVA, or a t-test. Post hoc analysis was performed using a Tukey test or a Bonferroni test. Correlation was calculated by Pearson Product moment

correlation (correlation coefficient = R). The strength of a linear model for the altropane ratio and behavioural tests was determined by linear regression analysis. Statistical significance was determined by $p > 0.05$.

Chapter 4: *In vitro* labeling of neural stem/progenitor cells with $[^{99m}Tc(CO)_3SAACQHIVTat_{47-58}]^+$

4.1 Background

Stem cell therapy is considered to be a promising treatment option for a number of neurological disorders. Transplantation of neural stem cells in the damaged brain offers therapeutic promise for PD, Alzheimer's disease, Huntington's disease, traumatic brain injury, and spinal cord injury (Redmond, Jr. *et al.*, 2007; Wu *et al.*, 2008; McBride *et al.*, 2004; Zhao *et al.*, 2002; Klein and Svendsen, 2005). At this time, cell transplantation therapy is highly variable, due in part to difficulties achieving reproducible cell grafts. The development of imaging techniques to visualize cell transplants in a reliable manner is necessary to standardize grafting technique and gain greater experimental control in pre-clinical and clinical studies.

Tat-based peptides are useful tools to incorporate radiolabels, fluorescent protein, proteins, or MRI contrast agents into cells (Polyakov *et al.*, 2000; Lewin *et al.*, 2000; Bhorade *et al.*, 2000; Gammon *et al.*, 2003; Saalik *et al.*, 2004). Tat peptides were originally derived from the HIV-1 tat protein involved in the replication of the HIV-1 virus (Frankel and Pabo, 1988). Entry of the tat peptide into the cell is proposed to be a two step process. The first step involves binding to the cell surface via ionic interactions of the positively-charged peptide to the negatively charged proteoglycans followed by induction of macropinocytosis (Kaplan *et al.*, 2005). When coupled to technetium-99m (^{99m}Tc), cells can be labeled with a relatively inexpensive and widely available

radionuclide. ^{99m}Tc has a half-life of approximately six hours and decays with an emission of 140-keV gamma-rays. These are optimal physical characteristics for gamma-camera imaging and therefore produce good resolution images (Chianelli *et al.*, 1997).

Two different methods can be used for labeling tat peptides with radioisotopes: direct and indirect labeling. Direct labeling involves conjugation of the radionuclide to the tat peptide without the use of a spacer or linking group (Lewin *et al.*, 2000; Polyakov *et al.*, 2000). Indirect labeling uses a spacer or linking group to indirectly attach a radionuclide to the tat peptide (Stephenson *et al.*, 2004a). The single amino acid chelate (SAAC) is a spacer that mimics a naturally occurring amino acid and can be incorporated into a peptide at any position (Stephenson *et al.*, 2004b). The SAACQHIVTat allows rhenium (Re) or ^{99m}Tc to be conjugated forming inert complexes that are structurally identically (Stephenson *et al.*, 2004a; Stephenson *et al.*, 2004b) (Figure 4.1).

Re-SAACQ fluoresces and the subcellular distribution can be determined by using epi-fluorescence microscopy (Stephenson *et al.*, 2004a). Because Re-SAACQ and ^{99m}Tc-SAACQ are isostructural, the subcellular distribution of the two forms of the tat peptide will be the same. Using direct labeling, the fluorophore is often exchanged for the radionuclide. Therefore, the peptides have slightly different structures and subcellular distribution cannot be determined.

Figure 4.1. (A) The Fmoc-protected single amino acid chelate (bisQuinoline) (SAACQ). (B) The corresponding iso-structural $[Re(CO)_3SAACQ]^+$ derivative. (C) The AcGRKKRRQRRR-SAACQ-G target peptide and (D) the [AcGRKKRRQRRR-$Re(CO)_3$SAACQ-G][Br] or [AcGRKKRRQRRR-$^{99m}Tc(CO)_3$SAACQ-G]$^+$ target peptide.

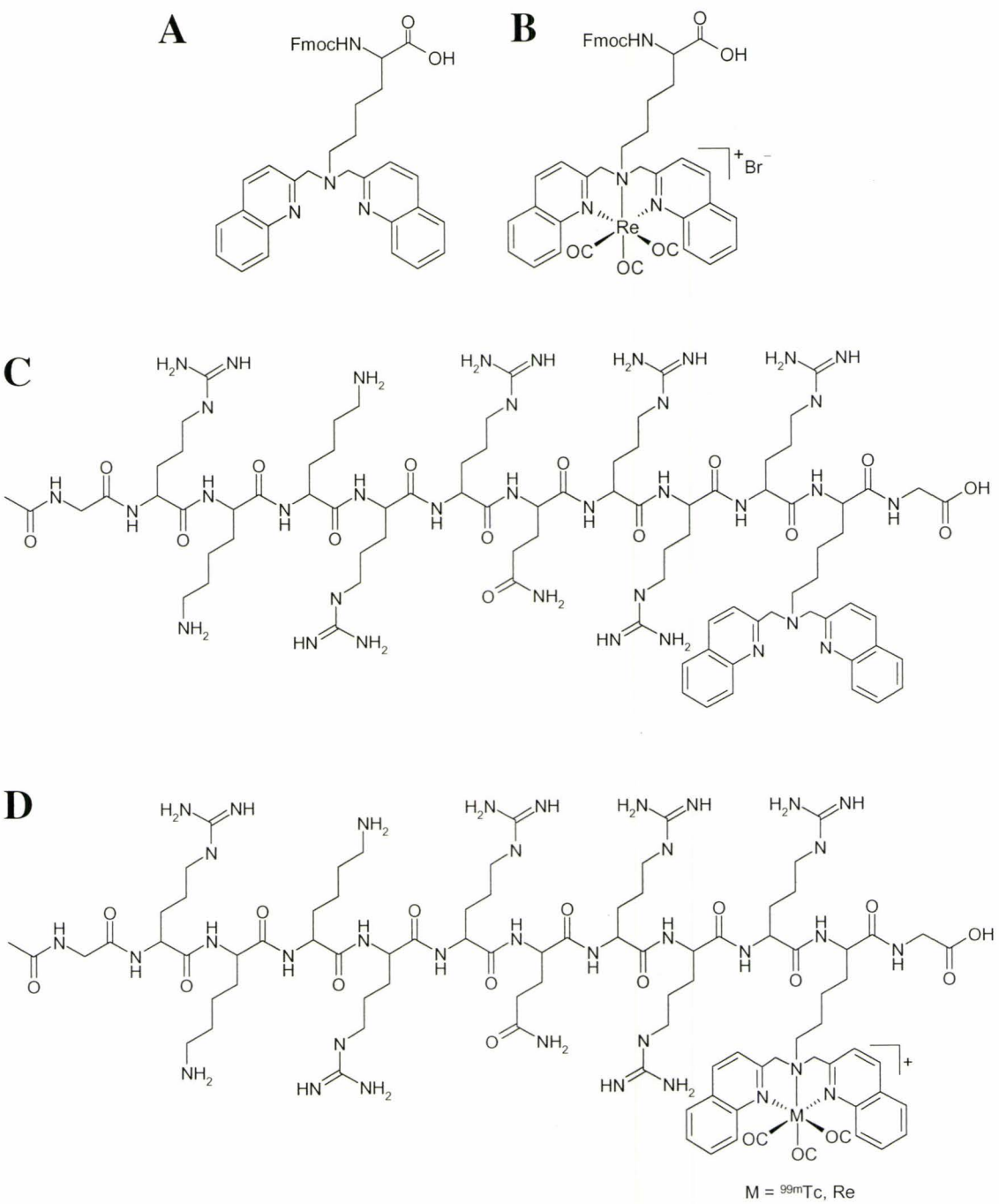
A
FmocHN
OH
B
FmocHN
OH
Br
Re
OC
C
D
M = 99mTc, Re

The first component of this thesis utilized [SAACQHIVTat$_{48-57}$] (SAACQ), Re-SAACQ, and ^{99m}Tc-SAACQ as labeling probes. This chapter also reports the results of the single-cell gel electrophoresis assay performed by Dr. Jennifer Lemon from Dr. Douglas Boreham's group at McMaster University.

4.2 Objective

The purpose of these experiments was to determine the distribution of the ^{99m}Tc-SAACQ peptide in NSPCs, define the parameters for NSPC labeling with ^{99m}Tc-SAACQ, and determine the effect of the probe on the biological parameters of NSPC viability, DNA integrity, proliferation and differentiation.

4.3 Results

4.3.1 Labeling NSPCs with Re-SAACQ and ^{99m}Tc-SAACQ

To radiolabel the permeation peptide (HIVTat$_{48-57}$) the SAAC was incorporated as a naturally occurring amino acid into the backbone of the peptide during synthesis. SAAC forms a well-defined product that is stable after labeling thereby preventing the premature loss of the isotope (Banerjee *et al.*, 2002; Stephenson *et al.*, 2004b). Because SAAC behaves as a naturally occurring amino acid, it can be incorporated into peptides in large quantities using an automated peptide synthesizer. Another advantage of this system is that the Re-SAAC peptides can be produced in a similar manner to SAAC peptides providing a non-radioactive isostructural standard that can be used as a reference standard when producing the ^{99m}Tc-SAAC peptides. For the purposes of these

experiments the SAACQ (SAAC-quinoline) was used because its Re-complex is luminescent. This is a unique feature of this system and allows for the uptake and distribution of the peptide in cells to be assessed prior to labeling with the ^{99m}Tc-SAACQ peptide.

Using Re-SAACQ, we determined the distribution of the tracer in NSPCs *in vitro* using epi-fluorescent microscopy. NSPCs were incubated with various concentrations of the tracer for varying amounts of time and fluorescent images were acquired (Figure 4.2). The tracer localizes to the nucleus with a large portion associating with the nuclear envelope and a smaller portion dispersed in the cytoplasm and in the nucleus. This is similar to what has been reported for a FITC-labeled HIV-Tat probe (Bhorade *et al.*, 2000). We did not observe unlabeled NSPCs in any of our cell preparations labeled with Re-SAACQ. This demonstrates that the addition of Re-SAACQ to the tat peptide backbone is not detrimental to the tracer uptake.

Once cell labeling was accomplished using Re-SAACQ, quantitative cell labeling was undertaken using ^{99m}Tc-SAACQ. NSPCs were incubated with varying amounts of ^{99m}Tc-SAACQ for 20 minutes. Following the incubation, cells were washed to remove any label that was not taken up into the cells and the amount of activity in the cell pellet was determined (Figure 4.3). The activity per cell was calculated assuming that the number of cells determined prior to labeling remained constant, which gives an

Figure 4.2. Re-SAACQ-labeled (A) neurosphere and (B) dissociated NSPCs. A high magnification of (B) is shown in (C). The Re-SAACQ localizes mainly to the nuclear envelope with some tracer present in the nucleus and cytosol.

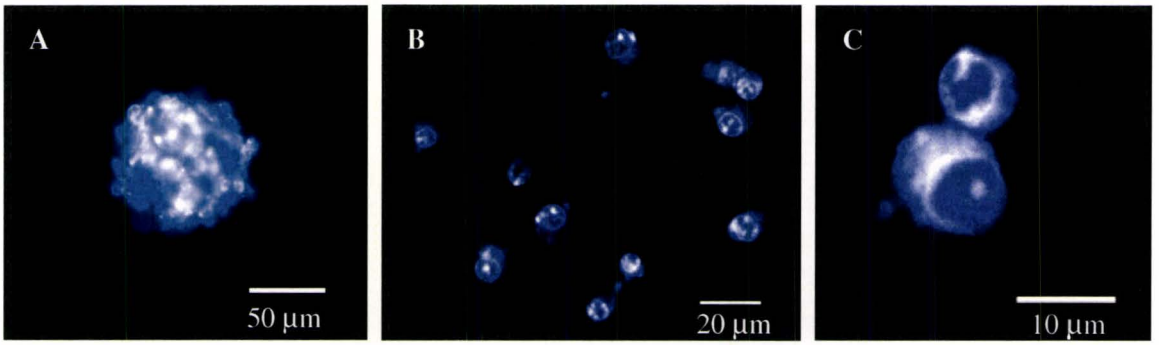
A
50 µm
B
20 µm
C
10 µm

Figure 4.3. The uptake of activity into cells versus varying initial incubation activities per cell. The cell uptake activity correlates significantly with the initial incubation activity per cell ($r = 0.76$, slope = 0.0186, intercept = -27.072, $p > 0.05$).

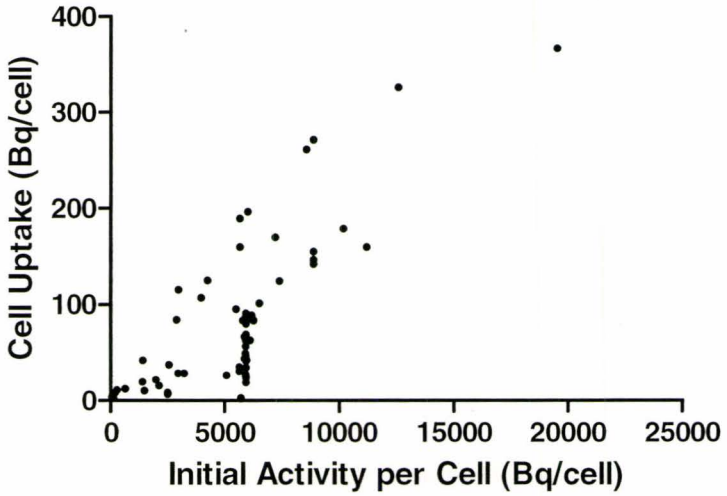
Cell Uptake (Bq/cell)
400
300
200
100
0
0
5000
10000
15000
20000
25000
Initial Activity per Cell (Bq/cell)

underestimation of cell uptake. Subsequent studies used approximately 0.006 MBq/cell for the initial incubation. Cell uptake activity ranged from 2 to 367 Bq/cell with an average uptake being 10-20 Bq/cell. The amount of activity obtained per cell is higher than reported in the literature where labeling resulted in 0.025 Bq/cell (de Vries et. el., 2005).

4.3.2 Efflux of ^{99m}Tc-SAACQ from NSPCs

Washout studies were also performed to determine the efflux of the label from the cells following the labeling procedure and the subsequent washes. Efflux of the label from the cells occurred for the first 20 minutes, which is consistent with the literature (Polyakov *et al.*, 2000). After 30 minutes, 59 ± 5% of the activity remained (n=4) (Table 4.1). A washout time of 30 minutes was used for the remainder of the studies. Upon repetition at the 30 minute time point, an average efflux of 28% was found and the cells retained 72% of the uptake activity (n=8). The difference observed from the initial washout study may be due to changes in the methodology for the cell labeling. The new method resulted in less cells being lost during the labeling and washout steps and therefore a greater amount of activity appeared to be retained due to an increase in cell number. The amount of ^{99m}Tc-SAACQ retained in the cells after efflux was sufficient for imaging and this amount is greater than the values reported in previous studies (Polyakov *et al.*, 2000).

Table 1. The average efflux of activity from the cells at various time points.

Efflux Time (min)	Average Activity after Efflux (Percent)
30	58.987
50	50.697
70	60.450
100	56.591

4.3.3 Viability of labeled NSPCs

An appropriate imaging probe will not affect the normal function of the cells after the labeling procedure. The viability of NSPCs was examined using a colorimetric dye-exclusion assay. NSPCs were incubated with approximately 0.006 MBq/cell for 20 minutes at 37°C. Viability of the labeled cells, determined at 2 and 24 hours post-labeling, was compared to NSPCs labeled with Re-SAACQ or SAACQ. There was no significant difference between ^{99m}Tc-SAACQ-, Re-SAACQ-, or SAACQ-labeled cells at 2 hours (99.0 ± 3.3%, 99.8 ± 1.3%, and 97.9 ± 3.3% respectively) or at 24 hours (95.7 ± 26.7%, 89.6 ± 2.9%, and 89.1 ± 14.5% respectively) (Figure 4.4). All groups were normalized to control cells that were incubated with an equal volume of 0.01M PBS. Normalization was done to account for differences in cell population heterogeneity within the culture and for the length of time the cells were in culture.

4.3.4 DNA damage of labeled NSPCs

Although there was no change in the viability of labeled cells, the colorimetric assay only provides information about the viability of the cells with respect to membrane integrity. To assess the integrity of the DNA, a single-cell gel electrophoresis assay was used to determine if the DNA was damaged during the incubation process or if damage resulted from the intracellular deposition, specifically, the nuclear localization of the tracer. This assay assesses single- and double-stranded DNA damage as well as apoptosis. The cells analyzed were incubated with similar amounts of tracer as per the colorimetric assays and they were assessed at 24 hours post-labeling. Control cells were

Figure 4.4. Viability of NSPCs labeled with SAACQ, Re-SAACQ, or ^{99m}Tc-SAACQ. There is no significant difference between the treatment groups. The viability is normalized to control cells (ANOVA, $n = 3$, $0 > 0.05$).

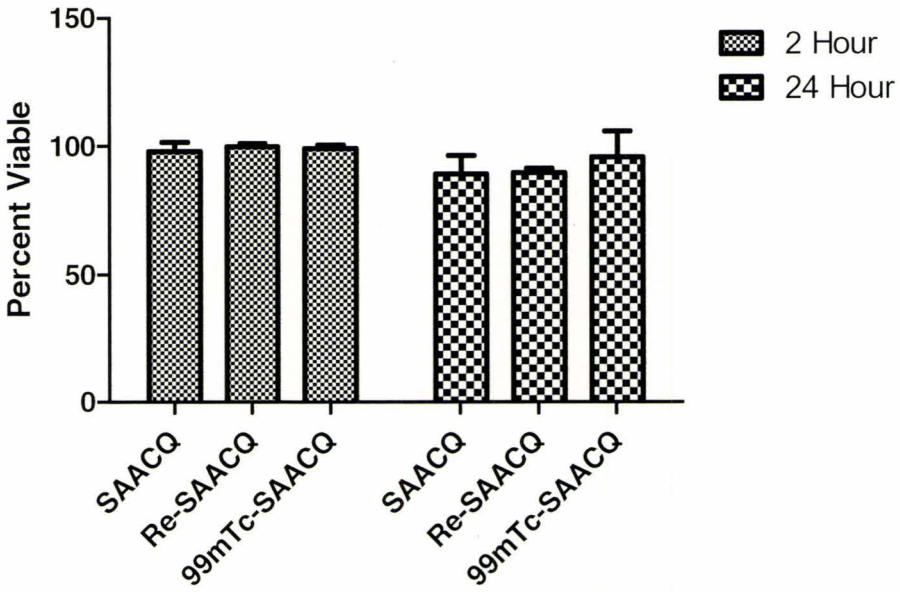
150
100
50
0
Percent Viable
2 Hour
24 Hour
SAACQ
Re-SAACQ
99mTc-SAACQ
SAACQ
Re-SAACQ
99mTc-SAACQ

incubated with an equal volume of 0.01 M PBS. Although there was greater variability than expected, there was no significant difference between the control and the ^{99m}Tc-SAACQ labeled cells (Figure 4.5). After NSPCs were incubated with the tracer, 36 ± 7% of cells appeared normal, while 27 ± 9% were apoptotic and an additional 37 ± 15% incurred a moderate amount of damage. These results indicate that the presence of the tracer did not appear to induce any additional damage to DNA when compared with the control cells 24 hours after labeling.

4.3.5 Proliferation of labeled NSPCs

The proliferation of NSPCs after labeling with ^{99m}Tc-SAACQ was assessed using the BrdU cell proliferation assay. After cell labeling, the cells were incubated with the BrdU reagent for 24 hours at 37°C and analyzed in parallel with the control cells. The assay assesses the amount of BrdU incorporated into newly synthesized DNA and is directly proportional to the number of cells that have divided within the 24 hour period. SAACQ-, Re-SAACQ-, and ^{99m}Tc-SAACQ-labeled NSPCs proliferation was normalized to control cells incubated with an equal volume of 0.01 M PBS. This accounts for differences in the primary cell line and the age of the cells. It has been demonstrated that the age of the cells can affect their proliferative ability (Ahlenius *et al.*, 2009). Re-SAACQ and SAACQ labeled cells did not significantly differ from one another (103.4 ± 7.8% and 108.5 ± 21.2% respectively) (Figure 4.6). ^{99m}Tc-SAACQ labeled cells showed a significant decrease in proliferation (25.4 ± 13.1%) compared to Re-SAACQ and

Figure 4.5. The comet assay distinguished cells undergoing early apoptosis (A) and late apoptosis (B), damaged cells (C), and undamaged cells (D). There was no significant difference in DNA damage between labeled and unlabeled cells (E) (ANOVA, $n = 3$, $p > 0.05$). This assay was performed with by the Dr. J. Lemon in Dr. D. Boreham's group at McMaster University.

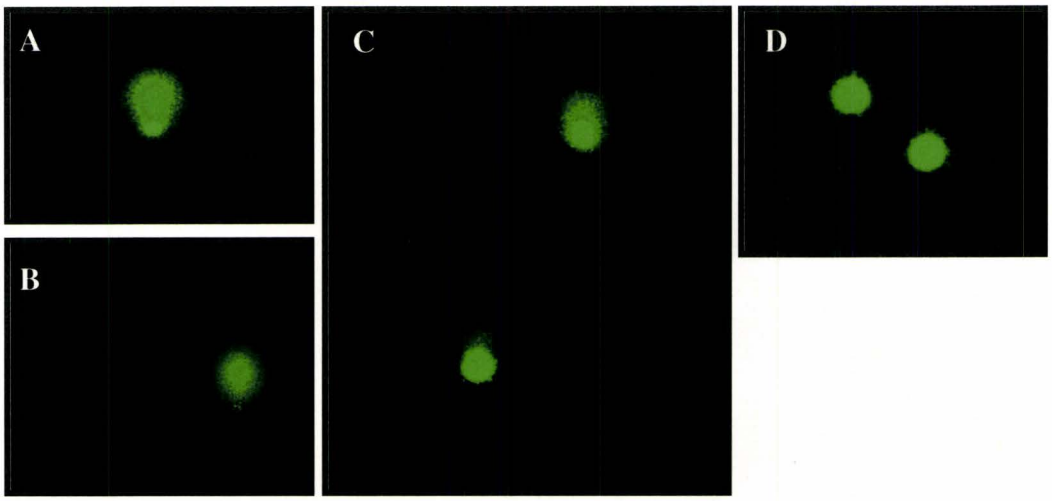
A
B
C
D

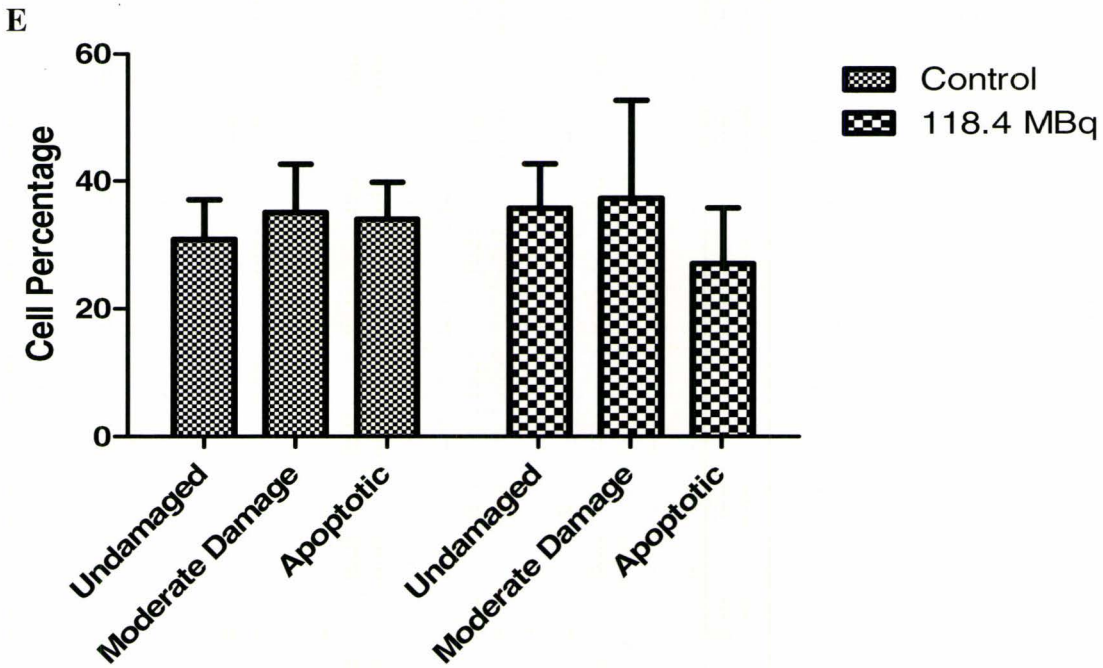
E
60
40
20
0
Cell Percentage
Control
118.4 MBq
Undamaged
Moderate Damage
Apoptotic
Undamaged
Moderate Damage
Apoptotic

Figure 4.6. Cell proliferation assessed by the BrdU cell proliferation assay. There is no significant difference between the proliferation of cells labeled with SAACQ or Re-SAACQ. There is a significant decrease in the proliferation of cells labeled with ^{99m}Tc-SAACQ (ANOVA, $n = 3$, $p < 0.05$).

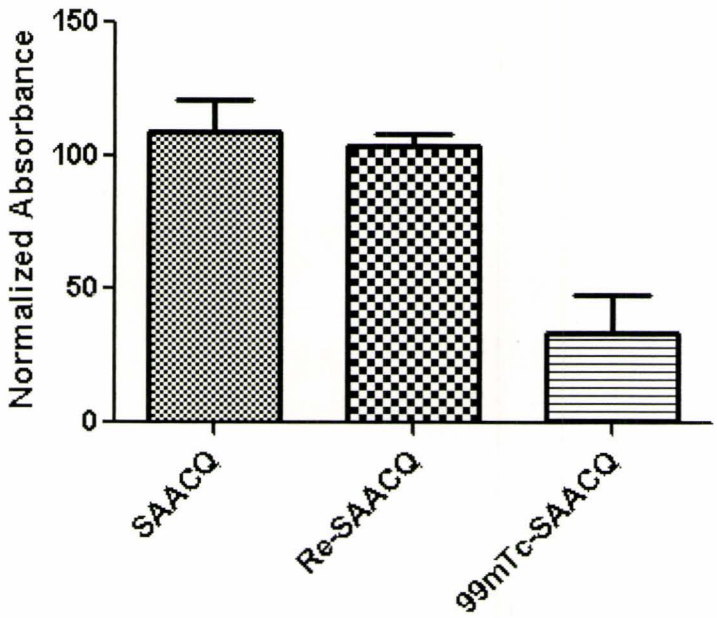
Normalized Absorbance
150
100
50
0
SAACQ
Re-SAACQ
99mTc-SAACQ

SAACQ labeled cells (Figure 4.6). This indicated that the difference in proliferation was most likely caused by ^{99m}Tc rather than the incorporation of the label into the cells.

4.3.6 Differentiation of labeled NSPCs

NSPCs isolated from wild-type mouse pups were labeled with SAACQ, Re-SAACQ, or ^{99m}Tc-SAACQ. Labeled cells were differentiated for 7 days in serum-free media containing 50% concentration of the growth factors EGF and FGF-2 or for 10 days in the same media with the addition of 1% fetal bovine serum. Cells were fixed in acetone and cell differentiation was assessed using epi-fluorescence immunocytochemistry. The neuronal and glial phenotypes were identified using antibodies to βIII-tubulin and GFAP respectively.

The percentages of neuronal and glial cells were expressed as a percentage of the total cell number determined by DAPI staining of the nuclei. The SAACQ, Re-SAACQ, and ^{99m}Tc-SAACQ groups were normalized to control cells to account for any differences in cell population due to differences in passage number. Differentiation after seven days was not sufficient for complete differentiation and therefore differentiation was extended to 10 days. The cells labeled with ^{99m}Tc-SAACQ showed variability in the percentage of cells that differentiated into neurons. Equally, there was variability in the percentage of cells that differentiated into neurons in the control group as well. There were more differentiated NSPCs identified as neurons in the ^{99m}Tc-SAACQ-labeled group in comparison to control cells (Figure 4.7). Representative images of labeled neurons and

astrocytes are shown in Figures 4.8b-d. When the differentiation of the cells was compared between the SAACQ, Re-SAACQ, and ^{99m}Tc-SAACQ groups, there was a tendency for increased neuronal differentiation in both the Re-SAACQ and ^{99m}Tc-SAACQ groups with ^{99m}Tc-SAACQ group showing the greatest amount of neuronal differentiation. However, because of the variability in the differentiation of the cells, this trend did not reach significance (Figure 4.8a).

4.4 Discussion

^{99m}Tc is the most widely used radionuclide in diagnostic medicine. It has a reasonably long half-life (6hrs) and is readily available in most hospitals making a ^{99m}Tc-based cell labeling agent accessible to the research community at a reasonable cost. This is of importance when considering the number of transplants undertaken in a typical pre-clinical study. An additional benefit of ^{99m}Tc is that it imparts a low dose burden that limits the potential radiation damage to labeled cells.

In this study we developed a novel method to label cells for imaging following transplanting the cells in the brain. By taking advantage of the unique properties of SAACQ, we were able to utilize the permeation peptide, HIVTat$_{48-57}$ in combination with SAACQ to efficiently label cells. With an isostructural Re-complex, we could visualize the distribution of the peptide within the cells using epi-fluorescent microscopy. 100% of

Figure 4.7. 10 day differentiation of NSPCs after labeling with ^{99m}Tc-SAACQ. There is a trend towards an increase in neuronal differentiation for NSPCs labeled with ^{99m}Tc-SAACQ in comparison with the control group (t-test, $n = 4$, $p > 0.05$).

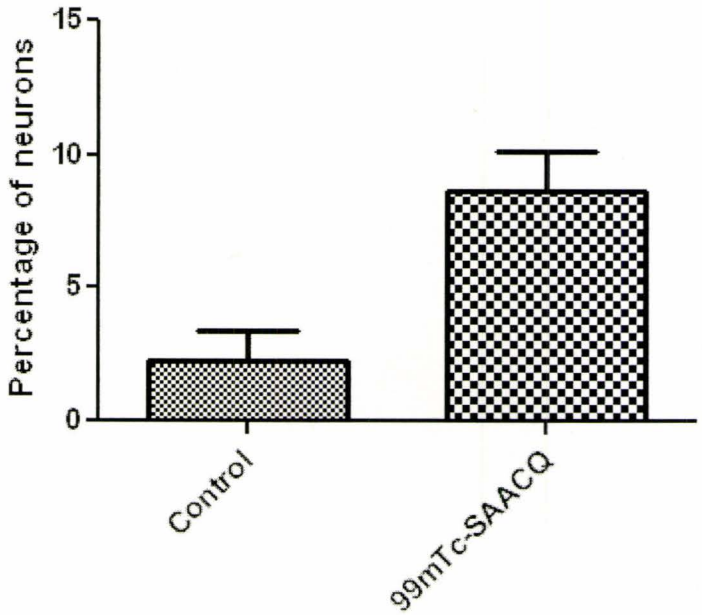
Percentage of neurons
15
10
5
0
Control
99mTc-SAACQ

Figure 4.8. Differentiation profiles of NSPCs labeled with SAACQ, Re-SAACQ, or ^{99m}Tc-SAACQ after 10 days *in vitro*. (A) Cells labeled with Re-SAACQ showed increased neuronal differentiation in comparison to the group of cells labeled with SAACQ. The highest number of neurons occurred in the ^{99m}Tc-SAACQ-labeled cells. However, because of the variability associated with *in vitro* differentiation of neurospheres, significance was not reached (ANOVA, $n = 4$, $p > 0.05$). Representative differentiation images of cells labeled with (B) the glial marker GFAP and (C) the neuronal marker βIII-tubulin. (E) The representative merged image showing the nuclear dye counterstain DAPI.

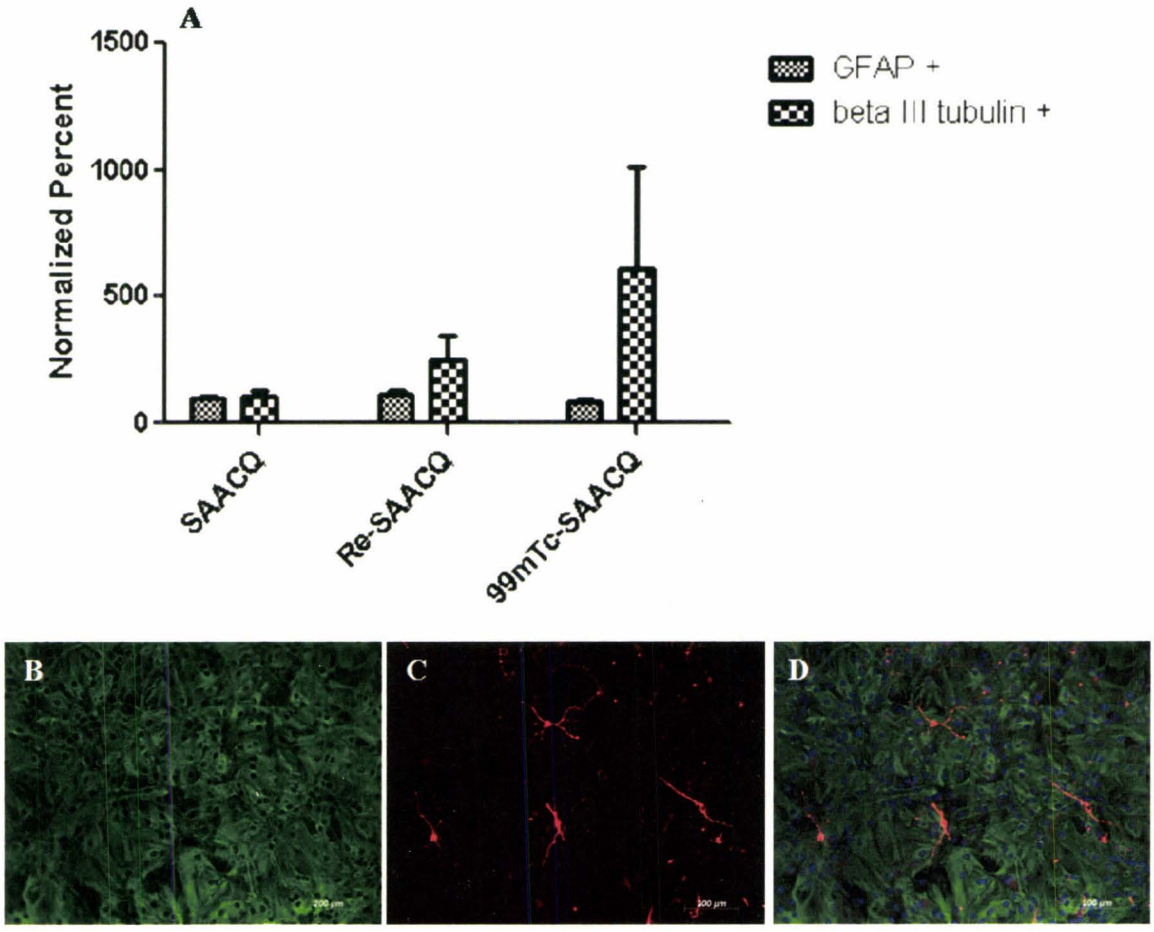
A
1500
1000
500
0
Normalized Percent
GFAP +
beta III tubulin +
SAACQ
Re-SAACQ
99mTc-SAACQ
B
C
D

the cells contained the fluorescent label. The label was preferentially localized to the outside of the nuclear envelope, but was also observed in the nucleus and cytoplasm of the cells. This spatial distribution is consistent with previous work on the uptake and distribution of tat-peptides (Bhorade *et al.*, 2000; Futaki *et al.*, 2001; Vives *et al.*, 1997; Bullok *et al.*, 2002).

We were able to efficiently label NSPCs with ^{99m}Tc-SAACQ and obtain high uptake values. This labeling strategy resulted in an average uptake of 10-20 Bq/cell, which is greater than previous reported values. The efflux of the label from the cells was also determined. After 30 minutes, approximately 72% of the label remained within the cells. This result is consistent with the literature indicating that efflux of labeled tat-peptides being complete after 20 minutes (Polyakov *et al.*, 2000). Our study showed a much greater retention of the label within the cells (compared with 17% retention; (Polyakov *et al.*, 2000)). The higher retention in our study may be due to the difference in the design of the tracer and/or the cell type used in the study.

Once cell labeling was accomplished, it was important to determine any negative biological effects of the label on the cells. Labeling murine NSPCs with ^{99m}Tc may be toxic to cells, introduce DNA damage, and/or interfere with the proliferation and differentiation capacity of the cells due to radiation-induced changes, thereby decreasing the potential use of the cells for therapeutic purposes. We investigated the toxicity of ^{99m}Tc-SAACQ to the NSPCs and found that the cells remained viable when compared

with cells labeled with Re-SAACQ and SAACQ at all time points analyzed. For this study we normalized the three labeled groups (^{99m}Tc-SAACQ, Re-SAACQ, and SAACQ) to the control cells incubated with an equal volume of 0.01 M PBS in order to account for differences in the primary cell cultures and differences in the age of the cells *in vitro*. Because the Re-SAACQ fluorescence intracellular distribution study showed the presence of the label in the nucleus, we examined the possibility of radiolytic damage to the DNA. We found there was no indication of DNA damage at 24 hours in comparison to control cells when assessed by the single-cell gel electrophoresis assay.

Interestingly, when cell proliferation was examined, there was a decrease in the proliferative capacity of the cells labeled with ^{99m}Tc-SAACQ in comparison to Re-SAACQ- and SAACQ-labeled cells. This may be due to radiation-induced damage to the DNA that can cause cell death or arrest the cell cycle. Radiation-induced apoptosis peaks in murine lymphocytes after exposure to ^{137}Cs at 8 hours and apoptosis declines rapidly after 16 hours (Lemon *et al.*, 2008). Because DNA damage was examined at 24 hours, ^{99m}Tc-induced DNA damage may have been repaired by this time or cells with un-repairable damage could have been eliminated by apoptosis.

^{99m}Tc-SAACQ has a nuclear localization signal and therefore can accumulate in close proximity to the DNA of the NSPCs (Vives *et al.*, 1997). ^{99m}Tc emits Auger electrons as it decays, which can cause DNA damage. Auger electrons travel less than 1 μm in distance and therefore must be in close proximity to the DNA of a cell to induce

any damage (Buchegger *et al.*, 2006). It has been calculated that the dose rate of ^{99m}Tc is an order of magnitude higher in the nucleus of a cell versus the cellular membrane (Faraggi *et al.*, 1994). The dose of ^{99m}Tc drops at the edge of the nucleus and is almost non-existent in the cytoplasm of the cell (Faraggi *et al.*, 1994). If the Auger electron emission results in DNA damage, it is possible for DNA repair to occur, however, the repair is frequently erroneous. Despite these concerns regarding the nuclear localization of ^{99m}Tc-SAACQ, Auger radiation energy released per decay is less than 1% for ^{99m}Tc and therefore may not be of significance. Fluorescent Re-SAACQ intracellular distribution showed strong nuclear envelope association with less tracer present in the cytosol and the nucleus, which implies there is a relatively little amount of ^{99m}Tc in close proximity to the DNA.

DNA damage caused by Auger electron emission from ^{99m}Tc has been reported in the literature (Ak *et al.*, 2002; Pedraza-Lopez *et al.*, 2000; Haefliger *et al.*, 2005). Haefliger *et al.* (2005) reported that DNA damage caused by nuclear localization of ^{99m}Tc did not result in a decrease in viability at 24 hours, but proliferation was inhibited at this time point. At 5 days there was nuclear damage and cell death occurred 9 days after labeling as a result of radiation-induced mitosis-linked death or radiation-induced cell senescence (Haefliger *et al.*, 2005). The authors noted that incubation with less activity produced initial cell damage but was followed by recovery and exponential growth. For their study, cells were incubated for 36 hours and the lowest concentration of peptide was in the nanomolar range whereas we incubated the cells for 20 minutes with peptide

concentrations in the picomolar range. Based on the decrease in the concentration of the radiolabeled peptide and the shortened incubation time in our study, it is possible that our cells experienced cell cycle arrest, slowing the proliferative capabilities of the labeled cells in comparison to the unlabeled peptide. DNA damage assays and apoptotic assays should be carried out at the 8 and 16 hour time points in order to verify DNA integrity of the ^{99m}Tc-SAACQ-labeled NSPCs.

The differentiation of NSPCs was examined after labeling with SAACQ, Re-SAACQ and ^{99m}Tc-SAACQ. Although it was not significant, there was a trend towards enhanced neuronal differentiation when cells were labeled with Re-SAACQ and ^{99m}Tc-SAACQ. The increase in neuronal differentiation is potentially useful since neuronal differentiation *in vitro* is typically less common than glial differentiation (Mokry *et al.*, 2005; Dromard *et al.*, 2007; Hattiangady *et al.*, 2007). However, certain studies do demonstrate a pronounced neuronal differentiation of neurospheres (Vroemen *et al.*, 2003). This highlights the heterogeneity of the cellular composition in neurospheres and may explain in part the variability seen in our differentiation study. In fact, βIII tubulin and GFAP expression have been seen in neurospheres suggesting that differentiation has already started and cell fate has already been determined before complete differentiation occurs (Roussa and Krieglstein, 2004). Antigen expression has been shown to be variable within the spheres (Brazel *et al.*, 2005). In spheres from the same region of the young adult mouse brain, 60% expressed GFAP and 15% expressed NG2, a glial precursor marker. The level of expression of these markers varied between individual

neurospheres. In addition, there was no overlap between GFAP positive and NG2 positive spheres indicating two distinct populations. In contrast to this, Dromard (2007) found that there was an overlap in the neurosphere expression of GFAP and NG2. This further supports the heterogeneity within the neurospheres.

Heterogeneity within the parent spheres will likely cause heterogeneity within the differentiated population of cells. This is indicated by the varying outcome in differentiation studies where some reports find a greater population of glial cells upon differentiation (Mokry *et al.*, 2005; Ader *et al.*, 2004) while other studies find a greater population of neuronal cells (Vroemen *et al.*, 2003). Although there is variability in the present differentiation study, the ^{99m}Tc-SAACQ-labeled group consistently showed greater neuronal differentiation suggesting that ^{99m}Tc-SAACQ causes the NSPCs to adopt a neuronal fate. This in combination with the decrease in the proliferation of the cells may be of value for certain transplantation studies. Typically, low neuronal numbers are seen in transplantation studies (Muraoka *et al.*, 2008) and there is concern of teratoma formation (Bjorklund *et al.*, 2002). Labeling the NSPCs with ^{99m}Tc-SAACQ may provide a method for decreasing the chances of teratoma formation, increasing neuronal differentiation, and permitting non-invasive visualization of the transplant with SPECT. It should be noted that *in vitro* differentiation is not necessarily reflective of *in vivo* differentiation and this area remains to be explored. How ^{99m}Tc-SAACQ is causing these changes to occur within the cell requires further investigation.

4.5 Conclusion

This study developed a new method for labeling NSPCs for visualization post-transplantation *in vivo* using SPECT. We were able to label NSPCs with ^{99m}Tc-SAACQ and achieve a relatively high uptake of activity that was retained within the cells. The use of ^{99m}Tc to label the cells makes this approach inexpensive and widely accessible. A successful labeling agent needs to maximize cellular uptake without compromising viability, proliferation, and differentiation of the NSCs. In addition, there should be no transfer of the radiotracer from dead or dying cells to surrounding live cells. In order to assess the labeled cells, the label must be contained within the cell of interest and not engulfed in surrounding macrophages, which can occur as cells die. Many strategies have been undertaken to label stem cells (Ford *et al.*, 1996; Aicher *et al.*, 2003; Chin *et al.*, 2003; Bai *et al.*, 2004; Ma *et al.*, 2005; Zhou *et al.*, 2005), however all of these methods have been complicated by expense, lack of availability of the isotope, poor cellular uptake, or undefined biological effects on the cells.

We developed a tracer that does not compromise the integrity of the DNA or the viability of the cells. The proliferation of the NSPCs is decreased; however, other studies have demonstrated that proliferation may only decrease for the first 24 hours post-labeling. It is of importance to determine if the decrease in proliferation is due to radiolytic damage that is not repaired, or if proliferation is slowed due to cell cycle arrest that occurs while the cells repair the damage. To assess this, it would be worthwhile to examine the viability and DNA integrity at 8 and 16 hours post-labeling. It would also be

of interest to assess the proliferative capacity of the NSPCs at later time points. We also found that there was a trend towards an increase in neuronal differentiation when cells were labeled with ^{99m}Tc-SAACQ in comparison to control cells. This increase in differentiation is interesting because it may provide a method to direct neuronal differentiation *in vivo*. In summary, a new method for labeling NSPCs to visualize cell transplants was developed. Further biological characterization is required to fully understand the effect of the tracer on the cells.

Chapter 5: Imaging neural stem/progenitor cells labeled with $[^{99m}Tc(CO)_3SAACQHIVTat_{47-58}]^+$ in rodents

5.1 Background

NSCs are capable of self-renewal and differentiation into the three main cell lineages of the CNS: astrocytes, oligodendrocytes, and neurons. NSCs can be isolated from the fetal, embryonic, and adult brain sources and they can be expanded *in vitro* as heterogeneous aggregates of cells. When isolating NSCs, NPCs are also obtained that contribute to the heterogeneity in the culture system. NPCs are more committed than NSCs, but they also maintain the potential to differentiate into the three cell lineages. The identification of NSCs from NPCs is difficult; however, the differentiation capacity of both neural stem and progenitor cells makes them an attractive therapeutic option.

NSPCs have been used for various experimental therapies and they have been shown to be effective to treat aspects of CNS disease and injury in animal models. NSPCs have been transplanted and shown to survive and differentiate into neurons in both the intact and diseased brain (Gage *et al.*, 1995; Nikkhah *et al.*, 2009). Studies in animals have also demonstrated the potential of NSPCs to integrate into the host environment and produce functional neurons that make connections with the host cells (Benninger *et al.*, 2003; Eriksson *et al.*, 2003; Lepore *et al.*, 2006). In addition, functional improvement after cell therapy has been seen in animal models of PD, spinal cord injury, and Alzheimer's disease (Redmond, Jr. *et al.*, 2007; Wu *et al.*, 2008; Klein and Svendsen, 2005).

NSPC therapy in animal models of PD has resulted in variable success. One study demonstrated that ESCs could be used to successfully treat PD; however, in these animals 40% had teratoma formation (Bjorklund *et al.*, 2002). Studies have also shown that although there is graft survival, functional recovery is not consistent (Svendsen *et al.*, 1997). Other studies have successfully demonstrated graft survival with the expression of tyrosine hydroxylase (TH), the rate limiting enzyme in dopamine production, and corresponding functional improvements (Hahn *et al.*, 2009). However, in clinical trials of PD, there has been little success with transplantation therapy and this treatment is still considered experimental despite numerous clinical trials (Hagell *et al.*, 1999; Lindvall *et al.*, 1994). There are many reasons that could contribute to the limited success of this cell therapy including the characteristics of the cells used for initial transplantation and the state of the host environment. Because these characteristics vary from study to study, it is difficult to make direct comparisons.

It is important to understand the conditions affecting initial transplant survival and the fate of the cells to decrease the variability in the transplant outcomes. Molecular imaging techniques give new information regarding certain transplant variables, such as the number of transplanted cells and the location of the transplant, which will increase successful outcomes. There is a need to standardize the transplant procedure using short-term assessment methods and to understand the fate of the transplanted cells using long-term tracking studies. In a previous study, it was found that despite the use of ultrasound-guided injection and highly trained personnel, cell injection was only performed correctly

approximately 50% of the time (de Vries *et al.*, 2005). With initial SPECT imaging of transplanted cells, the number of cells in the transplant can be calculated. The ability to monitor the number of cells injected into the host offers key quantitative and qualitative information about the transplant that, in turn improves the standardization of the procedures.

This chapter reports a calibration curve for the pinhole collimator prepared by Dr. Paul Shaffer from Dr. John Valliant's group at McMaster University to determine the number of cells in the mouse transplants.

5.2 Objective

To image cell transplants labeled with ^{99m}Tc-SAACQ using SPECT/CT in rodents.

5.3 Results

5.3.1 Imaging ^{99m}Tc-SAACQ-labeled NSPCs

To establish the working parameters, the initial visualization of NSPCs was determined by performing a subcutaneous injection of ^{99m}Tc-SAACQ-labeled cells into the posterior neck region of a 12-week old mouse. As expected, the dynamic SPECT scan did not show significant migration of the cells from the injection site up to 30 minutes after injection. This study provided proof of principle that ^{99m}Tc-SAACQ-labeled cells could be visualized using SPECT (Figure 5.1).

Figure 5.1. 30 minute dynamic SPECT/CT image of ^{99m}Tc-SAACQ-labeled cells injected subcutaneously into the posterior neck region of a 12-week old mouse. Cells (shown in red) do not migrate from the injection site.

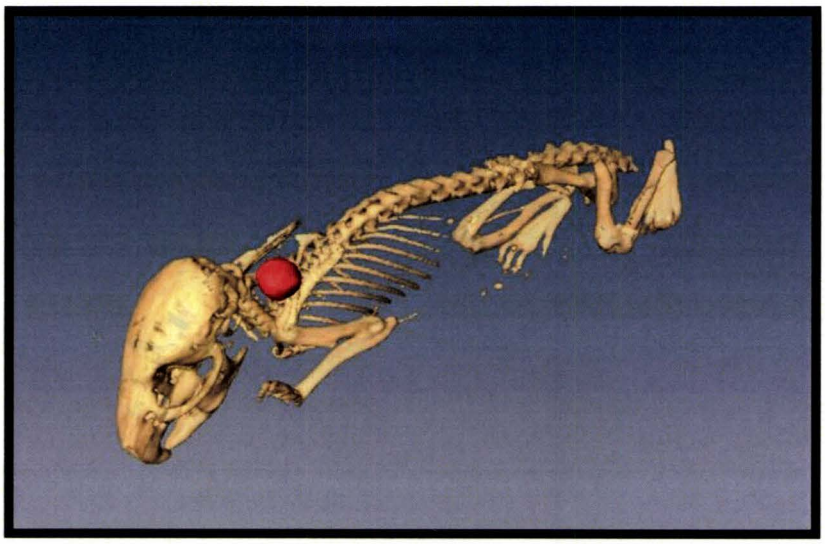

A calibration curve was made in order to determine the amount of activity in a region of interest (ROI) of a SPECT image based on the mean number of counts/acquisition time (Figure 5.2). Various amounts of pertechnetate were imaged with SPECT using a high-resolution parallel-hole collimator or a high-resolution pinhole collimator.

The decay-corrected amounts of activity were plotted against the mean number of counts/acquisition time. The mean values were obtained from an ROI placed around the cell transplant. After determining the mean counts/acquisition time for the transplant, the amount of activity was determined. The activity in the ROI that corresponded to the transplant and the activity/cell was used to determine the number of cells in the transplant. The calibration curve made from the high-resolution pinhole collimator (Figure 5.2a) was used for the subsequent transplantation studies in mice and the calibration curve made from the high-resolution parallel-hole collimator (Figure 5.2b) was used for the transplantation studies in rats. For the transplantation experiments, cells were labeled with the tracer prepared in high effective specific activity to avoid any effect on the cells caused by unlabeled tracer. In one study, cells prepared for transplantation contained 18 Bq/cell after efflux. An immediate benefit of SPECT imaging of ^{99m}Tc-SAACQ-labeled cells was highlighted as we were able to identify radioactivity, representing cells, adhered to the sides of the plastic 15 mL Falcon tubes used to wash and prepare the cells for transplantation (Figure 5.3). This mouse did not show the

Figure 5.2. Calibration curves were used to determine the number of cells in a given transplant. Calibration curves were made for (A) the high-resolution pinhole collimator and for (B) the high-resolution parallel-hole collimator. The high-resolution pinhole collimator calibration curve was prepared by Dr. P. Schaffer in D. J. Valliant's group at McMaster University.

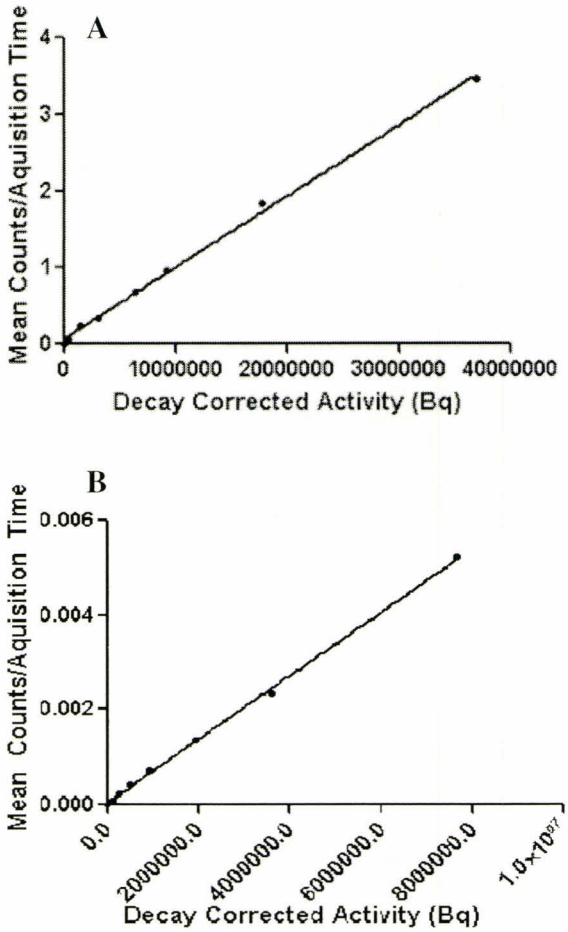
A
Mean Counts/Aquisition Time
0
1
2
3
4
0
10000000
20000000
30000000
40000000
Decay Corrected Activity (Bq)
B
Mean Counts/Aquisition Time
0.000
0.002
0.004
0.006
0.0
2000000.0
4000000.0
6000000.0
8000000.0
1.0×10^07
Decay Corrected Activity (Bq)

Figure 5.3. SPECT/CT image of ^{99m}Tc-SAACQ-labelled cells. Cells (shown in red) contain 18 Bq/cell of activity and are adhered to the inside of a 15 ml Falcon tube used for cell preparation.

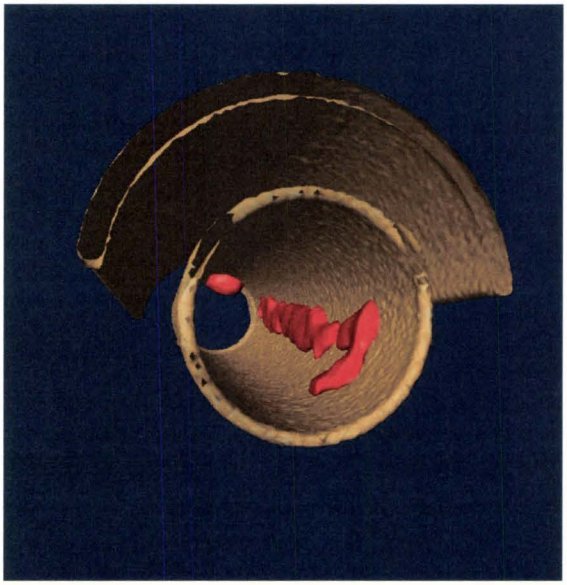

presence of labeled cells once stereotaxic injection was complete indicating that the majority of the cells remained in the plastic tube.

To address this issue of cells adhering to the Falcon tubes, the cells were prepared in silanized glass tubes and the labeled cells were then transplanted bilaterally into the striatum of a healthy, wildtype mouse. Cells contained 11 Bq/cell after efflux and the transplants were imaged with static planar and SPECT/CT 20 minutes post-transplantation (Figure 5.4a and b). This study demonstrated that 3-D imaging of cell transplants in the brain was feasible. However, the parallel-hole collimator did not offer the resolution needed to identify two transplant sites (Figure 5.4a). Following the acquisition of the initial images, the mouse was sacrificed and imaged for 15 hours with high-resolution pinhole SPECT/CT (Figure 5.4c and d). Using this collimator, both transplant sites could be resolved. Activity resided on the surface of the skull indicating that not all of the cells were located within the striatum. This was most likely due to reflux of the cells following the removal of the needle or the transfer of radioactivity to the skull during the transplantation procedure. Using a calibration curve, it was determined that approximately 5600 cells were present in the transplant sites.

5.3.2 Non-invasive SPECT imaging of labeled cell transplants

High-resolution pinhole SPECT/CT images were repeated to determine if the transplants could be imaged using this method in a shorter time frame to avoid euthanizing the subject. Cells were labeled with 10 Bq/cell for bilateral transplantation in

Figure 5.4. SPECT imaging of ^{99m}Tc-SAACQ transplanted cells. A bilateral transplant containing 11 Bq/cell after efflux is visualized with high resolution parallel-hole SPECT/CT in (A) a static planar image is shown in (B). High resolution pinhole SPECT/CT images of the same bilateral transplant are shown in (C) and (D). High resolution parallel-hole images were obtained over 30 minutes following a 10 minute static planar. High resolution pinhole SEPCT/CT images were obtained post-mortem over 15 hours. There is some activity that appears outside of the skull, which is most likely due to movement of the cells up the needle tract when the needle was retracted from the transplant site, or the transfer of activity from the syringe to the top of the skull.

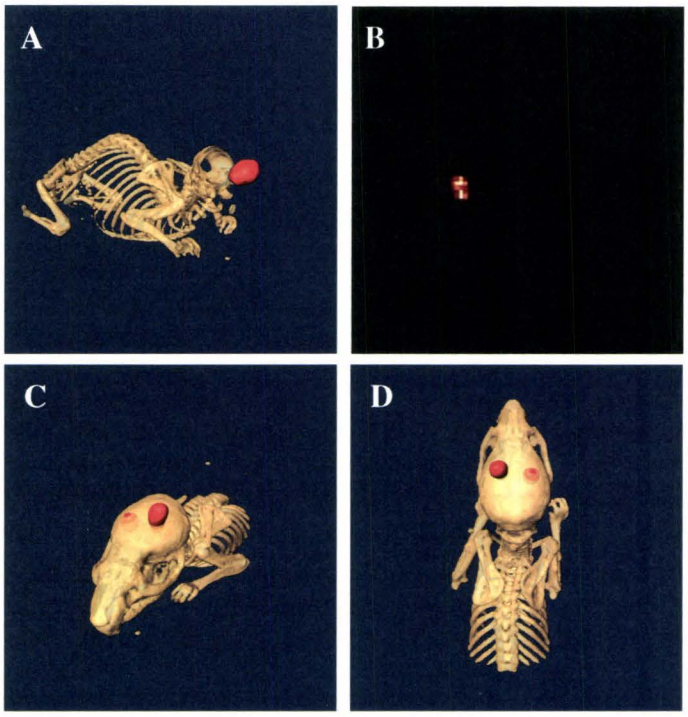
A
B
C
D

a healthy mouse. The mouse was anesthetized and a 2 hour pinhole image was acquired (Figure 5.5). Only one of the two transplant sites was visible containing approximately 840 cells. This indicates that the second site did not contain enough cells to generate an image despite attempts to evenly distribute the cells between the two transplant sites. The mouse recovered from the anesthesia without any adverse effects indicating that this procedure can be used to image the cells immediately after transplantation by non-invasive procedures.

5.3.3 Specificity of cell transplant images

To demonstrate the specificity of the procedure we determined the distribution of free ^{99m}Tc-SAACQ in the mouse brain in a comparison study. A similar amount of free ^{99m}Tc-SAACQ was injected into the striatum in an identical manner to the injection of the cells (Figure 5.6a). As expected, there was an increase in the distribution of the free peptide in comparison to the labeled cells. Tat peptides readily cross the blood brain barrier (Banks *et al.*, 2005), which is the most likely explanation for the accumulation of the activity seen in the abdominal area of the mouse in a planar image obtained 15 hours after injection of the isotope (Figure 5.6b).

Images of cell transplants labeled with ^{99m}Tc-SAACQ were also acquired in a rat in order to confirm that the labeled cells could be visualized in a different species using the same procedure. Labeled cells were transplanted into rats and images were taken immediately after surgery with SPECT/CT using a high resolution parallel-hole

Figure 5.5. A 2 hour pinhole SPECT/CT image of a bi-lateral transplant in healthy, wild-type mouse. The cell transplant contains approximately 840 cells labeled with 10 Bq/cell (shown in red) on one side. There were not enough cells transplanted on the other side to visualize the transplant.

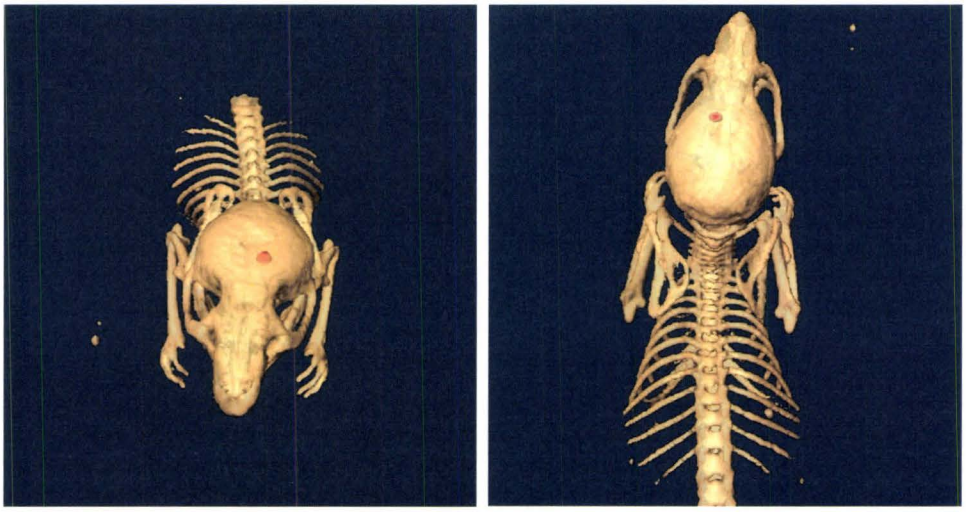

Figure 5.6. 1.85 MBq of free ^{99m}Tc-SAACQ injected bilaterally into the striatum of a healthy, wild-type mouse brain in a similar manner as a cell transplant. ^{99m}Tc-SAACQ distributes throughout the head of the animal and over time accumulates in the thorax and abdomen. The distribution of the radioligand is markedly different from when it is contained in cells. (A) Parallel-hole SPECT/CT and (B) Static-planar image of injected activity.

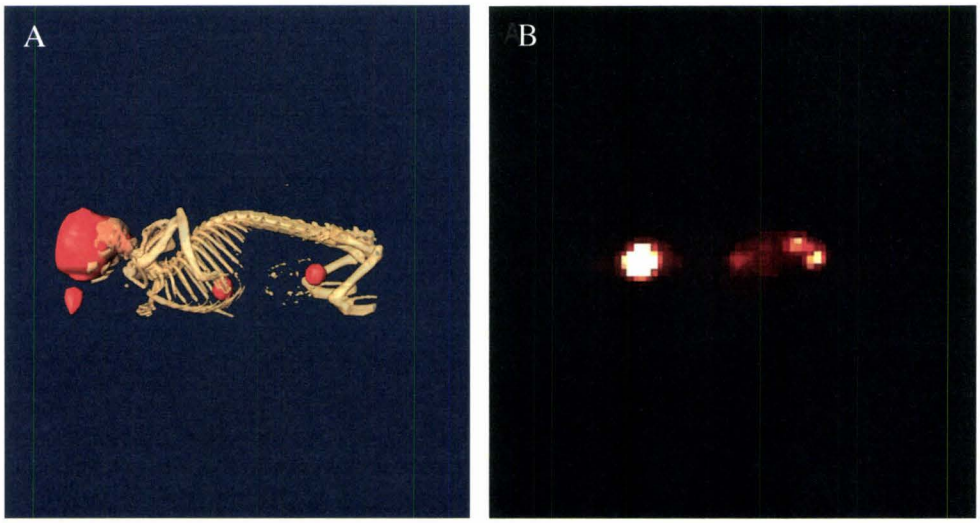
A
B

collimator. The number of cells in the transplant was determined using the calibration curve.

To illustrate the specificity of the image, two rats were transplanted with ^{99m}Tc-SAACQ labeled NSPCs or NSPCs double-labeled with cell tracker orange (a lipophilic dye) and ^{99m}Tc-SAACQ. Immediately after surgery a SPECT/CT image was acquired and the rats were euthanized and the brains were flash frozen for histology or phosphorimaging in order to confirm that the SPECT images corresponded to the transplanted cells. ^{99m}Tc-SAACQ labeled NSPCs transplanted into the striatum were visualized using SPECT and phosphorimaging (Figure 5.7a-d). The SPECT image of the transplanted cells and the phosphorimage demonstrate the specificity of the activity to the area of the transplanted cells. To further confirm this, NSPCs double-labeled with cell tracker orange and ^{99m}Tc-SAACQ were transplanted into the forebrain. The SPECT images correlated with the location of the cells as shown by histology (Figure 5.7e-j).

5.4 Discussion

Stem cell transplantation holds great promise as a viable therapy for PD. Despite some success in animal models, clinical trials using cell therapy for PD treatment has been disappointing (Hagell *et al.*, 1999; Lindvall *et al.*, 1994). The lack of efficacy is due in part to our limited understanding of the transplant parameters that influence cell fate. Avenues of research that enhance our knowledge of the factors affecting cell fate will aid in the development of stem cell therapy for the treatment of PD.

Figure 5.7. SPECT imaging of cells transplanted unilaterally into a rat. Cells transplanted into the striatum of a healthy rat and imaged with high-resolution parallel-hole SPECT/CT (A-C). The corresponding phosphorimage of the coronal section taken through the transplant area is shown in (D). Cell transplants were also double-labeled with both ^{99m}Tc-SAACQ and cell tracker orange. High-resolution parallel-hole SPECT/CT images were taken of cells transplanted into the forebrain of the animal (H-J) and coronal sections were taken for histology (E-G). Cells are shown in red and counterstained with DAPI.

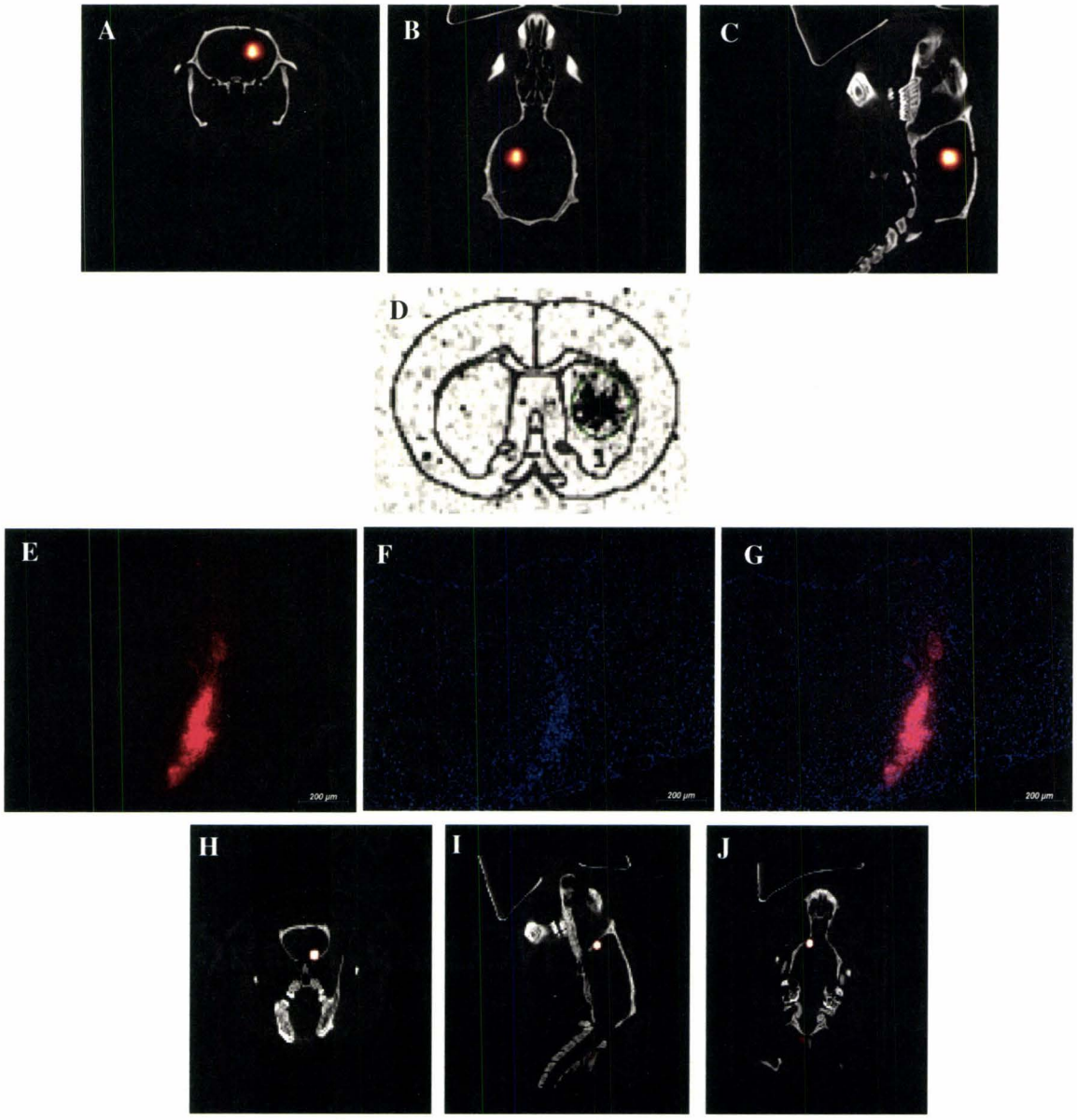
A
B
C
D
E
F
G
200 µm
200 µm
200 µm
H
I
J

Tracking stem cell fate after transplantation is essential to understand the mechanisms underlying stem cell engraftment and the associated functional benefits. To date, most studies that look at *in vivo* stem cell imaging utilize MRI. MRI allows for excellent spatial resolution with some groups reporting the ability to visualize single cells (Heyn *et al.*, 2006). However, in order to achieve that level of sensitivity with an MRI scanner, experimental, high-magnetic field scanners have often been employed limiting the direct translation to a clinical setting.

Long term tracking of cell transplants has also been demonstrated using SPECT (Blackwood *et al.*, 2009). SPECT imaging offers the sensitivity to monitor small numbers of cells. Imaging has been done with [^{111}In]tropolone and the cells could be monitored in the heart for 15 days post-transplantation (Blackwood *et al.*, 2009). ^{111}In is a relatively long-lived isotope (half-life = 2.83 days) and previous work has indicated that this isotope does not affect the viability or proliferation of bone marrow stem cells when taken up into the cytoplasm (Jin *et al.*, 2005). Studies utilizing ^{111}In-labelled cells have focused on cellular transplantation to the heart after myocardial infarction and not on PD treatment.

Defining the optimum parameters for transplantation is important to improve the consistency of the transplant procedures, which will lead to reliable and effective therapeutic outcomes. Labeling cells *in vitro* with ^{99m}Tc-SAACQ allowed us to visualize our neural cell transplants. We were able to visualize ^{99m}Tc-SAACQ-labeled cells in the

posterior neck region of a mouse giving proof-of-principle for cell imaging using the ^{99m}Tc-peptide with SPECT/CT *in vivo*. Using this technique we identified cells that were lost during the transplantation procedure by adhering to the tubes used in preparation of the cells for injection. By modifying our procedure we were able to visualize bi-lateral cell transplants in the mouse brain. When free ^{99m}Tc-SAACQ was injected using a method identical to cell transplantation, the distribution of the activity in the brain was markedly different from the cell transplants supporting the specificity of the signal to transplanted cells. We also verified the specificity of the signal using phosphorimaging and correlative histology.

Using a calibration curve, the number of transplanted cells could be determined. There was considerable variation in the number of cells comprising the transplants despite the attempts to replicate the transplant conditions. Even a bilateral transplant into the mouse showed variability in cell number with only one of the two transplant sites containing enough cells for detection with SPECT. This highlights the variability in the actual number of cells delivered to the transplant site. It is therefore of importance to establish precise transplantation parameters as it has been shown that the number of transplanted cells affects the outcome of the therapy (Terpstra *et al.*, 2007; Nikkhah *et al.*, 2009).

For a successful cell based therapy for PD to be achieved the following criteria has been stated for humans: (1) the grafted cells need to express a complete set of

biochemical mechanisms required for the production of DA as well as the correct morphological and physiological properties (Mendez *et al.*, 2005; Isacson *et al.*, 2003), (2) at least 100 000 grafted cells need to survive long term in the putamen (Hagell and Brundin, 2001), (3) the grafted cells need to re-establish the dense functional DA-releasing terminal synaptic network in the striatum, (4) the grafted cells need to be functionally integrated into the host neural circuitry (Piccini *et al.*, 2000). In previous animal studies it has been demonstrated that an average of 1-5% of NSPCs become TH-positive unless they are genetically altered by the overexpression of transcription factors such as Nurr1 (Wagner *et al.*, 1999). In order to improve the transplant procedure it may be necessary to induce DAergic cell fate *in vitro* prior to labeling. This would promote a greater number of cells to adopt a DAergic cell fate within the graft and allow for the determination of the number of cells transplanted into each striatum.

A limitation of the current procedure was the restriction on the number of cells that were able to be labeled for the transplantation procedure. It may be necessary to optimize the labeling procedure to decrease the initial incubation activity per cell in order to increase the number of cells that can be labeled. Currently, the initial activity per cell was approximately 6000 Bq/cell which allowed a maximum of 400, 000 cells to be labeled. The constraint on the number of cells that were able to be labeled was due to the amount of the ^{99m}Tc-SAACQ that could be produced on a given day. This resulted in an average uptake per cell of 20 Bq/cell. If the amount of initial activity per cell was decreased to be approximately 3400 Bq/cell a greater number of cells could be labeled

without a large sacrifice on the uptake of activity into the cell. In turn a greater number of cells could be transplanted, which may lead to better graft survival.

Currently, the method developed allows for the short term evaluation of the graft. Although this is necessary for standardizing the transplant procedure, it is also important to develop methods for the long-term tracking of cells. Ideally, a method to do this would allow for evaluation of the initial transplant and allow the transplanted cells to be monitored over time. This could be accomplished using radioisotopes with longer half-lives or MRI contrast agents. Lewin *et al.* (2000) developed a method that labeled the tat peptide with a fluorophore, ^{111}In, and a superparamagnetic iron oxide particle (SPIO). This allows the labeled cells to be monitored by fluorescence microscopy, SPECT, and MRI. Multimodality imaging would permit a greater amount of information to be obtained about the transplant. ^{99m}Tc would be more ideal for SPECT imaging in comparison to ^{111}In because of its lower dose burden. In fact, ^{111}In has been explored as a radiotherapeutic agent when delivered using the tat peptide because of the cytoxicity of the radionuclide when in close proximity to the DNA (Liu *et al.*, 2009). Combining our technology with a SPIO would allow for multimodality imaging. The initial transplant could be assessed using SPECT and long term tracking of the cells and the exact cell placement could be elucidated using MRI, which has exquisite resolution.

5.5 Conclusion

The methodology used in this study is an efficient and convenient way to monitor NSPC transplants in small animals. This technique can be used to verify the position of the cells and to determine the number of cells transplanted in real time by a non-invasive procedure. This tracer uses ^{99m}Tc, which is inexpensive, widely available, and commonly used in diagnostic medicine making this method of transplant monitoring feasible for clinical translation. ^{99m}Tc has a low dose burden and a 6 hour half-life that makes it useful for imaging over 24 hours. This is important especially when multiple transplants are needed. Although long-term trafficking studies are important to further monitor cell fate post-transplantation, we believe that characterizing the initial transplant will aid in standardizing the technique and will have significant impact on cell transplant therapy.

Chapter 6: [^{123}I]altropane imaging and behavioural analysis of the dopamine system in the 6-OHDA rat model of Parkinson's disease pre- and post-transplantaion

6.1 Background

PD is the second most prevalent neurodegenerative disease in North America. It is a progressive disorder characterized by the loss of DA neurons that project from the SNpc to the striatum (Dawson and Dawson, 2003). This leads to DA depletion, which results in the motor symptoms of PD (Dauer and Przedborski, 2003). Current therapies, such as oral dosing of L-DOPA, a DA precursor, focus on controlling the symptoms associated with PD (Dauer and Przedborski, 2003). L-DOPA replaces striatal DA and relieves many of the motor symptoms associated with the disease. However, prolonged use of L-DOPA results in dyskinesias that decrease the patients' quality of life (Chapuis *et al.*, 2005). Therefore, it is important to search for therapies aimed at protecting the remaining DA neurons or replacing the neurons lost during the disease progression.

Investigation of potential therapies can be carried out pre-clinically in animal models of the disease. The 6-OHDA rodent model is widely implemented because of the well characterized behavioural phenotypes associated with the DA deficiency (Ungerstedt, 1971; Bjorklund *et al.*, 2002). To assess the integrity of the DA system, behavioural tests and histology are commonly used. The motor asymmetries provide an indirect, qualitative measure of the DA depletion in the nigrostriatal system. Histological methods give excellent spatial resolution; however, they require sacrifice of the animal

which increases the number of animals needed per study and increases the variability within the study because one animal is not examined at multiple time points.

In vivo studies to investigate the intactness of the nigrostriatal projections have been carried out in humans and non-human primates using SPECT and positron emission tomography (PET). These techniques use radiotracers with a high specificity for the DAT, which is specifically expressed on DA neurons (Benamer *et al.*, 2000; Ravina *et al.*, 2005). With the development of designated small animal SPECT scanners, it is possible to examine the nigrostriatal projection system in rodent models of PD. DAT ligands for SPECT imaging include [^{99m}Tc]TRODAT (Mozley *et al.*, 2000), [^{123}I]β-CIT (Marek *et al.*, 2001), [^{123}I]IPT (Kim *et al.*, 1997), [^{123}I]FP-CIT (Booij *et al.*, 1997), and [^{123}I]altropane (Fischman *et al.*, 1998), which all display significantly reduced binding to the DAT in PD patients. The scan time for each ligand varies from 20-24 hours for [^{123}I]β-CIT to 3-4 hours for [^{123}I]FP-CIT and [^{99m}Tc]TRODAT (Abi-Dargham *et al.*, 1996; Kao *et al.*, 2001). [^{123}I]altropane imaging can be acquired in a scan time of 2 hours with peak uptake in the striatum occurring between 10 and 15 minutes (Fischman *et al.*, 1998). In addition, altropane is 28 times more specific for the DAT compared to the serotonin transporter in comparison to IPT and β-CIT, which are 2 times more specific (Madras *et al.*, 1998c).

New therapeutic strategies for PD are aimed at neuroprotective methods to slow disease progression or at permanently correcting the DA loss via cell therapy. To

advance cell therapies, it is necessary to accurately monitor the progression of the disease and the therapeutic response. The purpose of this study was to monitor DA loss and the response to NSPC transplants using [^{123}I]altropane in a rat model of PD.

6.2 Objective

For this component of the thesis, experiments were conducted to determine if [^{123}I]altropane is a good predictor of nigrostriatal system integrity. Nigrostriatal system integrity refers to the ascending pathway projections of the DA neurons that project from the SNpc to the caudate-putamen (striatum).

6.3 Results

6.3.1 [^{18}F]FMT and [^{99m}Tc]TRODAT PET and SPECT imaging

Initial studies were performed using [^{18}F]FMT and [^{99m}Tc]TRODAT to monitor the DAT by PET and SPECT respectively. We were unable to consistently visualize the DAT using these two markers (data shown in Appendix 2) and therefore we continued this study using [^{123}I]altropane as discussed below.

6.3.2 [^{123}I]altropane as a marker of the DAT in rats

[^{123}I]altropane has been used to image the DAT in human and non-human primates (Fischman *et al.*, 1998; Madras *et al.*, 1998b; Fernandez *et al.*, 2001). However, the use of [^{123}I]altropane to image the DAT in a rat using SPECT has not been demonstrated previously. Using phosphorimaging, [^{123}I]altropane showed binding that

was specific in the striatum of a normal rat (Figure 6.1). Using SPECT imaging we were able to image the striatum of both untreated and 6-OHDA lesioned rats (Figure 6.2). We were able to image complete and partial lesions (Figure 6.2b,d). This experiment demonstrated that [^{123}I]altropane binds specifically to the striatum in both wild-type and 6-OHDA lesioned rats and can differentiate between complete and partial lesions.

6.3.3 [^{123}I]altropane SPECT in a 6-OHDA model of PD: DA content

A unilateral lesion of the nigrostriatal system was introduced by a stereotaxic injection of 6-OHDA into the MFB. Rats were analyzed post-lesion with regard to the altropane ratio and the DA content in the striatum and SN. DA content was measured by DA HPLC (Figure 6.3).

In this model there was a significant correlation between the DA content in the striatum and the altropane ratios. Linear regression analysis demonstrated that altropane ratios are strongly related to DA content in the striatum (Figure 6.3a). However, there was no significant correlation between DA content in the SN and the altropane ratios (Figure 6.3b). Consistent with this finding, there was also no significant correlation of the DA content in the SN with the DA content in the striatum (Figure 6.3c).

Figure 6.1. Phosphorimage of [^{123}I]altropane binding in a coronal section of the adult rat brain. The dark intense zone marks binding of [^{123}I]altropane in the area of the striatum.

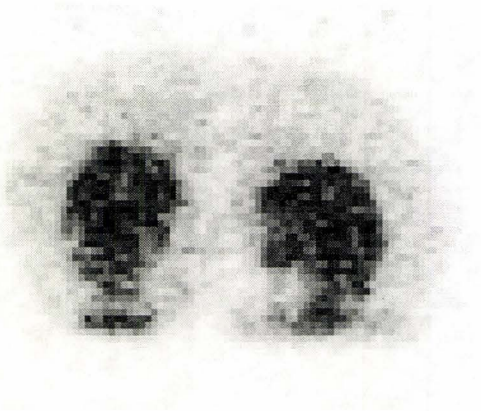

Figure 6.2. [^{123}I]altropane SPECT imaging in parkinsonian rats. Coronal and transverse SPECT images show [^{123}I]altropane binding in the striatum of untreated rats (A and C) and in 6-OHDA lesioned rats (B and D). [^{123}I]altropane can detect a complete lesion (B) with an altropane ratio that decreases from 0.86 pre-lesion to 0.15 post-lesion and a partial lesion (D) with an altropane ratio that decreases from 1.1 pre-lesion to 0.71 post-lesion. The bright region seen on (B) and (D) corresponds to a pertechnetate marker used to define the right side of the animal. Images were obtained two weeks post-lesion with dynamic SPECT/CT using a high-resolution parallel-hole collimator over the course of 30 minutes. Images shown are summed images of the dynamic SPECT/CT.

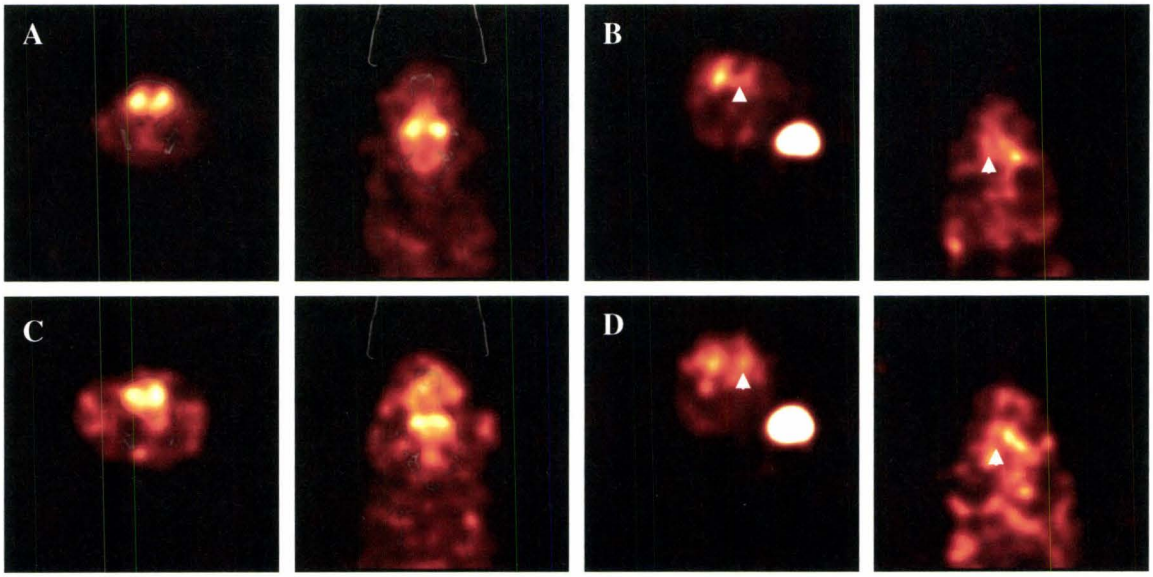
A
B
C
D

Figure 6.3. Linear regression analysis of parameters describing the nigrostriatal system in the 6-OHDA rat model of PD. There was a significant correlation of (A) the striatal DA content and the altropane ratio ($r^2 = 0.9756$, $n = 8$, $p < 0.05$). There is no correlation in (B) the SN DA content and the altropane ratio ($r^2 = 0.1720$, $n = 8$, $p > 0.05$) or in (C) the DA content in the SN and the striatum ($r^2 = 0.09698$, $n = 8$, $p > 0.05$).

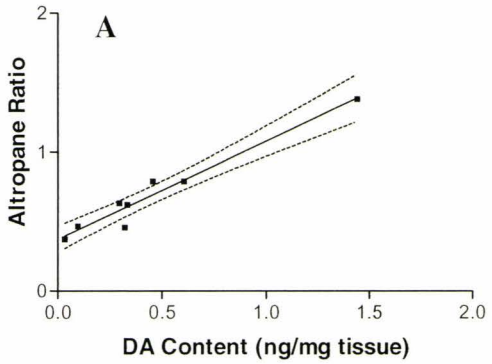
A
Altropane Ratio
DA Content (ng/mg tissue)
0
1
2
0.0
0.5
1.0
1.5
2.0

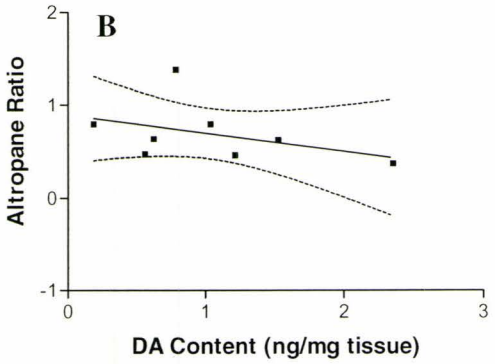
B
Altropane Ratio
DA Content (ng/mg tissue)
-1
0
1
2
0
1
2
3

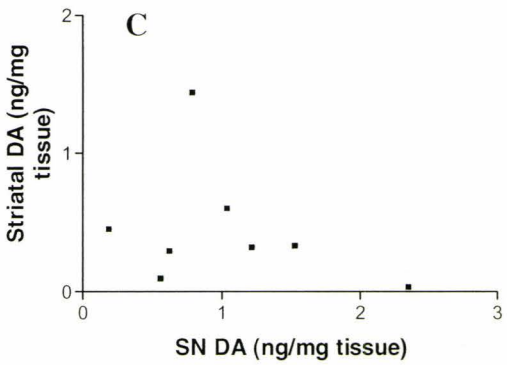
C
Striatal DA (ng/mg tissue)
SN DA (ng/mg tissue)
0
1
2
0
1
2
3

6.3.4 [^{123}I]altropane SPECT in a 6-OHDA model of PD: behaviour

A unilateral lesion of the nigrostriatal system was introduced by an injection of the neurotoxin 6-OHDA into the MFB. Rats in the transplant group received a transplant of NSPCs into the striatum. Behavioural analysis and [^{123}I]altropane imaging was carried out pre- and post-lesioning and at 1, 2, 3, 4, 6, 7, and 8 weeks after transplantation of the NSPCs.

At the given time points, rats underwent non-drug induced tests (cylinder and PIT tests) prior to [^{123}I]altropane SPECT imaging. Two days after SPECT imaging they were analyzed for drug-induced testing (rotational behaviour). Changes to the SPECT images due to the amphetamine challenge were avoided by performing drug-induced testing after SPECT imaging.

In this model there was a significant correlation between altropane ratios and contralateral paw preference in the cylinder test (Figure 6.4a) and a significant correlation between the altropane ratios and the PIT (Figure 6.4b). There was no significant correlation between the altropane ratios and the rotational behaviour (Figure 6.4c). Linear regression analysis was also performed on the data to determine if there was a strong relationship between the behavioural tests and the altropane fitting a linear model. This analysis showed that there was no strong relationship in the control or transplant group between the cylinder test and the altropane ratio ($r^2 = 0.1770$ and $r^2 = 0.07687$ respectively). Likewise, the analysis showed that there was no strong relationship in the

Figure 6.4. Correlation analysis of behavioural tests with [^{123}I]altropane binding in the striatum. The figure shows the correlation of (A) the altropane ratio and the contralateral paw use preference in the cylinder test ($r = -0.4208$, $n = 42$, $p < 0.05$ for control animals and $r = -0.2772$, $n = 75$, $p < 0.05$ for transplant animals) and (B) the altropane ratio and difference in distance moved between the ipsilateral and contralateral forelimb ($r = -0.5425$, $n = 41$, $p < 0.05$ for control animals and $r = -0.3040$, $n = 73$, $p < 0.05$ for transplant animals) and of (C) the altropane ratio and amphetamine-induced rotations per minute ($r = -0.2403$, $n = 42$, $p > 0.05$ for control animals and $r = -0.1498$, $n = 74$, $p > 0.05$).

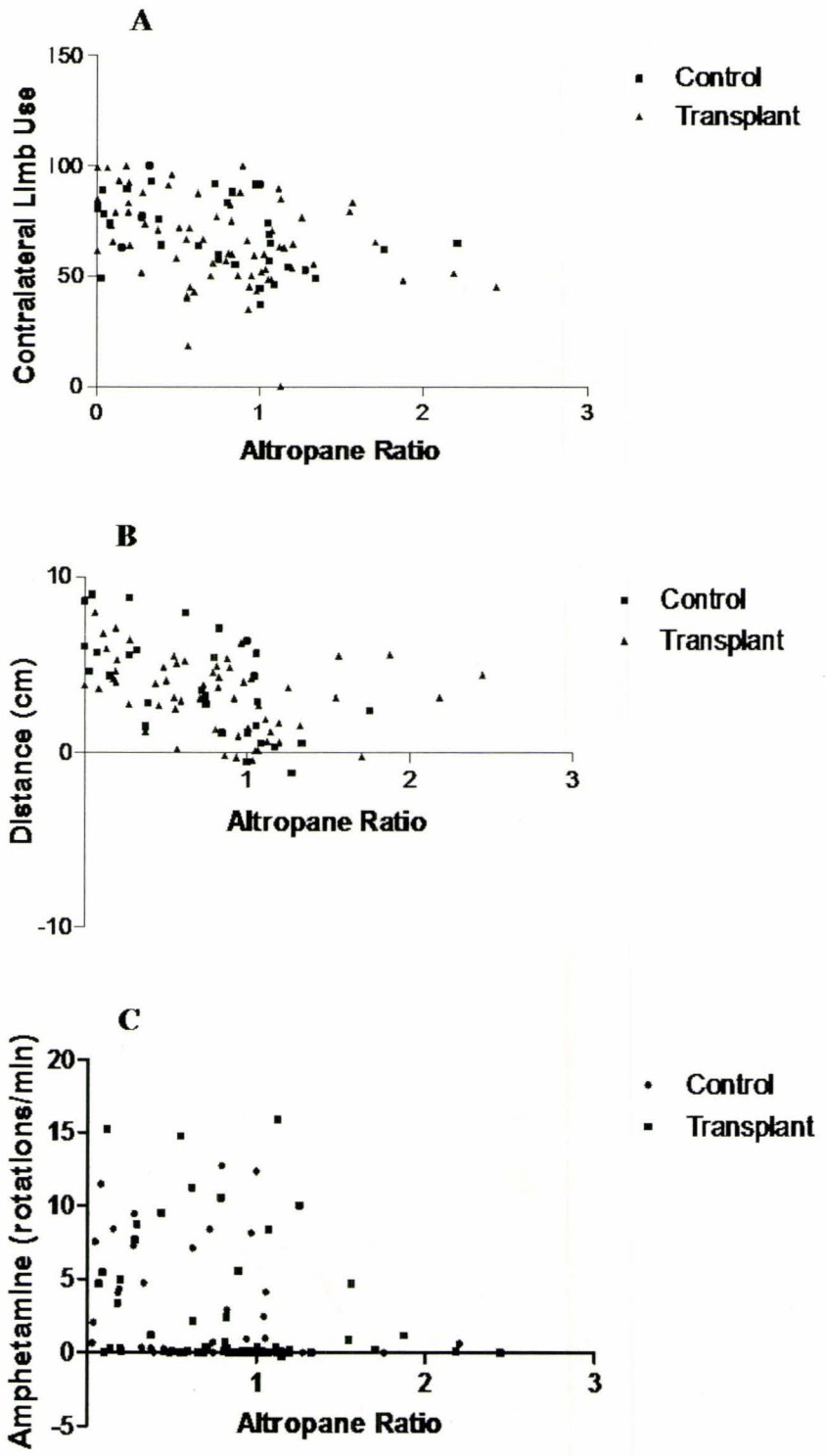
A
Contralateral Limb Use
150
100
50
0
0
1
2
3
Altropane Ratio
Control
Transplant
B
Distance (cm)
10
0
-10
1
2
3
Altropane Ratio
Control
Transplant
C
Amphetamine (rotations/min)
20
15
10
5
0
-5
1
2
3
Altropane Ratio
Control
Transplant

control or transplant group between the PIT and the altropane ratio ($r^2 = 0.2943$ and $r^2 = 0.09240$ respectively).

6.3.5 [^{123}I]altropane SPECT in a 6-OHDA model of PD: histology

At the 8 week post-transplant time point, rats were euthanized and the brains were processed for histological analysis. Cryosections were taken through the SN, striatum, and the transplant site and these sections were stained for the presence of TH. A well defined transplant was not obvious in any of the sections examined from the transplanted animals.

THir was compared with the altropane ratio at the 8 week post-transplant time point. With almost complete lesions, a decrease in TH staining in the right striatum (compared to the left striatum) corresponded to a decrease in the altropane ratio (Figure 6.5b). However, in rats with partial lesions, a decrease in the altropane ratio did not consistently correspond to reduced TH staining in the right striatum compared to the staining in the left striatum (Figure 6.5a). This may be because TH is not specific to DA neurons and therefore may be marking a larger population of neurons than indicated by [^{123}I]altropane.

6.3.6 [^{123}I]altropane SPECT imaging in a 6-OHDA model of PD: changes over time

Changes in the altropane ratio were examined over the duration of the experiments in both control and transplanted groups of animals. There were no

Figure 6.5. Representative images are shown at 8 weeks post-transplantation for the comparison of TH staining in the striatum with [^{123}I]altropane ratios. In (A) there is only a small difference in the DA content between the two striata assessed by TH staining, and there is a minor depletion of the DAT shown by an altropane ratio of 0.75. In (B) there is a marked difference between the intact and lesioned striatum with TH staining and there is a substantial depletion of the DAT shown by an altropane ratio of 0.26. Both animals are control animals.

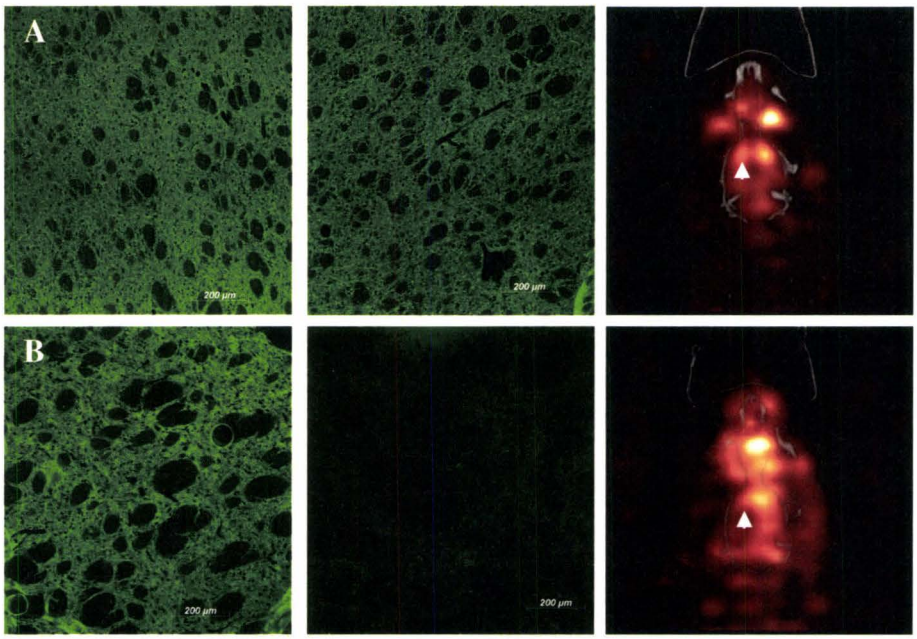
A
200 µm
200 µm
B
200 µm
200 µm

significant changes over time (Figure 6.6), which was expected in the transplant group because we were unable to find an obvious transplant with positive TH staining. Because animals in the control and transplant groups had lesions that ranged from partial to almost complete, this increased the variability in the groups and therefore contributed to the lack of significance when comparing the pre- and post-lesion time points. Due to [^{123}I]altropane availability near the end of the study, the data from week 7 (transplant n = 4, control n = 2) and week 8 (transplant n = 3, control n = 1) were combined because of a low number of animals in these groups.

6.4 Discussion

The present study examined if SPECT imaging with [^{123}I]altropane could be used to monitor disease progression and the therapeutic response in a 6-OHDA model of PD before and after the transplantation of NSPCs. Altropane has been used successfully to image the DAT in non-human primates (Madras *et al.*, 1998b), healthy volunteers and patients with PD (Madras *et al.*, 1998a; Fischman *et al.*, 1998). Imaging the nigrostriatal DA system in small animals has become a feasible approach with the development of small animal SPECT scanners. To this end, DAT imaging agents such as [^{99m}Tc]TRODAT and [^{123}I]FP-CIT have been used to image the DA system in mice and rats (Acton *et al.*, 2002; Scherfler *et al.*, 2002; Andringa *et al.*, 2005; Alvarez-Fischer *et al.*, 2007). To our knowledge, [^{123}I]altropane has not been used to evaluate the DA system in rats.

Figure 6.6. [^{123}I]altropane ratios for control and transplant animals over time. There were no significant changes in the [^{123}I]altropane ratios for either group ($p > 0.05$).

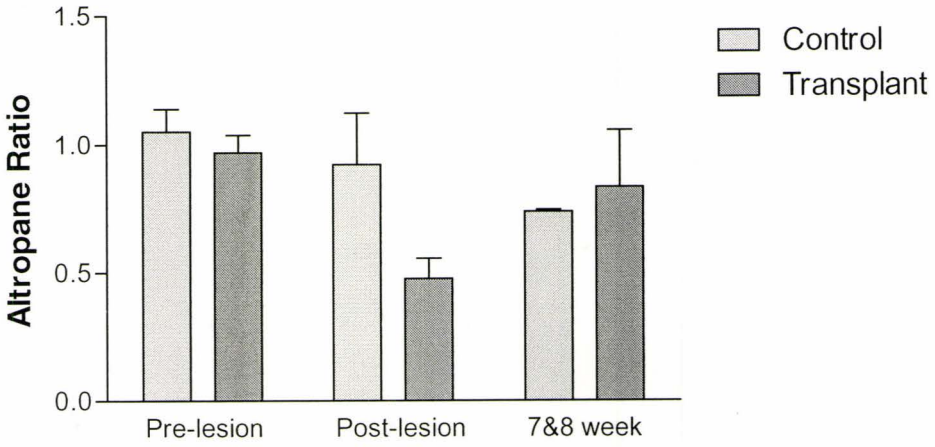
Altropane Ratio
1.5
1.0
0.5
0.0
Pre-lesion
Post-lesion
7&8 week
Control
Transplant

We have demonstrated that [^{123}I]altropane is taken up specifically in the striatum of rats. We correlated altropane ratios to the DA content in the striatum and the SN. There is an excellent correlation of the altropane ratios with the DA content in the striatum, however there was no significant correlation of the altropane ratios with DA content in the SN. This is consistent with findings for [^{123}I]FP-CIT binding ratios in the MPTP mouse model of PD where the authors reported a correlation with the DA content in the striatum, but not with TH positive neurons in the SN (Alvarez-Fischer *et al.*, 2007). In contrast, using the 6-OHDA mouse model, this study found that [^{123}I]FP-CIT binding ratios correlated with DA content in the striatum and TH positive neurons in the SN. Our data supports previous findings in that DAT imaging agents give excellent insight into the degree of denervation in the striatum, but they do not predict the integrity of the nigrostriatal system. Therefore, the results found in this study may impact the use of [^{123}I]altropane in clinical trials, especially those aimed at assessing neuroprotection strategies.

To further evaluate the information that can be derived from [^{123}I]altropane SPECT imaging, we sought to assess whether altropane ratios are predictive of the behavioural outcomes in the 6-OHDA model of PD. Behavioural analyses are commonly used to determine the extent of a lesion and the functional responses to therapy. This method provides an indirect measurement of the lesion size and the effects of a specific therapy; however, it does not give a quantitative assessment on therapeutic efficacy. We found a significant correlation between altropane ratios and the cylinder test and PIT in

both the transplant and control animals. In the rotational behaviour test, there was no significant correlation between altropane ratios and the rotations/min. However, linear regression analysis showed low r^2 values indicating that there is no strong relationship between the altropane ratio and the behavioural tests used in this study. Therefore the altropane ratio is not a good predictor of behavioural outcomes. This also supports our finding that [^{123}I]altropane does not predict the integrity of the nigrostriatal system as functional changes are related to disruption of the nigrostriatal pathway.

In cross-sectional studies in humans with PD, the reduction of [^{123}I]β-CIT correlated with declining clinical scores (Asenbaum *et al.*, 1997; Seibyl *et al.*, 1995). This was demonstrated for both the Hoehn and Yahr test and the Unified Parkinson's Disease Rating Scale (UPDRS). However, longitudinal studies have been unable to show a clear correlation between changes in [^{123}I]β-CIT uptake and the changes in clinical scores (Marek *et al.*, 2001). There were significant correlations between the initial scan and the initial UPDRS score and between the final scan and the final UPDRS score. However, when studied longitudinally, there was no correlation between the annual percentage change in the putamen, the caudate, or the total striatal [^{123}I]β-CIT uptake and the clinical progression measured by either the total or motor UPDRS scores (Marek *et al.*, 2001). This may be because neither the UPDRS scores nor the [^{123}I]β-CIT uptake are linear scales and therefore the rate of change may be differentially dependent on variables of the disease. In addition, UPDRS scores may reflect more general changes in functional status as opposed to [^{123}I]β-CIT binding, which is reflective of only the DA

neuronal integrity. Despite this, DAT ligands provide an objective biomarker of DA degeneration and an objective endpoint for therapeutic trials.

Similar to what is found in clinical trials, in our longitudinal study we found that the altropane ratios were not predictive of functional outcome as assessed by a variety of behavioural tests. This could be because the behavioural tests for the 6-OHDA rat model do not represent DA system degeneration in a linear fashion. In addition, the changes that behavioural tests represent are most likely reflective of changes that are not restricted to the DA nigrostriatal system.

When the altropane ratio was compared to coronal sections stained with TH, there was a decrease in the altropane ratio that corresponded with a decrease in TH staining with rats that showed an almost complete striatal lesion. However, there was no obvious relationship with rats showing a partial lesion. This may be because TH is also the rate limiting step in the production of DOPA, the precursor for DA, which in turn is the precursor for norepinephrine and epinephrine, both of which are found in the striatum. Therefore, TH staining may give an overestimation of DA neurons, whereas altropane gives a more representative assessment of DA levels in the striatum. This is supported by our finding that striatal DA levels correlate with altropane ratios.

When looking at the altropane ratios over time, there was no significant change in either the control or the transplant animals. This is expected in the transplant group

because we were unable to find an obvious transplant that survived the 8 week post-transplantation period. The absence of a transplant may be due to immune rejection of the grafted cells over time or the low number of cells initially injected into the brain.

The efficacy of the transplants may also be affected by the host environment. We transplanted NSPCs as opposed to cells directed into a DAergic phenotype because the microenvironment provided within the graft may support cell survival and DAergic cell fate. It has been reported that type 1 astrocytes from the VM provide trophic support for DA differentiation (Wagner *et al.*, 1999) and they are a major component of the cellular microenvironment for NSCs in the developing and mature brain (Alvarez-Buylla *et al.*, 2000). Astrocytes contribute to neuronal differentiation and survival through direct cell-to-cell interaction and the secretion of various factors (Kirchhoff *et al.*, 2001). Recently, it was shown that degenerating or necrotic striatum releases factors that can also contribute to TH-induction of human NSCs (Anwar *et al.*, 2008). In fact, induction of TH expression from the striatum has been demonstrated both *in vitro* (Ling *et al.*, 1998; Buytaert-Hoefen *et al.*, 2004) and *in vivo* (Bjorklund *et al.*, 2002; Yang *et al.*, 2002). Therefore, the host microenvironment can have a significant influence on the survival of the graft and on the DAergic differentiation of the cells within the graft.

Although we were unable to determine if altropane ratios were able to predict DA replacement in the striatum, our findings in this study support previous findings with [^{123}I]FP-CIT. Alvarez-Fischer *et al.* (2007) found that binding did not significantly

correlate with cell number in the SN. We also did not find a significant correlation between [^{123}I]altropane binding and SN DA content. In line with this result, we did not find a strong relationship between the altropane ratio and the behavioural tests indicative of function. This indicates that [^{123}I]altropane, and perhaps other DAT ligands, do not predict the integrity of the nigrostriatal system.

6.5 Conclusion

To summarize, our results strengthen the argument that DAT ligands can be used to predict the functional integrity of DA terminals in the striatum (Scherfler *et al.*, 2002; Andringa *et al.*, 2005; Alvarez-Fischer *et al.*, 2007). However, they also indicate that the interpretation of data from SPECT images of [^{123}I]altropane should be viewed in light of the fact that they may not indicate the integrity of the nigrostriatal system. This is important in efforts to use DAT imaging agents as a method to evaluate neuroprotective therapies.

Chapter 7: Future Directions

The purpose of this thesis was to develop a method to standardize transplant parameters and monitor the DA system using SPECT. Utilizing the radioactive tracer ^{99m}Tc-SAACQ, the number of transplanted cells can be determined. Previous studies report that differences in cell number affect the ability of the graft to integrate into the host striatum and subsequently affect the functional outcomes of the cell therapy (Terpstra *et al.*, 2007; Nikkhah *et al.*, 2009). This indicates that there are a threshold number of cells that must be transplanted in order to produce an effective treatment option. The ^{99m}Tc-SAACQ cell label used in this study represents a method to determine if sufficient quantities of cells have been transplanted.

Monitoring the DA system post-transplant using [^{123}I]altropane may predict the functional outcome based on the image acquired. We determined that [^{123}I]altropane does not provide information about the integrity of the nigrostriatal pathway; however, cell transplants are generally placed in the striatum and the connections between the SN and the striatum are not investigated. Our study demonstrated that [^{123}I]altropane does predict the DA content in the striatum. Since increasing the striatal DA content is the goal of cell transplantation [^{123}I]altropane may be an appropriate marker for the efficacy of cell therapy.

The present study found a significant decrease in cell proliferation when the cells were labeled with ^{99m}Tc-SAACQ. To determine whether the decrease is due to slowing

of the cell cycle while DNA repair occurs, cell death, or a temporary slowing of the cell cycle proliferation, viability and DNA integrity should be assessed at different time points. It would useful to assess viability and DNA damage at earlier time points and in combination with proliferation at longer time points in similar studies. This would provide a more complete picture of cell cycle patterns in the labeled cells. In addition, a trend towards neuronal differentiation was observed. It would be useful to characterize the differentiated labeled neurons in comparison to control neurons. This could be accomplished using neuronal markers to characterize the types of neurons differentiating *in vitro*.

In order to pursue the potential of this technology further, higher numbers of cells need to be transplanted to enhance the survival of the graft. By decreasing the amount of activity for the initial labeling, more cells could be labeled for transplantation. However, using a lower initial activity would require additional studies on the possible adverse biological effects. Because the viability and the amount of DNA damage were not altered in this study, it is unlikely that a lower amount of incubation activity will affect the NSPCs in this way. The proliferative capacity and differentiation of the cells will also need to be assessed at a lower initial labeling activity and compared to the changes seen with the initial labeling activity used in the present study.

This study did not see survival of the transplanted NSPCs. This could be due to immune rejection of the cells, the low number of cells transplanted, or the location of the

transplant. Transplanting a larger number of cells in multiple locations in the striatum may increase cell survival and functional outcome. The resulting graft should be assessed in terms of the ability to adopt a DAergic fate, integrate into the host striatum, and form functional synaptic connections. Standard immunostaining and slice culture electrophysiology could be used to probe these questions.

Finally, the use of [^{123}I]altropane to monitor the functional outcome of the grafted cells need to be established. This will be accomplished by using different transplant parameters as described above in order to determine the optimal conditions. The [^{123}I]altropane image should be correlated to striatal DA content, and the number of DAergic neurons as determined by histology. Comparing the [^{123}I]altropane image with various behavioural tests would also be of interest to determine if replacing striatal DA through transplantation correlates with functional outcome when DA is replaced in the striatum. Continuing efforts to define optimal transplant parameters will provide information that standard diagnostic techniques cannot generate and further develop this form of cell therapy for the treatment of PD.

Appendix 1: Reference Tissue Model

The reference tissue model is derived from the compartmental model that uses a reference tissue time activity curve (TAC) as an input in place of plasma input. A typical compartmental model for ligand-receptor kinetics is shown in Figure 1a and this fits the reversible tracer kinetics for both the target and reference tissues (Lammertsma *et al.*, 1996). The tracer kinetics of this model are based on the following assumptions: (1) there is rapid equilibrium between the free and non-specific binding of the tracer in the target tissue; (2) the concentration of the tracer is the same in the vascular space (C_P), free plus non-specific compartment (C_{F+NS}), and the specific compartment (C_S) for the target tissue, and in the free and free plus non-specific compartment (C_F and C_{F+NS}) for the reference tissue; and (3) the transport of the tracer follows first order kinetics. The reference tissue model assumes that the tracer contribution from the vascular space is negligible. Therefore, $C_T=C_{F+NS}+C_S$ and $C_R=C_F+C_{NS}$ where C_T and C_R are the concentrations of the tracer measured in the target and reference tissues respectively (Zhou *et al.*, 2007).

A common way to measure tracer binding kinetics is the distribution volume (DV). The tracer DV in the tissue is defined as the ratio of the tracer concentration in the target tissue to the tracer concentration in the plasma at equilibrium (Zhou *et al.*, 2007). A key assumption in the reference tissue model is that the DV in the free plus nonspecific

binding compartment is the same in the reference tissue and the target tissue. The binding potential (BP) is equal to the DV_T/DV_R-1=DVR-1.

The kinetics of the tracer from C_P to the tissue are determined by the rate constants K_1 and k_2. The ratio of K_1 to k_2 represents the DV. By assuming that the DV is constant across brain regions, C_P can be represented by the tracer kinetics from an alternate region, the reference tissue. The DVR or BP can be estimated directly using the reference tissue TAC as the input (Morris *et al.*, 2004).

The compartmental model in Figure 1.1a can be simplified by assuming there is rapid equilibrium between free and nonspecific binding in the reference tissue and there is rapid equilibrium between the free plus nonspecific binding in the target tissue. This allows the target tissue and the reference tissue to be modeled as single compartments (Figure 1.1b).

The simplified Logan plot with reference tissue analysis is used in this study to estimate the DVR and therefore the BP (BP=DVR-1).

$$\int_0^T C_T(t)dt/C_T(T) = DVR\{\int_0^T C_R(t)dt/C_T(T)\} + int \text{ (Logan } et\ al.\text{, 1996)}$$

DVR is estimated from the slope of the best fit line and used to estimate the binding potential. Representative images of [^{123}I]altropane images are shown with the corresponding binding potential as assessed by Logan analysis (Figure 1.2).

Figure 1.1. (A) A representative 2 compartment model used for receptor-ligand studies. (B) Simplified 2 compartment model that assumes the target tissue and reference tissues as single compartments.

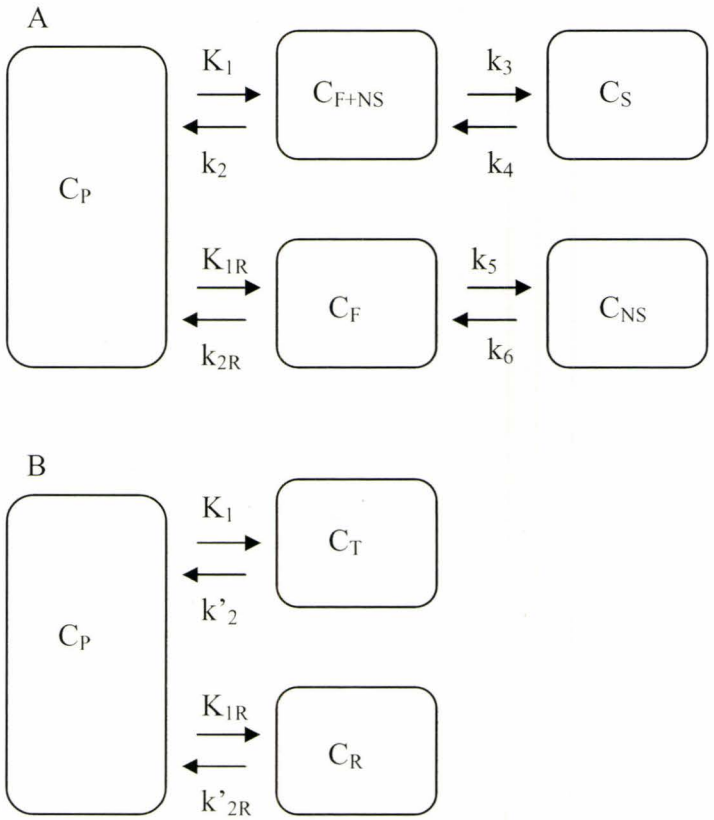
A
K_1
k_2
C_{F+NS}
k_3
k_4
C_S
C_P
K_{1R}
k_{2R}
C_F
k_5
k_6
C_{NS}
B
K_1
k'_2
C_T
C_P
K_{1R}
k'_{2R}
C_R

Figure 1.2. Representative [^{123}I]altropane SPECT images of rats 2 weeks post-lesion. (A) A partial lesion is shown. Logan analysis determines the binding potential to be 0.775 in the left striatum and -0.050 in the right striatum. (B) For a near complete lesion, Logan analysis determines the binding potential to be 0.346 in the left striatum and -0.204 in the right striatum. The right side of the animal is marked by a vial of pertechnetate corresponding to the bright signal seen on the lower right side of the image.

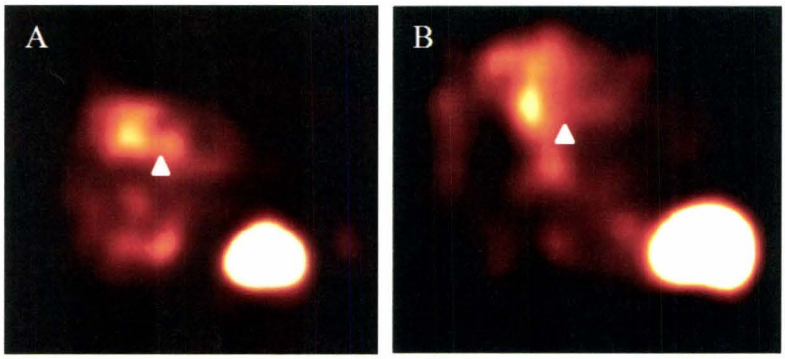
A
B

Appendix 2: Imaging with [^{18}F]FMT and [^{99m}Tc]TRODAT

SPECT imaging of the head of the animal was done using a low-energy, high resolution collimator over 64 angles around the head (32 angles per detector with 40 second projections). Projection data was reconstructed using OSEM iterative reconstruction with detector response compensation. A total of two iterations with eight subsets were used and reconstructed images were filtered with a 3D Gaussian filter with FWHM of 2 mm.

Accurate positioning of the rat brain was determined using the CT component of the X-SPECT system which has a flat panel detector FOV of 10cm x 10cm. CT information was acquired using 75-kVp X-rays, and a tube current of 265 μA with a spot size of 50 μm. 512 projections were acquired over 360° and reconstructed with a modified FeldKamp cone-beam reconstruction (Cobra-Exxim version 6.0). The resulting image had a matrix of 256 x 256 x 256 and a reconstructed voxel size of 155μm.

[^{18}F]FMT imaging was done using a Philips Mosaic Small Animal PET system (Cleveland, Ohio, USA). A 30 minute scan was acquired 60 minutes post-injection of the [^{18}F]FMT (injection was done without the use of anesthetic). For anatomical co-registration, a CT scan was acquired using the X-SPECT system as described above.

Despite different time points and different amounts of activity injected and injecting the tracers with and without Isoflurane, we were unable to consistently visualize the striatum of the normal rats with either tracer (Figure 2.1). [^{123}I]altropane allowed us to visualize the DAT in the striatum and therefore was used for the remainder of this study.

Figure 2.1. (A) [^{99m}Tc]TRODAT SPECT/CT image in a normal rat. Approximately 148 MBq of activity was injected via the tail vein. Possible uptake in the striatum is marked by an arrow. (B) [^{18}F]FMT PET/CT image of the striatum of a normal rat. Approximately 32.9 MBq of activity was administered via the tail-vein. The rat was injected without an anesthetic and was imaged 60 minutes post-injection.

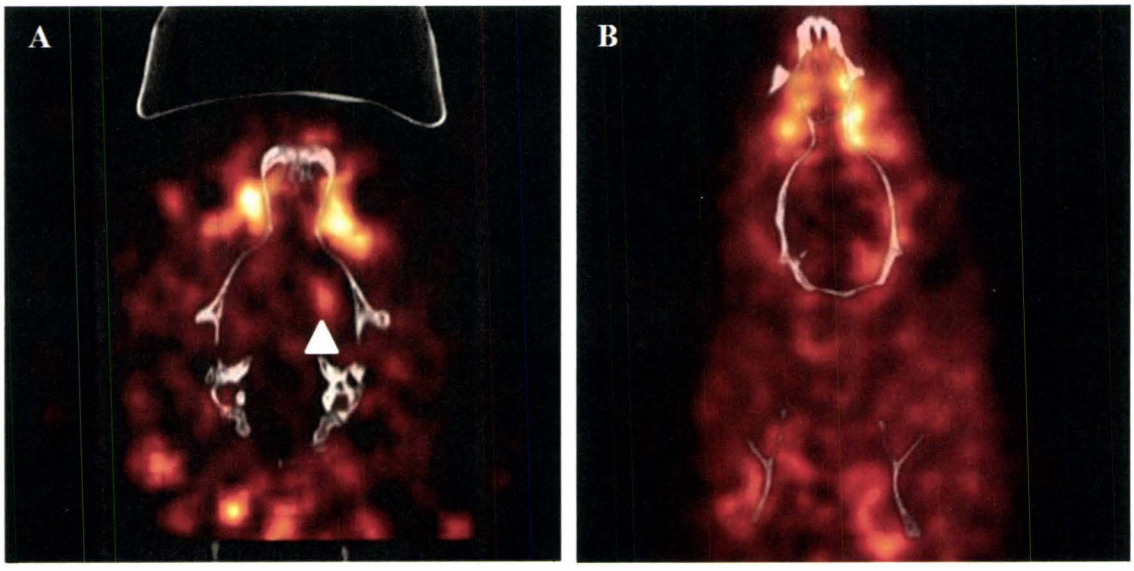
A
B

References

1. Aarsland D, Tandberg E, Larsen JP, Cummings JL (1996) Frequency of dementia in Parkinson disease. Arch Neurol 53:538-542.

2. Abi-Dargham A, Gandelman MS, DeErausquin GA, Zea-Ponce Y, Zoghbi SS, Baldwin RM, Laruelle M, Charney DS, Hoffer PB, Neumeyer JL, Innis RB (1996) SPECT imaging of dopamine transporters in human brain with iodine-123-fluoroalkyl analogs of beta-CIT. J Nucl Med 37:1129-1133.

3. Acton PD, Choi SR, Plossl K, Kung HF (2002) Quantification of dopamine transporters in the mouse brain using ultra-high resolution single-photon emission tomography. Eur J Nucl Med Mol Imaging 29:691-698.

4. Ader M, Schachner M, Bartsch U (2004) Integration and differentiation of neural stem cells after transplantation into the dysmyelinated central nervous system of adult mice. Eur J Neurosci 20:1205-1210.

5. Ahlenius H, Visan V, Kokaia M, Lindvall O, Kokaia Z (2009) Neural stem and progenitor cells retain their potential for proliferation and differentiation into functional neurons despite lower number in aged brain. J Neurosci 29:4408-4419.

6. Ahlskog JE, Kelly PJ, van Heerden JA, Stoddard SL, Tyce GM, Windebank AJ, Bailey PA, Bell GN, Blexrud MD, Carmichael SW (1990) Adrenal medullary transplantation into the brain for treatment of Parkinson's disease: clinical outcome and neurochemical studies. Mayo Clin Proc 65:305-328.

7. Aicher A, Brenner W, Zuhayra M, Badorff C, Massoudi S, Assmus B, Eckey T, Henze E, Zeiher AM, Dimmeler S (2003) Assessment of the tissue distribution of transplanted human endothelial progenitor cells by radioactive labeling. Circulation 107:2134-2139.

8. Ak I, Vardereli E, Durak B, Gulbas Z, Basaran N, Stokkel MP, Pauwels EK (2002) Labeling of mixed leukocytes with (99m)Tc-HMPAO causes severe chromosomal aberrations in lymphocytes. J Nucl Med 43:203-206.

9. Alvarez-Buylla A, Herrera DG, Wichterle H (2000) The subventricular zone: source of neuronal precursors for brain repair. Prog Brain Res 127:1-11.

10. Alvarez-Fischer D, Blessmann G, Trosowski C, Behe M, Schurrat T, Hartmann A, Behr TM, Oertel WH, Hoglinger GU, Hoffken H (2007) Quantitative [(123)I]FP-CIT pinhole SPECT imaging predicts striatal dopamine levels, but not number of nigral neurons in different mouse models of Parkinson's disease. Neuroimage 38:5-12.

11. Andringa G, Drukarch B, Bol JG, de Bruin K, Sorman K, Habraken JB, Booij J (2005) Pinhole SPECT imaging of dopamine transporters correlates with dopamine transporter immunohistochemical analysis in the MPTP mouse model of Parkinson's disease. Neuroimage 26:1150-1158.

12. Anwar MR, Andreasen CM, Lippert SK, Zimmer J, Martinez-Serrano A, Meyer M (2008) Dopaminergic differentiation of human neural stem cells mediated by co-cultured rat striatal brain slices. J Neurochem 105:460-470.

13. Aponso PM, Faull RL, Connor B (2008) Increased progenitor cell proliferation and astrogenesis in the partial progressive 6-hydroxydopamine model of Parkinson's disease. Neuroscience 151:1142-1153.

14. Arjona V, Minguez-Castellanos A, Montoro RJ, Ortega A, Escamilla F, Toledo-Aral JJ, Pardal R, Mendez-Ferrer S, Martin JM, Perez M, Katati MJ, Valencia E, Garcia T, Lopez-Barneo J (2003) Autotransplantation of human carotid body cell aggregates for treatment of Parkinson's disease. Neurosurgery 53:321-328.

15. Armstrong RJ, Tyers P, Jain M, Richards A, Dunnett SB, Rosser AE, Barker RA (2003) Transplantation of expanded neural precursor cells from the developing pig ventral mesencephalon in a rat model of Parkinson's disease. Exp Brain Res 151:204-217.

16. Asenbaum S, Brucke T, Pirker W, Podreka I, Angelberger P, Wenger S, Wober C, Muller C, Deecke L (1997) Imaging of dopamine transporters with iodine-123-beta-CIT and SPECT in Parkinson's disease. J Nucl Med 38:1-6.

17. Bai J, Ding W, Yu M, Du J, Liu Z, Jia B, Li L, Shen L, Tian J, Wang F (2004) Radionuclide imaging of mesenchymal stem cells transplanted into spinal cord. Neuroreport 15:1117-1120.

18. Banerjee SR, Levadala MK, Lazarova N, Wei L, Valliant JF, Stephenson KA, Babich JW, Maresca KP, Zubieta J (2002) Bifunctional single amino acid chelates for labeling of biomolecules with the [Tc(CO)(3)](+) and [Re(CO)(3)](+) cores. Crystal and molecular structures of [ReBr(CO)(3)(H(2)NCH(2)C(5)H(4)N)], [Re(CO)(3)[(C(5)H(4)NCH(2))(2)NH]]Br, [Re(CO)(3)[(C(5)H(4)NCH(2))(2)NCH(2)CO(2)H]]Br, [Re(CO)(3)[X(Y)NCH(2)CO(2)CH(2)CH(3)]]Br (X = Y = 2-pyridylmethyl; X = 2-pyridylmethyl, Y = 2-(1-methylimidazolyl)methyl; X = Y = 2-(1-methylimidazolyl)methyl), [ReBr(CO)(3)[(C(5)H(4)NCH(2))NH(CH(2)C(4)H(3)S)]], and [Re(CO)(3)[(C(5)H(4)NCH(2))N(CH(2)C(4)H(3)S)(CH(2)CO(2))]]. Inorg Chem 41:6417-6425.

19. Banks WA, Robinson SM, Nath A (2005) Permeability of the blood-brain barrier to HIV-1 Tat. Exp Neurol 193:218-227.

20. Barrio JR, Huang SC, Yu DC, Melega WP, Quintana J, Cherry SR, Jacobson A, Namavari M, Satyamurthy N, Phelps ME (1996) Radiofluorinated L-m-tyrosines: new in-vivo probes for central dopamine biochemistry. J Cereb Blood Flow Metab 16:667-678.

21. Benamer TS, *et al.* (2000) Accurate differentiation of parkinsonism and essential tremor using visual assessment of [123I]-FP-CIT SPECT imaging: the [123I]-FP-CIT study group. Mov Disord 15:503-510.

22. Benninger F, Beck H, Wernig M, Tucker KL, Brustle O, Scheffler B (2003) Functional integration of embryonic stem cell-derived neurons in hippocampal slice cultures. J Neurosci 23:7075-7083.

23. Bhorade R, Weissleder R, Nakakoshi T, Moore A, Tung CH (2000) Macrocyclic chelators with paramagnetic cations are internalized into mammalian cells via a HIV-tat derived membrane translocation peptide. Bioconjug Chem 11:301-305.

24. Bjorklund A, Schmidt RH, Stenevi U (1980) Functional reinnervation of the neostriatum in the adult rat by use of intraparenchymal grafting of dissociated cell suspensions from the substantia nigra. Cell Tissue Res 212:39-45.

25. Bjorklund A, Stenevi U (1979) Reconstruction of the nigrostriatal dopamine pathway by intracerebral nigral transplants. Brain Res 177:555-560.

26. Bjorklund LM, Sanchez-Pernaute R, Chung S, Andersson T, Chen IY, McNaught KS, Brownell AL, Jenkins BG, Wahlestedt C, Kim KS, Isacson O (2002) Embryonic stem cells develop into functional dopaminergic neurons after transplantation in a Parkinson rat model. Proc Natl Acad Sci U S A 99:2344-2349.

27. Bjugstad KB, Teng YD, Redmond DE, Jr., Elsworth JD, Roth RH, Cornelius SK, Snyder EY, Sladek JR, Jr. (2008) Human neural stem cells migrate along the nigrostriatal pathway in a primate model of Parkinson's disease. Exp Neurol 211:362-369.

28. Blackwood KJ, Lewden B, Wells RG, Sykes J, Stodilka RZ, Wisenberg G, Prato FS (2009) In vivo SPECT quantification of transplanted cell survival after engraftment using (111)In-tropolone in infarcted canine myocardium. J Nucl Med 50:927-935.

29. Blum D, Torch S, Lambeng N, Nissou M, Benabid AL, Sadoul R, Verna JM (2001) Molecular pathways involved in the neurotoxicity of 6-OHDA, dopamine

and MPTP: contribution to the apoptotic theory in Parkinson's disease. Prog Neurobiol 65:135-172.

30. Booij J, Tissingh G, Winogrodzka A, Boer GJ, Stoof JC, Wolters EC, van Royen EA (1997) Practical benefit of [123I]FP-CIT SPET in the demonstration of the dopaminergic deficit in Parkinson's disease. Eur J Nucl Med 24:68-71.

31. Brazel CY, Limke TL, Osborne JK, Miura T, Cai J, Pevny L, Rao MS (2005) Sox2 expression defines a heterogeneous population of neurosphere-forming cells in the adult murine brain. Aging Cell 4:197-207.

32. Buchegger F, Perillo-Adamer F, Dupertuis YM, Delaloye AB (2006) Auger radiation targeted into DNA: a therapy perspective. Eur J Nucl Med Mol Imaging 33:1352-1363.

33. Bull ND, Bartlett PF (2005) The adult mouse hippocampal progenitor is neurogenic but not a stem cell. J Neurosci 25:10815-10821.

34. Bullok KE, Dyszlewski M, Prior JL, Pica CM, Sharma V, Piwnica-Worms D (2002) Characterization of novel histidine-tagged Tat-peptide complexes dual-labeled with (99m)Tc-tricarbonyl and fluorescein for scintigraphy and fluorescence microscopy. Bioconjug Chem 13:1226-1237.

35. Bussell R, Jr., Eliezer D (2001) Residual structure and dynamics in Parkinson's disease-associated mutants of alpha-synuclein. J Biol Chem 276:45996-46003.

36. Buytaert-Hoefen KA, Alvarez E, Freed CR (2004) Generation of tyrosine hydroxylase positive neurons from human embryonic stem cells after coculture with cellular substrates and exposure to GDNF. Stem Cells 22:669-674.

37. Cadet JL, Brannock C (1998) Free radicals and the pathobiology of brain dopamine systems. Neurochem Int 32:117-131.

38. Cameron HA, Woolley CS, McEwen BS, Gould E (1993) Differentiation of newly born neurons and glia in the dentate gyrus of the adult rat. Neuroscience 56:337-344.

39. Chang JW, Wachtel SR, Young D, Kang UJ (1999) Biochemical and anatomical characterization of forepaw adjusting steps in rat models of Parkinson's disease: studies on medial forebrain bundle and striatal lesions. Neuroscience 88:617-628.

40. Chapuis S, Ouchchane L, Metz O, Gerbaud L, Durif F (2005) Impact of the motor complications of Parkinson's disease on the quality of life. Mov Disord 20:224-230.

41. Chianelli M, Signore A, Fritzberg AR, Mather SJ (1997) The development of technetium-99m-labelled interleukin-2: a new radiopharmaceutical for the in vivo detection of mononuclear cell infiltrates in immune-mediated diseases. Nucl Med Biol 24:579-586.

42. Chiasson BJ, Tropepe V, Morshead CM, van der Kooy D (1999) Adult mammalian forebrain ependymal and subependymal cells demonstrate proliferative potential, but only subependymal cells have neural stem cell characteristics. J Neurosci 19:4462-4471.

43. Chin BB, Nakamoto Y, Bulte JW, Pittenger MF, Wahl R, Kraitchman DL (2003) 111In oxine labelled mesenchymal stem cell SPECT after intravenous administration in myocardial infarction. Nucl Med Commun 24:1149-1154.

44. Choi WS, Yoon SY, Oh TH, Choi EJ, O'Malley KL, Oh YJ (1999) Two distinct mechanisms are involved in 6-hydroxydopamine- and MPP+-induced dopaminergic neuronal cell death: role of caspases, ROS, and JNK. J Neurosci Res 57:86-94.

45. Chojnacki A, Weiss S (2008) Production of neurons, astrocytes and oligodendrocytes from mammalian CNS stem cells. Nat Protoc 3:935-940.

46. Cohen G (1984) Oxy-radical toxicity in catecholamine neurons. Neurotoxicology 5:77-82.

47. Conti L, Pollard SM, Gorba T, Reitano E, Toselli M, Biella G, Sun Y, Sanzone S, Ying QL, Cattaneo E, Smith A (2005) Niche-independent symmetrical self-renewal of a mammalian tissue stem cell. PLoS Biol 3:e283.

48. Copray S, Balasubramaniyan V, Levenga J, de BJ, Liem R, Boddeke E (2006) Olig2 overexpression induces the in vitro differentiation of neural stem cells into mature oligodendrocytes. Stem Cells 24:1001-1010.

49. Damier P, Hirsch EC, Zhang P, Agid Y, Javoy-Agid F (1993) Glutathione peroxidase, glial cells and Parkinson's disease. Neuroscience 52:1-6.

50. Date I, Asari S, Ohmoto T (1995) Two-year follow-up study of a patient with Parkinson's disease and severe motor fluctuations treated by co-grafts of adrenal medulla and peripheral nerve into bilateral caudate nuclei: case report. Neurosurgery 37:515-518.

51. Date I, Imaoka T, Miyoshi Y, Ono T, Asari S, Ohmoto T (1996) Chromaffin cell survival and host dopaminergic fiber recovery in a patient with Parkinson's disease treated by cografts of adrenal medulla and pretransected peripheral nerve. Case report. J Neurosurg 84:685-689.

52. Date I, Yoshimoto Y, Imaoka T, Miyoshi Y, Furuta T, Asari S, Ohmoto T (1994) Cografts of adrenal medulla with peripheral nerve for Parkinson's disease. Cell Transplant 3 Suppl 1:S47-S49.

53. Dauer W, Przedborski S (2003) Parkinson's disease: mechanisms and models. Neuron 39:889-909.

54. Dawson TM, Dawson VL (2003) Molecular pathways of neurodegeneration in Parkinson's disease. Science 302:819-822.

55. de Vries IJ, Lesterhuis WJ, Barentsz JO, Verdijk P, van Krieken JH, Boerman OC, Oyen WJ, Bonenkamp JJ, Boezeman JB, Adema GJ, Bulte JW, Scheenen TW, Punt CJ, Heerschap A, Figdor CG (2005) Magnetic resonance tracking of dendritic cells in melanoma patients for monitoring of cellular therapy. Nat Biotechnol 23:1407-1413.

56. DeJesus OT, Endres CJ, Shelton SE, Nickles RJ, Holden JE (1997) Evaluation of fluorinated m-tyrosine analogs as PET imaging agents of dopamine nerve terminals: comparison with 6-fluoroDOPA. J Nucl Med 38:630-636.

57. Deumens R, Blokland A, Prickaerts J (2002) Modeling Parkinson's disease in rats: an evaluation of 6-OHDA lesions of the nigrostriatal pathway. Exp Neurol 175:303-317.

58. Doetsch F, Caille I, Lim DA, Garcia-Verdugo JM, Alvarez-Buylla A (1999a) Subventricular zone astrocytes are neural stem cells in the adult mammalian brain. Cell 97:703-716.

59. Doetsch F, Garcia-Verdugo JM, Alvarez-Buylla A (1997) Cellular composition and three-dimensional organization of the subventricular germinal zone in the adult mammalian brain. J Neurosci 17:5046-5061.

60. Doetsch F, Garcia-Verdugo JM, Alvarez-Buylla A (1999b) Regeneration of a germinal layer in the adult mammalian brain. Proc Natl Acad Sci U S A 96:11619-11624.

61. Doudet DJ, Chan GL, Jivan S, DeJesus OT, McGeer EG, English C, Ruth TJ, Holden JE (1999) Evaluation of dopaminergic presynaptic integrity: 6-[18F]fluoro-L-dopa versus 6-[18F]fluoro-L-m-tyrosine. J Cereb Blood Flow Metab 19:278-287.

62. Dromard C, Bartolami S, Deleyrolle L, Takebayashi H, Ripoll C, Simonneau L, Prome S, Puech S, Tran VB, Duperray C, Valmier J, Privat A, Hugnot JP (2007) NG2 and Olig2 expression provides evidence for phenotypic deregulation of

cultured central nervous system and peripheral nervous system neural precursor cells. Stem Cells 25:340-353.

63. Dunnett SB, Bjorklund A, Schmidt RH, Stenevi U, Iversen SD (1983) Intracerebral grafting of neuronal cell suspensions. IV. Behavioural recovery in rats with unilateral 6-OHDA lesions following implantation of nigral cell suspensions in different forebrain sites. Acta Physiol Scand Suppl 522:29-37.

64. Dunnett SB, Bjorklund A, Stenevi U, Iversen SD (1981) Behavioural recovery following transplantation of substantia nigra in rats subjected to 6-OHDA lesions of the nigrostriatal pathway. I. Unilateral lesions. Brain Res 215:147-161.

65. Elmaleh DR, Fischman AJ, Shoup TM, Byon C, Hanson RN, Liang AY, Meltzer PC, Madras BK (1996) Preparation and biological evaluation of iodine-125-IACFT: a selective SPECT agent for imaging dopamine transporter sites. J Nucl Med 37:1197-1202.

66. Erickson RI, Paucar AA, Jackson RL, Visnyei K, Kornblum H (2008) Roles of insulin and transferrin in neural progenitor survival and proliferation. J Neurosci Res 86:1884-1894.

67. Eriksson C, Bjorklund A, Wictorin K (2003) Neuronal differentiation following transplantation of expanded mouse neurosphere cultures derived from different embryonic forebrain regions. Exp Neurol 184:615-635.

68. Espejo EF, Montoro RJ, Armengol JA, Lopez-Barneo J (1998) Cellular and functional recovery of Parkinsonian rats after intrastriatal transplantation of carotid body cell aggregates. Neuron 20:197-206.

69. Falkenstein G, Rosenthal C, Reum T, Morgenstern R, Dobrossy M, Nikkhah G (2009) Pattern of long-term sensorimotor recovery following intrastriatal and--accumbens DA micrografts in a rat model of Parkinson's disease. J Comp Neurol 515:41-55.

70. Faraggi M, Gardin I, de Labriolle-Vaylet C, Moretti JL, Bok BD (1994) The influence of tracer localization on the electron dose rate delivered to the cell nucleus. J Nucl Med 35:113-119.

71. Fernandez HH, Friedman JH, Fischman AJ, Noto RB, Lannon MC (2001) Is altropane SPECT more sensitive to fluoroDOPA PET for detecting early Parkinson's disease? Med Sci Monit 7:1339-1343.

72. Fischman AJ, Babich JW, Elmaleh DR, Barrow SA, Meltzer P, Hanson RN, Madras BK (1997) SPECT imaging of dopamine transporter sites in normal and MPTP-Treated rhesus monkeys. J Nucl Med 38:144-150.

73. Fischman AJ, Bonab AA, Babich JW, Palmer EP, Alpert NM, Elmaleh DR, Callahan RJ, Barrow SA, Graham W, Meltzer PC, Hanson RN, Madras BK (1998) Rapid detection of Parkinson's disease by SPECT with altropane: a selective ligand for dopamine transporters. Synapse 29:128-141.

74. Flax JD, Aurora S, Yang C, Simonin C, Wills AM, Billinghurst LL, Jendoubi M, Sidman RL, Wolfe JH, Kim SU, Snyder EY (1998) Engraftable human neural stem cells respond to developmental cues, replace neurons, and express foreign genes. Nat Biotechnol 16:1033-1039.

75. Ford JW, Welling TH, III, Stanley JC, Messina LM (1996) PKH26 and 125I-PKH95: characterization and efficacy as labels for in vitro and in vivo endothelial cell localization and tracking. J Surg Res 62:23-28.

76. Frankel AD, Pabo CO (1988) Cellular uptake of the tat protein from human immunodeficiency virus. Cell 55:1189-1193.

77. Freed CR, Greene PE, Breeze RE, Tsai WY, DuMouchel W, Kao R, Dillon S, Winfield H, Culver S, Trojanowski JQ, Eidelberg D, Fahn S (2001) Transplantation of embryonic dopamine neurons for severe Parkinson's disease. N Engl J Med 344:710-719.

78. Fricker RA, Carpenter MK, Winkler C, Greco C, Gates MA, Bjorklund A (1999) Site-specific migration and neuronal differentiation of human neural progenitor cells after transplantation in the adult rat brain. J Neurosci 19:5990-6005.

79. Futaki S, Suzuki T, Ohashi W, Yagami T, Tanaka S, Ueda K, Sugiura Y (2001) Arginine-rich peptides. An abundant source of membrane-permeable peptides having potential as carriers for intracellular protein delivery. J Biol Chem 276:5836-5840.

80. Gage FH, Coates PW, Palmer TD, Kuhn HG, Fisher LJ, Suhonen JO, Peterson DA, Suhr ST, Ray J (1995) Survival and differentiation of adult neuronal progenitor cells transplanted to the adult brain. Proc Natl Acad Sci U S A 92:11879-11883.

81. Gammon ST, Villalobos VM, Prior JL, Sharma V, Piwnica-Worms D (2003) Quantitative analysis of permeation peptide complexes labeled with Technetium-99m: chiral and sequence-specific effects on net cell uptake. Bioconjug Chem 14:368-376.

82. Ganat YM, Silbereis J, Cave C, Ngu H, Anderson GM, Ohkubo Y, Ment LR, Vaccarino FM (2006) Early postnatal astroglial cells produce multilineage precursors and neural stem cells in vivo. J Neurosci 26:8609-8621.

83. Garcia AD, Doan NB, Imura T, Bush TG, Sofroniew MV (2004) GFAP-expressing progenitors are the principal source of constitutive neurogenesis in adult mouse forebrain. Nat Neurosci 7:1233-1241.

84. Gerlach M, Ben-Shachar D, Riederer P, Youdim MB (1994) Altered brain metabolism of iron as a cause of neurodegenerative diseases? J Neurochem 63:793-807.

85. Giasson BI, Duda JE, Murray IV, Chen Q, Souza JM, Hurtig HI, Ischiropoulos H, Trojanowski JQ, Lee VM (2000) Oxidative damage linked to neurodegeneration by selective alpha-synuclein nitration in synucleinopathy lesions. Science 290:985-989.

86. Glinka YY, Youdim MB (1995) Inhibition of mitochondrial complexes I and IV by 6-hydroxydopamine. Eur J Pharmacol 292:329-332.

87. Goetz CG, Stebbins GT, III, Klawans HL, Koller WC, Grossman RG, Bakay RA, Penn RD (1991) United Parkinson Foundation Neurotransplantation Registry on adrenal medullary transplants: presurgical, and 1- and 2-year follow-up. Neurology 41:1719-1722.

88. Goldman S (2005) Stem and progenitor cell-based therapy of the human central nervous system. Nat Biotechnol 23:862-871.

89. Graham DG, Tiffany SM, Bell WR, Jr., Gutknecht WF (1978) Autoxidation versus covalent binding of quinones as the mechanism of toxicity of dopamine, 6-hydroxydopamine, and related compounds toward C1300 neuroblastoma cells in vitro. Mol Pharmacol 14:644-653.

90. Greenamyre JT, Sherer TB, Betarbet R, Panov AV (2001) Complex I and Parkinson's disease. IUBMB Life 52:135-141.

91. Gritti A, Frolichsthal-Schoeller P, Galli R, Parati EA, Cova L, Pagano SF, Bjornson CR, Vescovi AL (1999) Epidermal and fibroblast growth factors behave as mitogenic regulators for a single multipotent stem cell-like population from the subventricular region of the adult mouse forebrain. J Neurosci 19:3287-3297.

92. Hack MA, Sugimori M, Lundberg C, Nakafuku M, Gotz M (2004) Regionalization and fate specification in neurospheres: the role of Olig2 and Pax6. Mol Cell Neurosci 25:664-678.

93. Haefliger P, Agorastos N, Renard A, Giambonini-Brugnoli G, Marty C, Alberto R (2005) Cell uptake and radiotoxicity studies of an nuclear localization signal peptide-intercalator conjugate labeled with [99mTc(CO)3]+. Bioconjug Chem 16:582-587.

94. Hagell P, Brundin P (2001) Cell survival and clinical outcome following intrastriatal transplantation in Parkinson disease. J Neuropathol Exp Neurol 60:741-752.

95. Hagell P, Schrag A, Piccini P, Jahanshahi M, Brown R, Rehncrona S, Widner H, Brundin P, Rothwell JC, Odin P, Wenning GK, Morrish P, Gustavii B, Bjorklund A, Brooks DJ, Marsden CD, Quinn NP, Lindvall O (1999) Sequential bilateral transplantation in Parkinson's disease: effects of the second graft. Brain 122 (Pt 6):1121-1132.

96. Hahn M, Timmer M, Nikkhah G (2009) Survival and early functional integration of dopaminergic progenitor cells following transplantation in a rat model of Parkinson's disease. J Neurosci Res 87:2006-2019.

97. Hattiangady B, Shuai B, Cai J, Coksaygan T, Rao MS, Shetty AK (2007) Increased dentate neurogenesis after grafting of glial restricted progenitors or neural stem cells in the aging hippocampus. Stem Cells 25:2104-2117.

98. Henry B, Crossman AR, Brotchie JM (1998) Characterization of enhanced behavioral responses to L-DOPA following repeated administration in the 6-hydroxydopamine-lesioned rat model of Parkinson's disease. Exp Neurol 151:334-342.

99. Herrera DG, Garcia-Verdugo JM, Alvarez-Buylla A (1999) Adult-derived neural precursors transplanted into multiple regions in the adult brain. Ann Neurol 46:867-877.

100. Hettiarachchi K, Green CE, Ramanathan-Girish S, Wu B, Jackson CJ, Ridge S, Salem MA, Lanser ME (2001) Analysis of 2beta-carbomethoxy-3beta-(4-fluorophenyl)-N-(3-iodo-E-allyl)nortropane in rat plasma. II. Pharmacokinetic profile in male and female Sprague-Dawley rats evaluated by capillary electrophoresis. J Chromatogr A 924:471-481.

101. Heyn C, Ronald JA, Mackenzie LT, MacDonald IC, Chambers AF, Rutt BK, Foster PJ (2006) In vivo magnetic resonance imaging of single cells in mouse brain with optical validation. Magn Reson Med 55:23-29.

102. Hirsch EC, Hoglinger G, Rousselet E, Breidert T, Parain K, Feger J, Ruberg M, Prigent A, Cohen-Salmon C, Launay JM (2003) Animal models of Parkinson's disease in rodents induced by toxins: an update. J Neural Transm Suppl89-100.

103. Hitoshi S, Tropepe V, Ekker M, van der KD (2002) Neural stem cell lineages are regionally specified, but not committed, within distinct compartments of the developing brain. Development 129:233-244.

104. Honer M, Hengerer B, Blagoev M, Hintermann S, Waldmeier P, Schubiger PA, Ametamey SM (2006) Comparison of [18F]FDOPA, [18F]FMT and [18F]FECNT for imaging dopaminergic neurotransmission in mice. Nucl Med Biol 33:607-614.

105. Hovakimyan M, Haas SJ, Schmitt O, Gerber B, Wree A, Andressen C (2008) Mesencephalic human neural progenitor cells transplanted into the adult hemiparkinsonian rat striatum lack dopaminergic differentiation but improve motor behavior. Cells Tissues Organs 188:373-383.

106. Howel LL, Byrd LD, McDonough AM, Iuvone PM, Bakay RA (2000) Behavioral evaluation of hemiparkinsonian MPTP monkeys following dopamine pharmacological manipulation and adrenal co-graft transplantation. Cell Transplant 9:609-622.

107. Huang WS, Ma KH, Chou YH, Chen CY, Liu RS, Liu JC (2003) 99mTc-TRODAT-1 SPECT in healthy and 6-OHDA lesioned parkinsonian monkeys: comparison with 18F-FDOPA PET. Nucl Med Commun 24:77-83.

108. Hughes AJ, Daniel SE, Blankson S, Lees AJ (1993) A clinicopathologic study of 100 cases of Parkinson's disease. Arch Neurol 50:140-148.

109. Hwang JJ, Liao MH, Yen TC, Wey SP, Lin KJ, Pan WH, Chen JC, Ting G (2002) Biodistribution study of [99mTc] TRODAT-1 alone or combined with other dopaminergic drugs in mice with macroautoradiography. Appl Radiat Isot 57:35-42.

110. Isacson O, Bjorklund LM, Schumacher JM (2003) Toward full restoration of synaptic and terminal function of the dopaminergic system in Parkinson's disease by stem cells. Ann Neurol 53 Suppl 3:S135-S146.

111. Jensen JB, Parmar M (2006) Strengths and limitations of the neurosphere culture system. Mol Neurobiol 34:153-161.

112. Jin Y, Kong H, Stodilka RZ, Wells RG, Zabel P, Merrifield PA, Sykes J, Prato FS (2005) Determining the minimum number of detectable cardiac-transplanted 111In-tropolone-labelled bone-marrow-derived mesenchymal stem cells by SPECT. Phys Med Biol 50:4445-4455.

113. Johansson CB, Momma S, Clarke DL, Risling M, Lendahl U, Frisen J (1999) Identification of a neural stem cell in the adult mammalian central nervous system. Cell 96:25-34.

114. Jordan S, Eberling JL, Bankiewicz KS, Rosenberg D, Coxson PG, VanBrocklin HF, O'Neil JP, Emborg ME, Jagust WJ (1997) 6-[18F]fluoro-L-m-tyrosine:

metabolism, positron emission tomography kinetics, and 1-methyl-4-phenyl-1,2,3,6-tetrahydropyridine lesions in primates. Brain Res 750:264-276.

115. Kao PF, Tzen KY, Yen TC, Lu CS, Weng YH, Wey SP, Ting G (2001) The optimal imaging time for [99Tcm]TRODAT-1/SPET in normal subjects and patients with Parkinson's disease. Nucl Med Commun 22:151-154.

116. Kaplan IM, Wadia JS, Dowdy SF (2005) Cationic TAT peptide transduction domain enters cells by macropinocytosis. J Control Release 102:247-253.

117. Kienzl E, Jellinger K, Stachelberger H, Linert W (1999) Iron as catalyst for oxidative stress in the pathogenesis of Parkinson's disease? Life Sci 65:1973-1976.

118. Kim HJ, Im JH, Yang SO, Moon DH, Ryu JS, Bong JK, Nam KP, Cheon JH, Lee MC, Lee HK (1997) Imaging and quantitation of dopamine transporters with iodine-123-IPT in normal and Parkinson's disease subjects. J Nucl Med 38:1703-1711.

119. Kim JH, Auerbach JM, Rodriguez-Gomez JA, Velasco I, Gavin D, Lumelsky N, Lee SH, Nguyen J, Sanchez-Pernaute R, Bankiewicz K, McKay R (2002) Dopamine neurons derived from embryonic stem cells function in an animal model of Parkinson's disease. Nature 418:50-56.

120. Kirchhoff F, Dringen R, Giaume C (2001) Pathways of neuron-astrocyte interactions and their possible role in neuroprotection. Eur Arch Psychiatry Clin Neurosci 251:159-169.

121. Klein C, Butt SJ, Machold RP, Johnson JE, Fishell G (2005) Cerebellum- and forebrain-derived stem cells possess intrinsic regional character. Development 132:4497-4508.

122. Klein S, Svendsen CN (2005) Stem cells in the injured spinal cord: reducing the pain and increasing the gain. Nat Neurosci 8:259-260.

123. Kriegstein A, Alvarez-Buylla A (2009) The glial nature of embryonic and adult neural stem cells. Annu Rev Neurosci 32:149-184.

124. Kung MP, Stevenson DA, Plossl K, Meegalla SK, Beckwith A, Essman WD, Mu M, Lucki I, Kung HF (1997) [99mTc]TRODAT-1: a novel technetium-99m complex as a dopamine transporter imaging agent. Eur J Nucl Med 24:372-380.

125. Lacorazza HD, Flax JD, Snyder EY, Jendoubi M (1996) Expression of human beta-hexosaminidase alpha-subunit gene (the gene defect of Tay-Sachs disease) in

mouse brains upon engraftment of transduced progenitor cells. Nat Med 2:424-429.

126. Lammertsma AA, Bench CJ, Hume SP, Osman S, Gunn K, Brooks DJ, Frackowiak RS (1996) Comparison of methods for analysis of clinical [11C]raclopride studies. J Cereb Blood Flow Metab 16:42-52.

127. Lee SH, Lumelsky N, Studer L, Auerbach JM, McKay RD (2000) Efficient generation of midbrain and hindbrain neurons from mouse embryonic stem cells. Nat Biotechnol 18:675-679.

128. Lemon JA, Rollo CD, McFarlane NM, Boreham DR (2008) Radiation-induced apoptosis in mouse lymphocytes is modified by a complex dietary supplement: the effect of genotype and gender. Mutagenesis 23:465-472.

129. Lepore AC, Han SS, Tyler-Polsz CJ, Cai J, Rao MS, Fischer I (2004) Differential fate of multipotent and lineage-restricted neural precursors following transplantation into the adult CNS. Neuron Glia Biol 1:113-126.

130. Lepore AC, Neuhuber B, Connors TM, Han SS, Liu Y, Daniels MP, Rao MS, Fischer I (2006) Long-term fate of neural precursor cells following transplantation into developing and adult CNS. Neuroscience 142:287-304.

131. Lewin M, Carlesso N, Tung CH, Tang XW, Cory D, Scadden DT, Weissleder R (2000) Tat peptide-derivatized magnetic nanoparticles allow in vivo tracking and recovery of progenitor cells. Nat Biotechnol 18:410-414.

132. Lindvall O, Brundin P, Widner H, Rehncrona S, Gustavii B, Frackowiak R, Leenders KL, Sawle G, Rothwell JC, Marsden CD, . (1990) Grafts of fetal dopamine neurons survive and improve motor function in Parkinson's disease. Science 247:574-577.

133. Lindvall O, Sawle G, Widner H, Rothwell JC, Bjorklund A, Brooks D, Brundin P, Frackowiak R, Marsden CD, Odin P, . (1994) Evidence for long-term survival and function of dopaminergic grafts in progressive Parkinson's disease. Ann Neurol 35:172-180.

134. Ling ZD, Potter ED, Lipton JW, Carvey PM (1998) Differentiation of mesencephalic progenitor cells into dopaminergic neurons by cytokines. Exp Neurol 149:411-423.

135. Liu X, Wang Y, Nakamura K, Kawauchi S, Akalin A, Cheng D, Chen L, Rusckowski M, Hnatowich DJ (2009) Auger radiation-induced, antisense-mediated cytotoxicity of tumor cells using a 3-component streptavidin-delivery nanoparticle with 111In. J Nucl Med 50:582-590.

136. Logan J, Fowler JS, Volkow ND, Wang GJ, Ding YS, Alexoff DL (1996) Distribution volume ratios without blood sampling from graphical analysis of PET data. J Cereb Blood Flow Metab 16:834-840.

137. Lois C, Alvarez-Buylla A (1993) Proliferating subventricular zone cells in the adult mammalian forebrain can differentiate into neurons and glia. Proc Natl Acad Sci U S A 90:2074-2077.

138. Lois C, Alvarez-Buylla A (1994) Long-distance neuronal migration in the adult mammalian brain. Science 264:1145-1148.

139. Lopez-Lozano JJ, Bravo G, Abascal J, Brera B, Millan I (1999) Clinical outcome of cotransplantation of peripheral nerve and adrenal medulla in patients with Parkinson's disease. Clinica Puerta de Hierro Neural Transplantation Group. J Neurosurg 90:875-882.

140. Lopez-Lozano JJ, Bravo G, Abascal J, Brera B, Pascual ML, Martinez R, de la Torre C, Moreno R (1996) Clinical experience with cotransplantation of peripheral nerve and adrenal medulla in patients with Parkinson's disease. Transpl Int 9 Suppl 1:S485-S491.

141. Lundblad M, Andersson M, Winkler C, Kirik D, Wierup N, Cenci MA (2002) Pharmacological validation of behavioural measures of akinesia and dyskinesia in a rat model of Parkinson's disease. Eur J Neurosci 15:120-132.

142. Luquin MR, Montoro RJ, Guillen J, Saldise L, Insausti R, Del RJ, Lopez-Barneo J (1999) Recovery of chronic parkinsonian monkeys by autotransplants of carotid body cell aggregates into putamen. Neuron 22:743-750.

143. Luthman J, Fredriksson A, Sundstrom E, Jonsson G, Archer T (1989) Selective lesion of central dopamine or noradrenaline neuron systems in the neonatal rat: motor behavior and monoamine alterations at adult stage. Behav Brain Res 33:267-277.

144. Ma B, Hankenson KD, Dennis JE, Caplan AI, Goldstein SA, Kilbourn MR (2005) A simple method for stem cell labeling with fluorine 18. Nucl Med Biol 32:701-705.

145. Ma Y, Feigin A, Dhawan V, Fukuda M, Shi Q, Greene P, Breeze R, Fahn S, Freed C, Eidelberg D (2002) Dyskinesia after fetal cell transplantation for parkinsonism: a PET study. Ann Neurol 52:628-634.

146. Madras BK, Gracz LM, Fahey MA, Elmaleh D, Meltzer PC, Liang AY, Stopa EG, Babich J, Fischman AJ (1998a) Altropane, a SPECT or PET imaging probe

for dopamine neurons: III. Human dopamine transporter in postmortem normal and Parkinson's diseased brain. Synapse 29:116-127.

147. Madras BK, Gracz LM, Meltzer PC, Liang AY, Elmaleh DR, Kaufman MJ, Fischman AJ (1998b) Altropane, a SPECT or PET imaging probe for dopamine neurons: II. Distribution to dopamine-rich regions of primate brain. Synapse 29:105-115.

148. Madras BK, Meltzer PC, Liang AY, Elmaleh DR, Babich J, Fischman AJ (1998c) Altropane, a SPECT or PET imaging probe for dopamine neurons: I. Dopamine transporter binding in primate brain. Synapse 29:93-104.

149. Marek K, Innis R, van DC, Fussell B, Early M, Eberly S, Oakes D, Seibyl J (2001) [123I]beta-CIT SPECT imaging assessment of the rate of Parkinson's disease progression. Neurology 57:2089-2094.

150. Marin C, Aguilar E, Bonastre M, Tolosa E, Obeso JA (2005) Early administration of entacapone prevents levodopa-induced motor fluctuations in hemiparkinsonian rats. Exp Neurol 192:184-193.

151. Massoud TF, Gambhir SS (2003) Molecular imaging in living subjects: seeing fundamental biological processes in a new light. Genes Dev 17:545-580.

152. McBride JL, Behrstock SP, Chen EY, Jakel RJ, Siegel I, Svendsen CN, Kordower JH (2004) Human neural stem cell transplants improve motor function in a rat model of Huntington's disease. J Comp Neurol 475:211-219.

153. McGregor KH, Gil J, Lahiri S (1984) A morphometric study of the carotid body in chronically hypoxic rats. J Appl Physiol 57:1430-1438.

154. Meikle SR, Kench P, Kassiou M, Banati RB (2005) Small animal SPECT and its place in the matrix of molecular imaging technologies. Phys Med Biol 50:R45-R61.

155. Mendez I, Sanchez-Pernaute R, Cooper O, Vinuela A, Ferrari D, Bjorklund L, Dagher A, Isacson O (2005) Cell type analysis of functional fetal dopamine cell suspension transplants in the striatum and substantia nigra of patients with Parkinson's disease. Brain 128:1498-1510.

156. Mokry J, Karbanova J, Filip S (2005) Differentiation potential of murine neural stem cells in vitro and after transplantation. Transplant Proc 37:268-272.

157. Morris ED, Endres CJ, Schmidt KC, Christian BT, Muzic Jr RF, Risher RE (2004) Kinetic Modeling in Positron Emission Tomography. In: Emission

Tomography: The Fundamentals of PET and SPECT (Wernick MN, Aarsvold JN, eds), pp 499-536. New York: Elsevier Academic Press.

158. Morshead CM, Garcia AD, Sofroniew MV, van der KD (2003) The ablation of glial fibrillary acidic protein-positive cells from the adult central nervous system results in the loss of forebrain neural stem cells but not retinal stem cells. Eur J Neurosci 18:76-84.

159. Morshead CM, van der Kooy D (2001) A new 'spin' on neural stem cells? Curr Opin Neurobiol 11:59-65.

160. Mozley PD, Schneider JS, Acton PD, Plossl K, Stern MB, Siderowf A, Leopold NA, Li PY, Alavi A, Kung HF (2000) Binding of [99mTc]TRODAT-1 to dopamine transporters in patients with Parkinson's disease and in healthy volunteers. J Nucl Med 41:584-589.

161. Muraoka K, Shingo T, Yasuhara T, Kameda M, Yuen WJ, Uozumi T, Matsui T, Miyoshi Y, Date I (2008) Comparison of the therapeutic potential of adult and embryonic neural precursor cells in a rat model of Parkinson disease. J Neurosurg 108:149-159.

162. Nahmias C, Wahl L, Chirakal R, Firnau G, Garnett ES (1995) A probe for intracerebral aromatic amino-acid decarboxylase activity: distribution and kinetics of [18F]6-fluoro-L-m-tyrosine in the human brain. Mov Disord 10:298-304.

163. Nikkhah G, Rosenthal C, Falkenstein G, Roedter A, Papazoglou A, Brandis A (2009) Microtransplantation of dopaminergic cell suspensions: further characterization and optimization of grafting parameters. Cell Transplant 18:119-133.

164. O'Keeffe FE, Scott SA, Tyers P, O'Keeffe GW, Dalley JW, Zufferey R, Caldwell MA (2008) Induction of A9 dopaminergic neurons from neural stem cells improves motor function in an animal model of Parkinson's disease. Brain 131:630-641.

165. Offen D, Ziv I, Sternin H, Melamed E, Hochman A (1996) Prevention of dopamine-induced cell death by thiol antioxidants: possible implications for treatment of Parkinson's disease. Exp Neurol 141:32-39.

166. Olsson M, Nikkhah G, Bentlage C, Bjorklund A (1995) Forelimb akinesia in the rat Parkinson model: differential effects of dopamine agonists and nigral transplants as assessed by a new stepping test. J Neurosci 15:3863-3875.

167. Ostenfeld T, Joly E, Tai YT, Peters A, Caldwell M, Jauniaux E, Svendsen CN (2002) Regional specification of rodent and human neurospheres. Brain Res Dev Brain Res 134:43-55.

168. Palmer TD, Markakis EA, Willhoite AR, Safar F, Gage FH (1999) Fibroblast growth factor-2 activates a latent neurogenic program in neural stem cells from diverse regions of the adult CNS. J Neurosci 19:8487-8497.

169. Palmer TD, Ray J, Gage FH (1995) FGF-2-responsive neuronal progenitors reside in proliferative and quiescent regions of the adult rodent brain. Mol Cell Neurosci 6:474-486.

170. Palumbo A, Napolitano A, Barone P, d'Ischia M (1999) Nitrite- and peroxide-dependent oxidation pathways of dopamine: 6-nitrodopamine and 6-hydroxydopamine formation as potential contributory mechanisms of oxidative stress- and nitric oxide-induced neurotoxicity in neuronal degeneration. Chem Res Toxicol 12:1213-1222.

171. Parker WD, Jr., Boyson SJ, Parks JK (1989) Abnormalities of the electron transport chain in idiopathic Parkinson's disease. Ann Neurol 26:719-723.

172. Pedraza-Lopez M, Ferro-Flores G, Mendiola-Cruz MT, Morales-Ramirez P (2000) Assessment of radiation-induced DNA damage caused by the incorporation of 99mTc-radiopharmaceuticals in murine lymphocytes using single cell gel electrophoresis. Mutat Res 465:139-144.

173. Peremans K, Cornelissen B, Van Den BB, Audenaert K, Van de WC (2005) A review of small animal imaging planar and pinhole spect Gamma camera imaging. Vet Radiol Ultrasound 46:162-170.

174. Perlow MJ, Freed WJ, Hoffer BJ, Seiger A, Olson L, Wyatt RJ (1979) Brain grafts reduce motor abnormalities produced by destruction of nigrostriatal dopamine system. Science 204:643-647.

175. Perumal AS, Tordzro WK, Katz M, Jackson-Lewis V, Cooper TB, Fahn S, Cadet JL (1989) Regional effects of 6-hydroxydopamine (6-OHDA) on free radical scavengers in rat brain. Brain Res 504:139-141.

176. Piccini P, Lindvall O, Bjorklund A, Brundin P, Hagell P, Ceravolo R, Oertel W, Quinn N, Samuel M, Rehncrona S, Widner H, Brooks DJ (2000) Delayed recovery of movement-related cortical function in Parkinson's disease after striatal dopaminergic grafts. Ann Neurol 48:689-695.

177. Polyakov V, Sharma V, Dahlheimer JL, Pica CM, Luker GD, Piwnica-Worms D (2000) Novel Tat-peptide chelates for direct transduction of technetium-99m and

rhenium into human cells for imaging and radiotherapy. Bioconjug Chem 11:762-771.

178. Ravina B, *et al.* (2005) The role of radiotracer imaging in Parkinson disease. Neurology 64:208-215.

179. Redmond DE, Jr., Bjugstad KB, Teng YD, Ourednik V, Ourednik J, Wakeman DR, Parsons XH, Gonzalez R, Blanchard BC, Kim SU, Gu Z, Lipton SA, Markakis EA, Roth RH, Elsworth JD, Sladek JR, Jr., Sidman RL, Snyder EY (2007) Behavioral improvement in a primate Parkinson's model is associated with multiple homeostatic effects of human neural stem cells. Proc Natl Acad Sci U S A 104:12175-12180.

180. Reynolds BA, Weiss S (1992) Generation of neurons and astrocytes from isolated cells of the adult mammalian central nervous system. Science 255:1707-1710.

181. Roussa E, Krieglstein K (2004) GDNF promotes neuronal differentiation and dopaminergic development of mouse mesencephalic neurospheres. Neurosci Lett 361:52-55.

182. Saalik P, Elmquist A, Hansen M, Padari K, Saar K, Viht K, Langel U, Pooga M (2004) Protein cargo delivery properties of cell-penetrating peptides. A comparative study. Bioconjug Chem 15:1246-1253.

183. Sanchez-Pernaute R, Studer L, Bankiewicz KS, Major EO, McKay RD (2001) In vitro generation and transplantation of precursor-derived human dopamine neurons. J Neurosci Res 65:284-288.

184. Sawamoto K, Nakao N, Kakishita K, Ogawa Y, Toyama Y, Yamamoto A, Yamaguchi M, Mori K, Goldman SA, Itakura T, Okano H (2001) Generation of dopaminergic neurons in the adult brain from mesencephalic precursor cells labeled with a nestin-GFP transgene. J Neurosci 21:3895-3903.

185. Schaffer P, Gleave JA, Lemon JA, Reid LC, Pacey LK, Farncombe TH, Boreham DR, Zubieta J, Babich JW, Doering LC, Valliant JF (2008) Isostructural fluorescent and radioactive probes for monitoring neural stem and progenitor cell transplants. Nucl Med Biol 35:159-169.

186. Schallert T, Fleming SM, Leasure JL, Tillerson JL, Bland ST (2000) CNS plasticity and assessment of forelimb sensorimotor outcome in unilateral rat models of stroke, cortical ablation, parkinsonism and spinal cord injury. Neuropharmacology 39:777-787.

187. Schallert T, Woodlee MT (2005) Orienting and Placing. In: The behavior of the laboratory rat: A handbook with tests (Whishaw IQ, Kolb B, eds), pp 129-140. New York: Oxford Universtiy Press.

188. Scherfler C, Donnemiller E, Schocke M, Dierkes K, Decristoforo C, Oberladstatter M, Kolbitsch C, Zschiegner F, Riccabona G, Poewe W, Wenning G (2002) Evaluation of striatal dopamine transporter function in rats by in vivo beta-[123I]CIT pinhole SPECT. Neuroimage 17:128-141.

189. Schwarz J, Schwarz SC, Dorigo O, Stutzer A, Wegner F, Labarca C, Deshpande P, Gil JS, Berk AJ, Lester HA (2006) Enhanced expression of hypersensitive alpha4* nAChR in adult mice increases the loss of midbrain dopaminergic neurons. FASEB J 20:935-946.

190. Seaberg RM, van der Kooy D (2002) Adult rodent neurogenic regions: the ventricular subependyma contains neural stem cells, but the dentate gyrus contains restricted progenitors. J Neurosci 22:1784-1793.

191. Seibyl JP, Marek KL, Quinlan D, Sheff K, Zoghbi S, Zea-Ponce Y, Baldwin RM, Fussell B, Smith EO, Charney DS, . (1995) Decreased single-photon emission computed tomographic [123I]beta-CIT striatal uptake correlates with symptom severity in Parkinson's disease. Ann Neurol 38:589-598.

192. Seri B, Garcia-Verdugo JM, McEwen BS, Alvarez-Buylla A (2001) Astrocytes give rise to new neurons in the adult mammalian hippocampus. J Neurosci 21:7153-7160.

193. Sherman MY, Goldberg AL (2001) Cellular defenses against unfolded proteins: a cell biologist thinks about neurodegenerative diseases. Neuron 29:15-32.

194. Shihabuddin LS, Horner PJ, Ray J, Gage FH (2000) Adult spinal cord stem cells generate neurons after transplantation in the adult dentate gyrus. J Neurosci 20:8727-8735.

195. Simola N, Morelli M, Carta AR (2007) The 6-hydroxydopamine model of Parkinson's disease. Neurotox Res 11:151-167.

196. Sinclair SR, Fawcett JW, Dunnett SB (1999) Dopamine cells in nigral grafts differentiate prior to implantation. Eur J Neurosci 11:4341-4348.

197. Song HJ, Stevens CF, Gage FH (2002) Neural stem cells from adult hippocampus develop essential properties of functional CNS neurons. Nat Neurosci 5:438-445.

198. Soto-Otero R, Mendez-Alvarez E, Hermida-Ameijeiras A, Munoz-Patino AM, Labandeira-Garcia JL (2000) Autoxidation and neurotoxicity of 6-

hydroxydopamine in the presence of some antioxidants: potential implication in relation to the pathogenesis of Parkinson's disease. J Neurochem 74:1605-1612.

199. Spencer TJ, Biederman J, Madras BK, Dougherty DD, Bonab AA, Livni E, Meltzer PC, Martin J, Rauch S, Fischman AJ (2007) Further evidence of dopamine transporter dysregulation in ADHD: a controlled PET imaging study using altropane. Biol Psychiatry 62:1059-1061.

200. Stephenson KA, Banerjee SR, Besanger T, Sogbein OO, Levadala MK, McFarlane N, Lemon JA, Boreham DR, Maresca KP, Brennan JD, Babich JW, Zubieta J, Valliant JF (2004a) Bridging the gap between in vitro and in vivo imaging: isostructural Re and 99mTc complexes for correlating fluorescence and radioimaging studies. J Am Chem Soc 126:8598-8599.

201. Stephenson KA, Zubieta J, Banerjee SR, Levadala MK, Taggart L, Ryan L, McFarlane N, Boreham DR, Maresca KP, Babich JW, Valliant JF (2004b) A new strategy for the preparation of peptide-targeted radiopharmaceuticals based on an fmoc-lysine-derived single amino acid chelate (SAAC). automated solid-phase synthesis, NMR characterization, and in vitro screening of fMLF(SAAC)G and fMLF[(SAAC-Re(CO)3)+]G. Bioconjug Chem 15:128-136.

202. Studer L, Tabar V, McKay RD (1998) Transplantation of expanded mesencephalic precursors leads to recovery in parkinsonian rats. Nat Neurosci 1:290-295.

203. Suhonen JO, Peterson DA, Ray J, Gage FH (1996) Differentiation of adult hippocampus-derived progenitors into olfactory neurons in vivo. Nature 383:624-627.

204. Suslov ON, Kukekov VG, Ignatova TN, Steindler DA (2002) Neural stem cell heterogeneity demonstrated by molecular phenotyping of clonal neurospheres. Proc Natl Acad Sci U S A 99:14506-14511.

205. Svendsen CN, Caldwell MA, Shen J, ter Borg MG, Rosser AE, Tyers P, Karmiol S, Dunnett SB (1997) Long-term survival of human central nervous system progenitor cells transplanted into a rat model of Parkinson's disease. Exp Neurol 148:135-146.

206. Tabar V, Panagiotakos G, Greenberg ED, Chan BK, Sadelain M, Gutin PH, Studer L (2005) Migration and differentiation of neural precursors derived from human embryonic stem cells in the rat brain. Nat Biotechnol 23:601-606.

207. Takagi Y, Nishimura M, Morizane A, Takahashi J, Nozaki K, Hayashi J, Hashimoto N (2005) Survival and differentiation of neural progenitor cells

derived from embryonic stem cells and transplanted into ischemic brain. J Neurosurg 103:304-310.

208. Tatsch K (2001) Imaging of the dopaminergic system in parkinsonism with SPET. Nucl Med Commun 22:819-827.

209. Terpstra BT, Collier TJ, Marchionini DM, Levine ND, Paumier KL, Sortwell CE (2007) Increased cell suspension concentration augments the survival rate of grafted tyrosine hydroxylase immunoreactive neurons. J Neurosci Methods 166:13-19.

210. Thonhoff JR, Ojeda L, Wu P (2009) Stem Cell-Derived Motor Neurons: Applications and Challenges in Amyotrophic Lateral Sclerosis. Curr Stem Cell Res Ther.

211. Toledo-Aral JJ, Mendez-Ferrer S, Pardal R, Echevarria M, Lopez-Barneo J (2003) Trophic restoration of the nigrostriatal dopaminergic pathway in long-term carotid body-grafted parkinsonian rats. J Neurosci 23:141-148.

212. Tonchev AB, Yamashima T, Sawamoto K, Okano H (2005) Enhanced proliferation of progenitor cells in the subventricular zone and limited neuronal production in the striatum and neocortex of adult macaque monkeys after global cerebral ischemia. J Neurosci Res 81:776-788.

213. Tropepe V, Sibilia M, Ciruna BG, Rossant J, Wagner EF, van der KD (1999) Distinct neural stem cells proliferate in response to EGF and FGF in the developing mouse telencephalon. Dev Biol 208:166-188.

214. Turkington TG (2001) Introduction to PET instrumentation. J Nucl Med Technol 29:4-11.

215. Ungerstedt U (1968) 6-Hydroxy-dopamine induced degeneration of central monoamine neurons. Eur J Pharmacol 5:107-110.

216. Ungerstedt U (1971) Postsynaptic supersensitivity after 6-hydroxy-dopamine induced degeneration of the nigro-striatal dopamine system. Acta Physiol Scand Suppl 367:69-93.

217. Ungerstedt U, Arbuthnott GW (1970) Quantitative recording of rotational behavior in rats after 6-hydroxy-dopamine lesions of the nigrostriatal dopamine system. Brain Res 24:485-493.

218. Vives E, Brodin P, Lebleu B (1997) A truncated HIV-1 Tat protein basic domain rapidly translocates through the plasma membrane and accumulates in the cell nucleus. J Biol Chem 272:16010-16017.

219. Vroemen M, Aigner L, Winkler J, Weidner N (2003) Adult neural progenitor cell grafts survive after acute spinal cord injury and integrate along axonal pathways. Eur J Neurosci 18:743-751.

220. Wagner J, Akerud P, Castro DS, Holm PC, Canals JM, Snyder EY, Perlmann T, Arenas E (1999) Induction of a midbrain dopaminergic phenotype in Nurr1-overexpressing neural stem cells by type 1 astrocytes. Nat Biotechnol 17:653-659.

221. Wang TY, Sen A, Behie LA, Kallos MS (2006) Dynamic behavior of cells within neurospheres in expanding populations of neural precursors. Brain Res 1107:82-96.

222. Watts RL, Subramanian T, Freeman A, Goetz CG, Penn RD, Stebbins GT, Kordower JH, Bakay RA (1997) Effect of stereotaxic intrastriatal cografts of autologous adrenal medulla and peripheral nerve in Parkinson's disease: two-year follow-up study. Exp Neurol 147:510-517.

223. Wei P, Liu J, Zhou HL, Han ZT, Wu QY, Pang JX, Liu S, Wang TH (2007) Effects of engrafted neural stem cells derived from GFP transgenic mice in Parkinson's diseases rats. Neurosci Lett 419:49-54.

224. Weiss S, Dunne C, Hewson J, Wohl C, Wheatley M, Peterson AC, Reynolds BA (1996) Multipotent CNS stem cells are present in the adult mammalian spinal cord and ventricular neuroaxis. J Neurosci 16:7599-7609.

225. Westerlund U, Moe MC, Varghese M, Berg-Johnsen J, Ohlsson M, Langmoen IA, Svensson M (2003) Stem cells from the adult human brain develop into functional neurons in culture. Exp Cell Res 289:378-383.

226. Wictorin K, Brundin P, Sauer H, Lindvall O, Bjorklund A (1992) Long distance directed axonal growth from human dopaminergic mesencephalic neuroblasts implanted along the nigrostriatal pathway in 6-hydroxydopamine lesioned adult rats. J Comp Neurol 323:475-494.

227. Woodlee MT, Asseo-Garcia AM, Zhao X, Liu SJ, Jones TA, Schallert T (2005) Testing forelimb placing "across the midline" reveals distinct, lesion-dependent patterns of recovery in rats. Exp Neurol 191:310-317.

228. Woodlee MT, Kane JR, Chang J, Cormack LK, Schallert T (2008) Enhanced function in the good forelimb of hemi-parkinson rats: Compensatory adaptation for contralateral postural instability? Exp Neurol 211:511-517.

229. Wu S, Sasaki A, Yoshimoto R, Kawahara Y, Manabe T, Kataoka K, Asashima M, Yuge L (2008) Neural stem cells improve learning and memory in rats with Alzheimer's disease. Pathobiology 75:186-194.

230. Yandava BD, Billinghurst LL, Snyder EY (1999) "Global" cell replacement is feasible via neural stem cell transplantation: evidence from the dysmyelinated shiverer mouse brain. Proc Natl Acad Sci U S A 96:7029-7034.

231. Yang M, Stull ND, Berk MA, Snyder EY, Iacovitti L (2002) Neural stem cells spontaneously express dopaminergic traits after transplantation into the intact or 6-hydroxydopamine-lesioned rat. Exp Neurol 177:50-60.

232. Yasuhara T, Borlongan CV, Date I (2006) Ex vivo gene therapy: transplantation of neurotrophic factor-secreting cells for cerebral ischemia. Front Biosci 11:760-775.

233. Youdim MB, Riederer PF (2004) A review of the mechanisms and role of monoamine oxidase inhibitors in Parkinson's disease. Neurology 63:S32-S35.

234. Zbarsky V, Datla KP, Parkar S, Rai DK, Aruoma OI, Dexter DT (2005) Neuroprotective properties of the natural phenolic antioxidants curcumin and naringenin but not quercetin and fisetin in a 6-OHDA model of Parkinson's disease. Free Radic Res 39:1119-1125.

235. Zhao LR, Duan WM, Reyes M, Keene CD, Verfaillie CM, Low WC (2002) Human bone marrow stem cells exhibit neural phenotypes and ameliorate neurological deficits after grafting into the ischemic brain of rats. Exp Neurol 174:11-20.

236. Zhou R, Thomas DH, Qiao H, Bal HS, Choi SR, Alavi A, Ferrari VA, Kung HF, Acton PD (2005) In vivo detection of stem cells grafted in infarcted rat myocardium. J Nucl Med 46:816-822.

237. Zhou Y, Resnick SM, Ye W, Fan H, Holt DP, Klunk WE, Mathis CA, Dannals R, Wong DF (2007) Using a reference tissue model with spatial constraint to quantify [11C]Pittsburgh compound B PET for early diagnosis of Alzheimer's disease. Neuroimage 36:298-312.